NMR survey of reflected Brownian motion

Denis S. Grebenkov*

Laboratoire de Physique de la Matière Condensée, C.N.R.S.–Ecole Polytechnique, 91128 Palaiseau, France
and Unité de Recherche en Résonance Magnétique Médicale, C.N.R.S.–Université Paris-Sud XI, 91405 Orsay, France

(Published 17 August 2007)

Restricted diffusion is a common feature of many physicochemical, biological, and industrial processes. Nuclear magnetic resonance techniques are often used to survey the atomic or molecular motion in confining media by applying inhomogeneous magnetic fields to encode the trajectories of spin-bearing particles. The diversity and complexity of diffusive NMR phenomena, observed in experiments, result from the specific properties of reflected Brownian motion. Here the focus is on the mathematical aspects of this stochastic process, their physical interpretations, and their practical applications. The main achievements in this field, from Hahn's discovery of spin echoes to present-day research, are presented in a unified mathematical language. A long-standing problem of restricted diffusion under arbitrary magnetic field is reformulated in terms of multiple correlation functions of the reflected Brownian motion. Many classical results are retrieved, extended, and critically discussed.

DOI: 10.1103/RevModPhys.79.1077 PACS number(s): 82.56.Lz, 02.50.Cw, 76.60.Lz, 05.60.−k

CONTENTS

I. Introduction 1078
II. A Historical Overview 1080
A. Free diffusion by NMR 1080
B. Bloch-Torrey equation 1081
C. Effect of a geometrical restriction 1082
D. Narrow-pulse approximation 1082
E. Restricted diffusion in simple domains 1084
F. Gaussian phase approximation 1084
G. Multiexponential magnetization decay 1085
H. Non-Gaussian behavior 1085
I. Studying porous media 1088
J. Nonlinear magnetic fields 1089
K. Diffusive edge enhancement 1089
L. Conventional numerical techniques 1090
M. Matrix formalisms 1091
III. Multiple Correlation Functions 1091
A. Physical assumptions 1092
B. General formulation 1093
C. Application to spin echoes 1095
D. Temporal profiles of the magnetic field 1097
1. Simple spin echo 1097
2. CPMG spin echoes 1097
3. Oscillating profile 1098
4. Arbitrary coherence pathway 1098
E. Spatial profiles of the magnetic field 1098
1. Linear gradient 1098
2. Parabolic magnetic field 1098
F. Basic confining domains 1098
1. Slab 1099
2. Cylinder 1099
3. Sphere 1100
IV. Slow-diffusion Regime ($p \ll 1$) 1100
A. Leading term of the second moment 1100
B. Higher-order moments 1101
C. Correction term to the second moment 1102
D. Several temporal profiles 1104
E. Discussion of the correction term 1104
V. Motional-Narrowing Regime ($p \gg 1$) 1106
A. Leading terms 1106
B. Corrections to the leading term 1106
1. Stejskal-Tanner temporal profile 1106
2. CPMG temporal profile 1107
3. Oscillating temporal profile 1108
VI. Discussion 1108
A. Numerical implementation 1108
B. Odd-order moments 1110
1. First moment 1110
2. Antisymmetric temporal profiles 1111
C. Cumulant expansion 1111
D. Apparent diffusion coefficient 1112
E. Narrow-pulse approximation 1113
F. Localization regime 1115
G. Transition between different regimes 1116
H. Inverse spectral problem 1117
I. Application to porous media 1118
VII. Conclusion 1119
Acknowledgments 1121
Appendix A: Fourth Moment in the Slow-Diffusion Regime 1121
1. First-order contribution 1121
2. Second-order contribution 1121
Appendix B: Laplace Transform Summation Technique 1122
1. Consequences of the Mittag-Leffler theorem 1124
2. Example: Slab geometry and parabolic profile 1124
3. Analogy with the return-to-the-origin probability 1125
4. Relation to spectral zeta functions 1125
Appendix C: Fourth Moment in the Motional-Narrowing Regime 1126
Appendix D: Multiple Propagator Approach 1126
Appendix E: Even-Order Moments in the Narrow-Pulse Approximation 1128

*Electronic address: denis.grebenkov@polytechnique.edu

 ©2007 The American Physical Society

List of Symbols 1128
References 1129

I. INTRODUCTION

A particle diffusing in a confining medium is a general model for a number of physical, chemical, biological, and industrial processes. It may describe organic molecules or metabolites in biological cells[1] or brain tissue,[2] reactive species near porous catalysts,[3] ions near rough electrodes or cellular membranes,[4] oxygen in human lungs,[5] water molecules in cements[6] or rocks,[7] etc. When such a particle encounters an interface, they may interact in different ways depending on their physical and chemical properties. The interaction at the microscopic level can often be represented in terms of "reflection" and "absorption" at the interface. In the former case, the particle does not change its state and continues to diffuse in the bulk. In the latter case, the motion of the particle is terminated, either by absorption on or transfer through the interface, by chemical transformation into another particle, or by surface relaxation in a nuclear magnetic resonance (NMR) experiment, etc.[8] As a consequence, the random motion of a labeled particle is additionally complicated by multiple reflections on the interface.

In mathematics, this stochastic process is known as (partially) reflected Brownian motion.[9] It can be rigorously constructed for confining domains with smooth boundaries as a solution of the stochastic differential equation accounting for reflections on the boundary.[10] Although still governed by a Laplacian field, this Brownian process presents many new and interesting features due to the geometrical restriction. Its effects have been noted in areas as diverse as physiology [diffusional screening in mammalian lungs, Felici *et al.* (2005)], electrochemistry (e.g., constant phase angle frequency regime of the spectroscopic impedance of a rough metallic electrode[11]), and nuclear magnetic resonance [e.g., a multiexponential decay of the water proton signal in biological cells, Brownstein and Tarr (1977, 1979); see below].

NMR is of particular interest as being a method to "label" or "encode" Brownian trajectories of spin-bearing particles by using magnetic fields.[12] To illustrate the idea, consider nuclei of spin 1/2, e.g., water protons. Under a constant magnetic field B_0, these nuclei have two states with energies μB_0 and $-\mu B_0$, respectively, where μ is the nuclear magnetic moment.[13] The energy difference corresponds to the resonant or Larmor frequency $\omega_0 = 2\mu B_0/\hbar = \gamma B_0$, $2\pi\hbar$ being Planck's constant and $\gamma = 2\mu/\hbar$ the nuclear gyromagnetic ratio.[14] At thermal equilibrium, a difference of state populations creates a magnetization that is oriented along the direction of the magnetic field (traditionally, it is denoted as the z axis). A brief application of a periodic magnetic field B_1 rotating in the transverse plane xy with Larmor frequency γB_0 flips the spin magnetizations into this plane. When this so-called 90° radio-frequency (rf) pulse ceases, the spin magnetizations precess with the same Larmor frequency γB_0 in the transverse plane and relax to their equilibrium states (parallel to the axis z). For a

[1] Finkelstein (1987); Alberts *et al.* (1994); Pfeuffer *et al.* (1998).
[2] Nicholson (1985, 2001); Le Bihan (2003).
[3] Sahimi *et al.* (1990); Coppens (1999).
[4] Nyikos and Pajkossy (1986); Halsey and Leibig (1992); Sapoval (1994, 1996).
[5] Weibel (1984); Sapoval *et al.* (2002); Felici *et al.* (2004, 2005); Grebenkov, Filoche, *et al.* (2005).
[6] Halperin *et al.* (1994); Nestle *et al.* (2001); Plassais *et al.* (2003, 2005).
[7] Kenyon (1992); Kleinberg *et al.* (1994, 1996a); Song *et al.* (2000); Sen (2004).
[8] In the two last examples, the particle can still diffuse, but its state has been changed, for example, the nuclear magnetization has been lost. Since this particle does not contribute to the process in question any more, it can be thought of as being absorbed.
[9] Itô and McKean (1965); Port and Stone (1978); Freidlin (1985); Borodin and Salminen (1996); Bass (1998); Revuz and Yor (1999); Yor (2001); Grebenkov (2006a).
[10] As for ordinary differential equations, an infinitesimal increase of the stochastic process $\hat{W}_t$ can be expressed as $d\hat{W}_t = dW_t + \mathbf{n}(\hat{W}_t)\mathbb{I}_{\partial\Omega}(\hat{W}_t)d\ell_t$, $\hat{W}_0 = \mathbf{r}_0$, $\ell_0 = 0$, where W_t is the (ordinary) Brownian motion, $\mathbf{n}(\mathbf{r})$ is the unit normal to the boundary $\partial\Omega$ at $\mathbf{r}$, $\mathbb{I}_{\partial\Omega}$ is the indicator function of the boundary, $\mathbf{r}_0$ is the starting point, and ℓ_t is the measure of how much time the walker spent on the boundary until t. The first term governs the usual Brownian dynamics in the bulk, while the second term contributes only for collisions with the boundary and ensures that Brownian motion is indeed reflected. Note that this equation simultaneously determines both processes, the reflected Brownian motion $\hat{W}_t$ and its local time ℓ_t [see Freidlin (1985) for details].
[11] de Levie (1965); Armstrong and Burnham (1976); Nyikos and Pajkossy (1985); Sapoval *et al.* (1988); Halsey and Leibig (1992); Grebenkov (2006a, 2006c).
[12] An introduction to NMR can be found in Abragam (1961) and Callaghan (1991). Various aspects of NMR are collected in the encyclopedia by Grant and Harris (1996). Some general aspects of Brownian motion are discussed by Duplantier (2005) and Frey and Kroy (2005). Principles and application of self-diffusion measurements by NMR are described by Kärger *et al.* (1988) and Ardelean and Kimmich (2003). There is a special emphasis on diffusive motion in porous media and its applications in Klafter and Drake (1989), Kimmich (1997), Blümich (2000), and Havlin and ben Avraham (2002). Tutorials for using NMR to probe a geometry were written by Song (2003) and Sen (2004). Characterization of porous media with NMR methods is reviewed by Watson and Chang (1997), Barrie (2000), and Watson *et al.* (2002). Transport and geometrical properties of porous media are discussed in Scheidegger (1974), Dullien (1991), Kärger and Ruthven (1992), Sahimi (1995), and Wong (1999). A collection of papers on fundamental properties of diffusion is published in Kärger *et al.* (2005). Stochastic problems in physics were discussed by Chandrasekhar (1943).
[13] For protons, $\mu = 1.410\,606\,71 \times 10^{-26}$ J/T (Mohr and Taylor, 2005).
[14] For protons, $\gamma \approx 2.675 \times 10^8$ rad T^{-1} s^{-1}, and $\gamma \approx 2.038 \times 10^8$ rad T^{-1} s^{-1} for helium-3 (Mohr and Taylor, 2005).

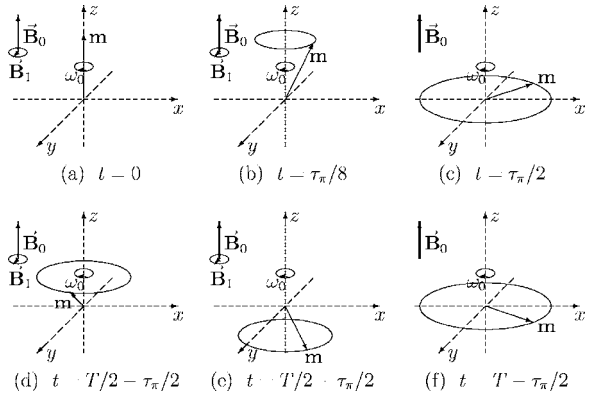

FIG. 1. Schematic illustration of echo formation. In a static field B_0 along the z axis, the spins precess around this axis with the Larmor frequency $\omega_0=\gamma B_0$, and their magnetizations are directed along z. (a) At time $t=0$, one applies a periodic magnetic field B_1 (rf pulse) rotating in the transverse plane xy with frequency ω_0. (b) Still precessing, each magnetization is turning, linearly in time, toward the transverse plane. (c) When $t=\tau_\pi/2$ (here $\gamma B_1\tau_\pi=\pi$), the magnetizations lie in the transverse plane, and the periodic magnetic field ceases. (d) During the period $\Delta T=T/2-\tau_\pi$, the magnetizations slowly relax to the longitudinal direction (axis z). At $t=T/2-\tau_\pi/2$, another rf pulse is applied. (e) Acting during the time τ_π, it inverts the longitudinal direction of the magnetizations. (f) When this 180° rf pulse is turned off, the slow relaxation during the subsequent time period ΔT returns the magnetizations into the transverse plane (f). Moreover, these magnetizations turn out to be partially refocused so that they form a macroscopic signal (an echo) at $t=T-\tau_\pi/2$. To get a simpler view of the action of the rf pulses, one could consider the coordinate frame rotating around the z axis with the frequency ω_0. Throughout this review, the rf pulses are assumed to be very short allowing their durations ($\tau_\pi/2$ and τ_π) to be neglected.

simple spin-echo experiment, the second 180° rf pulse at time $T/2$ is applied to refocus the magnetizations to form an echo at time T, as illustrated in Fig. 1.

If the magnetic field B_0 is not spatially homogeneous, some spins precess faster than others, depending on their location in space. Consequently, application of a time-dependent inhomogeneous magnetic field $B_t(\mathbf{r})$, directed along the z axis, can be used to encode the positions of nuclei. The total phase accumulated along the trajectory $\mathbf{r}(t)$ of a nucleus during the time from 0 to T is then

$$\varphi=\gamma\int_0^T dt\, B_t(\mathbf{r}(t)). \tag{1}$$

The macroscopic signal E measured at time T is formed by the entire ensemble of the spins diffusing in the confining domain Ω. The individual transverse magnetizations, conveniently written in a complex form $e^{i\varphi}$, have thus to be averaged over this ensemble. In most experiments, the number of spins is so large that one can average over all stochastic trajectories of reflected Brownian motion $\mathbf{r}(t)$,

$$E=\mathbb{E}\{e^{i\varphi}\}, \tag{2}$$

with φ being considered here as a functional of $\mathbf{r}(t)$. For convenience, the signal in Eq. (2) is normalized to 1 if $B_t(\mathbf{r})\equiv 0$ and no relaxation is present. Note that the expectation $\mathbb{E}$ includes the average over starting points with a given initial density $\rho_0(\mathbf{r})$ of spins distributed in the bulk. Since each Brownian trajectory is "weighted" by the functional in Eq. (1), some parts of this complex process can be emphasized by varying the temporal and spatial dependences of the applied magnetic field $B_t(\mathbf{r})$. One thus has a powerful experimental tool to survey reflected Brownian motion. Studying the attenuation of the macroscopic signal E in different magnetic fields, one can retrieve useful information about the diffusive motion itself (e.g., the diffusion coefficient) and the confining geometry. For this reason, NMR is widely used to probe complex morphology of natural and artificial materials (e.g., rocks, soils, cements, colloids) or biological tissues (e.g., brain, lung, bone, kidney). In such experiments, the time scale typically ranges between milliseconds and seconds during which the nuclei travel distances between a few microns (for liquids) and a few millimeters (for gases), depending on their diffusion coefficient.

In this review, we indicate and discuss the main theoretical achievements in this field, from Hahn's discovery of spin echoes in 1950 to present-day research. The actual understanding of diffusive phenomena comes from the intensive work of many scientists over half a century. Different theoretical approaches and mathematical concepts have been employed during the course of this long investigation: random walks and stochastic processes, partial differential equations, density matrices, Green functions, the Laplace operator eigenbasis, spectral and Fourier analysis, random fields, etc. If Hahn's original work described the simplest case of unrestricted diffusion in a time-independent linear magnetic-field gradient, further progress consisted of extending these results to include, for instance, geometrical restriction of diffusing nuclei or temporal dependence and spatial inhomogeneity of the magnetic field. Each technique was focused on a particular extension. So Stejskal and Tanner included an arbitrary temporal dependence for unrestricted diffusion while Robertson, and later Neuman, studied restricted diffusion in simple domains for specific temporal and spatial profiles. The diversity of theoretical approaches developed in the last few decades made the comparison between them and the understanding of fundamental properties of reflected Brownian motion difficult. A single mathematical approach to diffusive NMR phenomena should clarify the state of the art and could bring new ideas to this field. The multiple-correlation-function description is used throughout this review to retrieve, discuss, and extend many classical results. This technique allows one to tackle the problem of diffusive motion in any geometrical confinement and for arbitrary temporal and spatial profiles of the magnetic field.

To keep the review to a reasonable size, the scope of

issues presented herein has been carefully considered. The main focus is on mathematical aspects of restricted diffusion and their physical interpretation. The slow-diffusion and motional-narrowing regimes as well as the underlying Gaussian phase approximation and the related notion of the apparent diffusion coefficient are investigated in detail. Many other concepts like the local gradient approximation, the problem of odd moments, cumulant expansion, the localization regime, and the narrow-pulse approximation naturally appear. The use of NMR to probe complex morphologies is also discussed, in particular the problem of finding the surface-to-volume ratio. At the same time, a number of interesting issues could not be included; for example, diffusion in anisotropic media and the related tensorial formalism [see Güllmar *et al.* (2005); Kingsley (2006)], multidimensional distribution functions involving diffusion, and longitudinal and transverse relaxations,[15] or numerous applications in medicine and the oil industry. Anomalous diffusion, Knudsen ballistic motion, and other "strange" kinetics, which may occur, for instance, in nanoporous materials, are not considered.[16]

The paper is organized as follows. In the next section, we give a short historical overview to emphasize the main contributions to this field. In Sec. III, the multiple correlation function (MCF) description will be presented in detail to investigate the macroscopic signal attenuation due to restricted diffusion in the presence of an arbitrary magnetic field. The moments of the accumulated phase will be expressed in a compact matrix form involving the Laplace operator eigenbasis in a confining domain. This general description will then be applied to study spin echoes, the most typical experimental situation. In fact, the rephasing condition, required for echo formation, will make this technique more appropriate for theoretical and numerical use. Different choices of temporal and spatial profiles of the magnetic field will be discussed, including linear gradients and parabolic magnetic fields. The explicit formulas of the two matrices $\mathcal{B}$ and Λ, determining all the moments, will be given for three basic domains (slab, cylinder, and sphere). Section IV is devoted to a detailed study of the slow-diffusion regime, where the classical results will be retrieved in a general form and then critically discussed. In Sec. V, the leading and correction terms of the moments will be found for the motional-narrowing regime. In Sec. VI, we tackle several related topics, from the numerical implementation of the MCF description to the cancellation of odd moments. A comparison between theoretical and experimental measurements will be reported. The issues of the localization regime, cumulant expansion, and unrestricted diffusion will also be discussed. The problems of studying realistic porous media and their potential solutions will be outlined. In the Conclusion, we summarize the essential results and reveal a number of unsolved problems and further perspectives. Some interesting but cumbersome techniques outlined in the review are placed in the Appendixes.

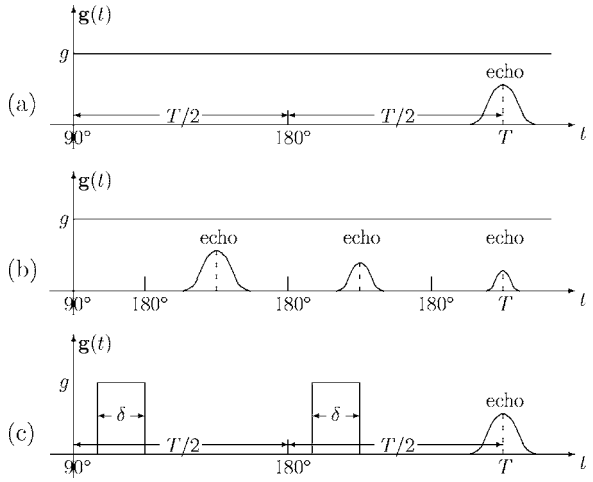

FIG. 2. Typical spin-echo sequences. (a) Formation of a spin echo at time T by application of a 180° rf pulse in steady gradient profile (Hahn experiment). (b) Periodic repetition of 180° rf pulses creates a train of spin echoes (Carr-Purcell experiment). (c) Pulsed gradient spin-echo formation (Stejskal-Tanner experiment).

II. A HISTORICAL OVERVIEW

We start with a short historical overview to emphasize the main contributions and steps in understanding diffusive NMR phenomena. This section serves as a guide to numerous results that are briefly discussed here, while a more detailed analysis is presented in the following sections.

A. Free diffusion by NMR

The origin of diffusive NMR phenomena can be attributed to Hahn's discovery of spin echoes in 1950. Application of a 180° rf pulse[17] [Fig. 2(a)] leads to refocusing of spin magnetizations, which creates an experimentally measurable signal called a "spin echo." Since this macroscopic signal is formed by local contributions of numerous nuclei, it somehow reflects the properties of the whole ensemble. Spin-spin interaction, field inhomogeneities, motion of nuclei, and other related effects determine the spin-echo amplitude and can

[15] Song *et al.* (2002); Hürlimann and Venkataramanan (2002); Venkataramanan *et al.* (2002); Callaghan *et al.* (2003); Seland *et al.* (2004); McDonald *et al.* (2005); Wilson and Hürlimann (2006), and references therein. See also Kleinberg (1994, 1996b) for transverse relaxation times distributions.

[16] Bouchaud and Georges (1990); Metzler and Klafter (2000); Kimmich (2002); Zaslavsky (2002).

[17] In the original Hahn experiment, the second rf pulse was of 90° that could invert the spin magnetizations as well. In particular, the prefactor in Eq. (3) was 1/3 which would correspond to a steady gradient without a 180° rf pulse. The factor 1/12 was found by Carr and Purcell (1954). The produced spin echo is often called "Hahn's echo" regardless of the duration of the second rf pulse (90° or 180°).

thus be investigated by means of NMR measurements. For instance, the attenuation of the macroscopic signal E due to free (or unrestricted) diffusion under steady magnetic field of a linear gradient g and duration T was found to be

$$E = \exp[-D\gamma^2 g^2 T^3/12], \tag{3}$$

where D is the free self-diffusion coefficient. On the one hand, the above relation helps to estimate the effect of diffusive motion when studying, for example, spin-spin relaxations. On the other hand, it accesses a direct experimental measurement of the diffusion coefficient by NMR. Hahn's averaging procedure was improved by Das and Saha in 1954. Another approach involving the spectral density function was proposed by Schearer and Walters in 1965.

This fundamental result was further extended by different authors. Carr and Purcell (1954) proposed repeatedly applying 180° rf pulses in order to produce a train of multiple spin echoes as shown in Fig. 2(b). They used a random-walk approach to derive the signal attenuation due to free diffusion for the kth echo:[18]

$$E = \exp[-D\gamma^2 g^2 T^3/12k^2]. \tag{4}$$

Again, the effect of diffusive motion can either be eliminated by taking a large number of echoes or be investigated by studying the dependence on k. Its experimental realization was later improved by Meiboom and Gill (1958) and it is now known as the Carr-Purcell-Meiboom-Gill (CPMG) sequence.

Douglass and McCall (1958) improved Hahn's analysis and gave another experimental verification. From the probabilistic point of view, the accumulated phase φ is a random variable whose distribution is determined by the properties of the diffusive motion, the applied magnetic field, and the geometry of confining medium. If there is no geometrical restriction, the Brownian motion can be thought of as a sum of *independent* infinitesimal spatial displacements of a diffusing nucleus. In this case, the central limit theorem (Feller, 1971) ensures a Gaussian distribution of the random phase φ in Eq. (1):

$$\mathbb{P}(\varphi) = (2\pi\mathbb{E}\{\varphi^2\})^{-1/2} \exp\left(-\frac{\varphi^2}{2\mathbb{E}\{\varphi^2\}}\right). \tag{5}$$

Like its Fourier transform, the signal is completely determined by the second moment $\mathbb{E}\{\varphi^2\}$:

$$E = \exp[-\mathbb{E}\{\varphi^2/2\}]. \tag{6}$$

Douglass and McCall found the second-order moment $\mathbb{E}\{\varphi^2/2\}$ to be equal to $2D\gamma^2 g^2(\tau^3 - \tau^2 T + T^3/6)$, where τ is the moment of the 180° pulse. Taking $\tau = T/2$, one gets $\mathbb{E}\{\varphi^2/2\} = D\gamma^2 g^2 T^3/12$ in agreement with Eq. (3).

Stejskal and Tanner (1965) proposed to replace a steady gradient by a pulsed gradient to facilitate the measurement and to enlarge the ranges of applicability. A typical pulsed gradient profile is shown in Fig. 2(c). If there is no gradient during the rf pulses, their amplitude has no need to be particularly large; in turn, no gradient at echo time T makes the determination of the echo amplitude more precise. In their paper, Stejskal and Tanner found the signal attenuation due to free diffusion for an arbitrary temporal profile of a linear magnetic-field gradient $\mathbf{g}(t)$:

$$E = \exp\left[-D\gamma^2\left(\int_0^T dt\, \mathbf{G}^2(t) - 4\mathbf{G}(T/2)\int_{T/2}^T dt\, \mathbf{G}(t) + 2T\mathbf{G}^2(T/2)\right)\right], \tag{7}$$

where $\mathbf{G}(t) = \int_0^t dt' \mathbf{g}(t')$ and the 180° rf pulse is applied at time $T/2$. This general relation and its derivatives for particular temporal profiles were widely used until the present day for theoretical and experimental purposes. For instance, the signal attenuation for the pulsed gradient shown in Fig. 2(c) was found to be

$$E = \exp[-D\gamma^2 g^2 \delta^2 (T/2 - \delta/3)]. \tag{8}$$

One retrieves Eq. (3) by taking $\delta = T/2$. We thoroughly discuss these results in the following sections.

B. Bloch-Torrey equation

An alternative description of diffusive NMR phenomena was proposed by Torrey (1956). To account for the diffusive motion, he modified the Bloch equation (Bloch, 1946) for the spin magnetization $\mathfrak{m}(\mathbf{r},t)$,

$$\left(\frac{\partial}{\partial t} - D\Delta + i\gamma \mathbf{g}\cdot\mathbf{r}\right)\mathfrak{m}(\mathbf{r},t) = 0, \tag{9}$$

by introducing the Laplace operator $\Delta = \nabla^2$, ∇ being the gradient operator. Looking for a solution of the one-dimensional equation in the form $\mathfrak{m}(x,t) = A(t)e^{-i\gamma g x t}$, Torrey retrieved Eqs. (3) and (4) in a simpler way. A bulk relaxation might be incorporated into this Bloch-Torrey equation through an additional constant term in parentheses.

Introduction of appropriate boundary conditions makes Eq. (9) suitable for describing restricted diffusion in a confining domain Ω. In general, the Fourier (also known as Robin, or mixed, or relaxing) boundary condition is used to take into account the surface relaxation or permeability of the boundary $\partial\Omega$:

$$D\frac{\partial}{\partial n}\mathfrak{m}(\mathbf{r},t) + \rho\mathfrak{m}(\mathbf{r},t) = 0, \tag{10}$$

where ρ is the surface relaxivity (or interface permeability) and $\partial/\partial n$ is the outward normal derivative. The above relation is nothing else than a conservation law: at each boundary point, the fluxes of magnetization from the bulk and through the boundary are equal. The sur-

[18] Throughout the review, T denotes the time of the last measurement, i.e., the whole duration of the sequence. For example, T is the moment of the last echo in Eq. (4). Note that T is often denoted as 2Δ in the literature.

face relaxivity ρ can widely range from being negligible in some tissues to being of the order of several microns per second or greater for sedimentary rocks. The role of the Fourier boundary condition for the Laplacian transport phenomena has been thoroughly discussed (Sapoval, 1994; Filoche and Sapoval, 1999; Grebenkov *et al.*, 2003, 2006). Even without the diffusion-sensitizing gradient $\mathbf{g}$, the surface relaxation would attenuate the magnetization (Brownstein and Tarr, 1977, 1979). This situation is described in Sec. II.G.

If the interface is impermeable for spin-bearing particles and does not contain magnetic impurities which could lead to surface relaxation ($\rho=0$), the above relation is reduced to the Neumann (or reflecting) boundary condition on the interface $\partial\Omega$:

$$\frac{\partial}{\partial n}\mathfrak{m}(\mathbf{r},t)=0. \tag{11}$$

The Neumann boundary condition (11) was used by Kaplan (1959) to describe electron-spin resonance in metals.

The initial condition to this boundary value problem is determined by the spin density $\rho_0(\mathbf{r})$ at time $t=0$ and by the way these spins were excited. In most cases, the initial spin density is uniform over the sample. If the 90° rf pulse is spatially homogeneous, each spin magnetization is flipped into the transverse plane in a similar way, so that the initial magnetization is proportional to the initial density. On the other hand, inhomogeneous rf pulses (e.g., with a linear gradient) can be used to create a nonuniform initial magnetization.

Once the magnetization $\mathfrak{m}(\mathbf{r},t)$ is found by solving the Bloch-Torrey equation with a given initial condition, the signal amplitude E at time T is obtained by the integration of $\mathfrak{m}(\mathbf{r},T)$, weighted by some pickup function $\tilde{\rho}(\mathbf{r})$ of the measuring coil or antenna, over the whole confining domain Ω:

$$E=\int_\Omega d\mathbf{r}\,\mathfrak{m}(\mathbf{r},T)\tilde{\rho}(\mathbf{r}). \tag{12}$$

After Wayne and Cotts (1966) solved numerically the Bloch-Torrey equation in a laminar system with the reflecting boundary condition, this approach became a common tool to investigate diffusive NMR phenomena.

C. Effect of a geometrical restriction

Relations (3)–(7) were derived for unrestricted diffusion, when nuclei diffused freely in an infinite reservoir. The presence of a restrictive frontier drastically influences the motion and the consequent signal attenuation (Fig. 3). Woessner used the spin-echo technique to experimentally demonstrate the effect of a geometrical restriction, measuring the signal attenuation for water molecules in a geological core and in aqueous suspensions of silica spheres (Woessner, 1960, 1961, 1963). Although $\ln E$ was still proportional to g^2, the ratio $D'=-\ln E/(\gamma^2 g^2 T^3/12)$ was not equal to the free diffusion coefficient D of water. Woessner called this ratio a spin-echo diffusion coefficient: it is now known as the effective, time-dependent, or apparent diffusion coefficient. The decrease of D' with T was attributed to the growing proportion $\sqrt{DT}/L$ of molecules whose motion was restricted by boundaries of the reservoir of size L.

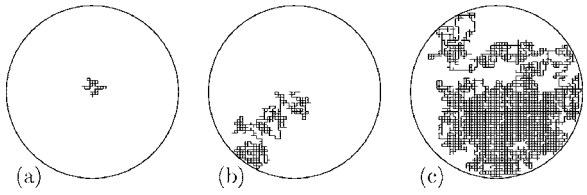

FIG. 3. Random-walk simulations of reflected Brownian motion confined inside a circle of radius L, for three values of the ratio $p=DT/L^2$: (a) 0.1, (b) 1, (c) 10. In all cases, diffusion is started from the center.

The size of a geometrical confinement is a natural length scale for restricted diffusion. At this point, it is worth mentioning the other length scales of the problem:

- diffusion length $L_p=\sqrt{DT}$, showing the average distance explored by spins during time T;
- gradient length $L_q=(\gamma g T)^{-1}$, over which the magnetic-field gradient g yields a phase spread of the order of 2π;[19]
- relaxation length $L_h=D/\rho$, which is the distance a particle should travel near the boundary before surface relaxation effects reduce its expected magnetization.

As we will see, different regimes of restricted diffusion depend on how short some of these lengths are with respect to the others.

D. Narrow-pulse approximation

The first theoretical treatment of *restricted* diffusion was proposed by Stejskal (1965) and Tanner and Stejskal (1968). Stejskal modified the Bloch-Torrey equation (9) to include the case of anisotropic, restricted diffusion, and flow. Then restricted diffusion was studied by using the pulsed (field) gradient spin-echo (PGSE) method which relates the signal attenuation to the intermediate scattering function:

$$\mathrm{ISF}(\mathbf{k})=\mathbb{E}\{e^{-i\mathbf{k}\cdot\mathbf{r}(\tau)}e^{i\mathbf{k}\cdot\mathbf{r}(0)}\}. \tag{13}$$

In fact, if the duration δ of the gradient pulses is much smaller than their separation time[20] τ, the integral in Eq. (1) can be reduced to

[19] In the literature, one can also find the dephasing length $L_{\mathrm{deph}}=(D/\gamma g)^{1/3}$ over which the spins travel to gain a phase spread of the order 2π with their diffusion coefficient D. It is simply a combination of the two other lengths, $L_{\mathrm{deph}}=(L_p^2 L_q)^{1/3}$.

[20] The separation τ between two gradient pulses is not necessarily related to the echo time T (albeit $\tau\leqslant T$). For conve-

$$\varphi \approx \gamma\delta[\mathbf{g}\cdot\mathbf{r}(0) - \mathbf{g}\cdot\mathbf{r}(\tau)], \tag{14}$$

known as the short-gradient-pulse or narrow-pulse approximation (NPA). The sign is changed due to the 180° rf pulse. The first gradient pulse encodes the position $\mathbf{r}$ of a nucleus at time $t=0$ by the factor $e^{i\gamma\delta\mathbf{g}\cdot\mathbf{r}(0)}$, while the second gradient pulse labels the position $\mathbf{r}'$ of the same nucleus at time $t=\tau$ by the factor $e^{-i\gamma\delta\mathbf{g}\cdot\mathbf{r}(\tau)}$. The probability density $G_\tau(\mathbf{r},\mathbf{r}')$ to diffuse from $\mathbf{r}=\mathbf{r}(0)$ to $\mathbf{r}'=\mathbf{r}(\tau)$ during time τ is known as the propagator, heat kernel, or Green's function of diffusion equation (see Sec. III.B). The average over initial and final positions with a uniform initial density $\rho_0(\mathbf{r})=1/V$ leads to the macroscopic signal

$$E \simeq \frac{1}{V}\int_\Omega d\mathbf{r}\int_\Omega d\mathbf{r}'\,G_\tau(\mathbf{r},\mathbf{r}')e^{i\gamma\delta\mathbf{g}\cdot(\mathbf{r}-\mathbf{r}')}, \tag{15}$$

where V is the volume of the domain Ω. When $\delta\to 0$ and simultaneously $|\mathbf{g}|\to\infty$ in such a way that $\mathbf{k}=\gamma\delta\mathbf{g}$ remains fixed, one gets ISF($\mathbf{k}$). This function can also be directly measured in dynamic light scattering (Bishop *et al.*, 1986) and employed in theoretical studies of transport in disordered systems (Guyer, 1988).

The crucial simplification of this approach relies on an explicit manifestation of the confining geometry via the propagator. The PGSE method allows the Fourier transform of the propagator to be measured experimentally, thus providing a simple way to probe a complex morphology by NMR. This technique, also called the q-space imaging method, was widely applied for both theoretical and experimental studies (Callaghan, 1984, 1991; Stilbs, 1987). For instance, Packer and Rees (1972) used this method to determine droplet size distributions in emulsions. Kärger and Heink (1983) performed a PGSE experiment to characterize molecular transport in microporous crystallites (zeolites of different kinds and sizes) through the properties of the propagator. Cory and Garroway (1990) pointed out how an NMR measurement of translational displacement probabilities could be used as an indicator of compartmentation.

The related effect of diffusive diffraction was experimentally discovered by Callaghan *et al.* (1991, 1992) from proton NMR studies of a water-saturated, orientationally disordered, loosely packed array of monodisperse polystyrene spheres. The analogy with light, x-ray, and neutron scattering was also discussed by Cotts (1991) and by Barrall *et al.* (1992). The diffusive diffraction in a slab geometry and in a cylindrical pore was reported by Coy and Callaghan (1994), and by Söderman and Jönsson (1995) and by Gibbs (1997), respectively. Balinov *et al.* (1994) observed similar effects in a highly concentrated water-oil emulsion. Their manifestation in the case of porous media was discussed by Bergman and Dunn (1994) and by Sen *et al.* (1995). Frey *et al.* (1988) analyzed the pulsed gradient spin-echo experiments with absorbing walls. Mitra and Sen (1992) and Callaghan (1995) considered the effect of surface relaxation. In particular, its influence on the apparent diffusion coefficient in the long-time limit was studied by Sen *et al.* (1994). Lennon and Kuchel (1994) reported the enhancement of the diffractionlike effect in the presence of surface relaxation sinks. Sen (2003) studied restricted diffusion between permeable walls by using the PGSE technique. The relation between pulsed gradient NMR measurements of restricted diffusion and the return-to-the-origin probability was pointed out by Mitra *et al.* (1995) and by Schwartz *et al.* (1997). Modal analysis of correlations between relaxation and diffusive diffraction measurements in fluid-saturated isolated pores with relaxing surfaces was developed by Marinelli *et al.* (2003). King *et al.* (1994) used the q-space concept for imaging of the brain. The time-dependent diffusion coefficient of water in a biological system (packed erythrocytes) was measured by Latour *et al.* (1994). In turn, Mair *et al.* (2001) utilized PGSE measurements with xenon-129 gas to find both the pore surface-to-volume ratio and the tortuosity of porous media (glass bead packs). An original approach to describe the diffusive diffraction in a porous medium was developed by Stepišnik (1998) who proposed expressing the nonuniform spin phase distribution in a pore as a series of waves with wave vectors characterizing the geometry and boundaries of confinement. Rodts and Levitz (2001) suggested a time-domain analysis allowing the interpretation of PGSE data in porous systems in terms of the material's length scale. This approach gave new insight into the micro-macro transition for diffusive transport. An overview of spatial coherence phenomena arising from translational spin motion in gradient spin-echo experiments was given by Callaghan *et al.* (1999). The use of a PGSE technique as a tool for studying translational diffusion was reviewed by Price (1997, 1998).

In experiments, the gradient pulses cannot be made with arbitrarily small duration δ and arbitrarily large intensity $|\mathbf{g}|$ since both these quantities are limited by the hardware setup. The validity of the approximate relations (14) and (15) depends on whether the nuclei can be considered as immobile during time δ. The characteristic diffusion time L^2/D might be a time scale for comparison to δ. This condition is particularly difficult to satisfy for gas diffusion which has seen a considerable rise in interest during the last decade.

The applicability of the NPA in various NMR contexts was investigated by different authors. Blees (1994) numerically solved a modified Bloch-Torrey equation by using a finite-difference method in order to quantify the effect of finite-duration gradient pulses. For the same purpose, Linse and Söderman (1995) performed Brownian dynamic simulations for molecules entrapped in planar, cylindrical, and spherical geometries. Mitra and Halperin (1995) showed how the finite duration of gradient pulses made isolated pores appear smaller than their actual size. Wang *et al.* (1995) proposed a criterion of applicability of the NPA by considering restricted diffusion in simple domains (slab, cylinder, and sphere). Monte Carlo simulations were also implemented by Duh

nience, we use $\tau=T/2$ in the review (note that one often takes $\tau=T$).

et al. (2001) to demonstrate a strong deviation from approximate theoretical results in the case of intermediate and long sequences. Mair, Sen, *et al.* (2002) showed a breakdown of the narrow-pulse approximation by analyzing the restricted diffusion of xenon in model porous media (random packs of monodisperse glass beads). For the case of unbounded homogeneous porous media, Zielinski and Sen (2003c) used a Padé approximation of the time-dependent diffusion coefficient to compare the effects of narrow- and finite-width pulses. Malmborg *et al.* (2004) studied highly concentrated emulsions to show how the duration of the gradient pulse influences NMR diffusion experiments. It should be noted that the unavoidable heterogeneity in natural materials reduces diffraction effects, making it even more challenging to use this technique in practice for experimental characterization of porous structures. We discuss the narrow-pulse approximation in Sec. VI.E.

E. Restricted diffusion in simple domains

Robertson (1966) applied a quantum-mechanics operator formalism to study restricted diffusion in a slab geometry between two parallel planes. Using a formal analogy, the Laplace operator in the Bloch-Torrey equation (9) with the Neumann boundary condition (11) could be interpreted as a Hamiltonian of a free particle in a specific potential well, while the term containing a linear magnetic-field gradient represented a perturbative interaction. The magnetization $\mathfrak{m}(\mathbf{r},t)$ was then expanded over eigenfunctions $u_m(\mathbf{r})$ of the Laplace operator in an interval

$$\mathfrak{m}(\mathbf{r},t) = \sum_m c_m(t) u_m(\mathbf{r}). \tag{16}$$

An infinite-dimensional system of linear differential equations was obtained for unknown coefficients $c_m(t)$ (see also Sec. VI.A). A further analysis of the density matrix $c_m(t)c^*_{m'}(t)$ led to

$$-\ln E \simeq q^2 \sum_{m=0}^{\infty} \frac{8}{\pi^4(2m+1)^4}\left(\frac{1}{\pi^2(2m+1)^2 p} - \frac{3-4e^{-\pi^2(2m+1)^2 p/2}+e^{-\pi^2(2m+1)^2 p}}{\pi^4(2m+1)^4 p^2}\right), \tag{17}$$

where $q=\gamma g L T$ and $p=DT/L^2$. For small time T ($p \ll 1/\pi^2$), a series expansion of the exponential functions in Eq. (17) yields the relation (3). For long enough T ($p \gg 2/\pi^2$), Robertson found a new behavior of the signal attenuation due to restricted diffusion in a slab geometry, which is now called the motionally averaging or motional-narrowing regime:

$$E \simeq \exp[-\gamma^2 g^2 L^4 T/120D]. \tag{18}$$

Although $\ln E$ is still proportional to g^2, the dependence on the echo time T, the diffusion coefficient D, and the slab width L is drastically different in comparison with Eq. (3) for free diffusion. For instance, the nuclei with higher D diffuse more rapidly, but the related signal attenuation is, contrarily to intuition, smaller. A sharp dependence on the size of the confining domain appears here as a characteristic feature of restricted diffusion. This behavior was experimentally observed in a laminar system by Wayne and Cotts (1966). We discuss the motional-narrowing regime in detail in Sec. V.

Robertson's work had deep impact on the further development of this field. High sensitivity to geometrical confinement stimulated interest in restricted diffusion as a method for probing confining morphologies of porous materials and biological tissues by using NMR. A number of far-reaching extensions were made. Another quantum-mechanics-oriented approach was suggested by Cates, Schaefer, and White (1988) and Cates, White, *et al.* (1988). They used standard perturbative theory to study the slow-diffusion and motional-narrowing regimes for any magnetic-field inhomogeneity, with special emphasis on restricted diffusion in a sphere. Stepišnik (1981, 1985) developed the density matrix calculation for a more general case including, for instance, strong dipolar coupling. In particular, the NMR spin-echo attenuation in a magnetic-field gradient was related to the velocity autocorrelation function.[21]

The eigenfunction expansion became the usual tool to investigate restricted diffusion. For instance, Brownstein and Tarr (1979) used it to explain multiexponential relaxation for water in biological cells (see Sec. II.G). Bergman (1997) studied the low-lying diffusion eigenstates and their contribution at long times. Song (2000a) reported an experimental demonstration of the excitation and detection of a wide range of eigenmodes in porous media by exploring the inhomogeneous internal magnetic field in the pore space. This technique was then applied to characterize multiple length scales in rocks by Song *et al.* (2000).

Finally, Robertson's operator formalism can be considered as a prototype for efficient numerical techniques like multiple-propagator or stepwise-gradient approaches (see Sec. II.M). In particular, the concepts of the multiple-correlation-function description given in Sec. III were first seen in the work of Robertson.

F. Gaussian phase approximation

Neuman (1974) retrieved and extended Robertson's results by considering the accumulation of phase shifts during diffusive motion. In the limit of short diffusion times, only a small fraction of nuclei can "feel" the presence of reflecting boundaries, and their contribution to the accumulated phase can be neglected. One thus retrieves a Gaussian distribution (5). In the opposite limit of very long diffusion times, each spin explores the bulk several times during a small time interval. At this time scale, the spatial displacements of a spin can be seen as independent "jumps" at randomly chosen bulk points, and the central limit theorem leads again to the relation

[21] See Stepišnik (1993); Stepišnik and Callaghan (2000); Stepišnik *et al.* (2001).

(5). Neuman assumed that the Gaussian distribution was valid for the intermediate case as well. This assumption, now known as the Gaussian phase approximation (GPA), reduces the difficult problem of resolving the Bloch-Torrey equation in a confining medium to the calculation of the second moment $\mathbb{E}\{\varphi^2\}$, which is generally simpler. In particular, Neuman used Dini's expansions (Watson, 1962) to carry out an analytical calculation of restricted diffusion in a slab, a cylinder, and a sphere. For these basic domains, the heat kernel and the Laplace operator eigenbasis are known explicitly (see Table I).

After Neuman's work, the Gaussian phase approximation was repeatedly used by many authors. Murday and Cotts (1968) experimentally observed restricted diffusion of liquid lithium in spherical droplets and confirmed the GPA. McGregor (1990) related the transverse relaxation rate to autocorrelation functions, calculated them for three basic domains, and then retrieved and checked the GPA predictions experimentally with the diffusion of helium-3 nuclei. To explain transverse relaxation processes in porous sedimentary rocks, Kleinberg and Horsfield (1990) modeled pores as spherical cavities and then applied Neuman's results. Hayden *et al.* (2004) used them to fit their experimental measurements for restricted diffusion of hyperpolarized helium-3 in a cylindrical pore. Kuchel *et al.* (1996) extended Neuman's relation for a sphere to account for surface and bulk relaxation. The theory of macroscopic signal formation in the presence of structure-specific magnetic-field inhomogeneities developed by Sukstanskii and Yablonskiy (2003, 2004) was based on the Gaussian phase approximation. The accuracy of the GPA was numerically investigated by different authors. For example, Balinov *et al.* (1993) used Brownian dynamics to simulate the motion of spins confined to spheres and between planes.

The Gaussian phase approximation and Neuman's results will be discussed in detail in Secs. IV and V.

G. Multiexponential magnetization decay

Mathematical analysis of the Bloch-Torrey equation is significantly complicated by the fact that the operator on the left-hand side of Eq. (9) is not Hermitian. In contrast, without a diffusion-sensitizing gradient, the Bloch-Torrey equation is reduced to the ordinary diffusion or heat equation. The surface relaxation mechanism is still represented through the Fourier boundary condition (10). Expanding the magnetization $\mathfrak{m}(\mathbf{r},t)$ over the Laplace operator eigenbasis, Brownstein and Tarr (1977, 1979) found multiexponential signal decay

$$E = \sum_m I_m e^{-T/T_m}, \tag{19}$$

where T_m and I_m are the relaxation time and the relative intensity of the mth eigenmode. Both these quantities contain useful information about the confining geometry. For weak surface relaxation, the ground eigenmode is nearly constant and its inverse relaxation time is proportional to the surface relaxivity and the surface-to-volume ratio. Brownstein and Tarr gave several examples (simple domains like a slab, a cylinder, and a sphere) and illustrated the efficiency of their formalism by explaining a multiexponential decay of the proton-spin relaxation for water in biological cells.

Many authors employed or extended these results. In the case of weakly coupled pores, the magnetization decay inside each pore depends on its size. The multiexponential decay of the overall signal at long time yields thus directly the pore size distribution[22] (Mendelson, 1990). On the other hand, an excitation of particular eigenmodes by NMR can be used to extract further information on the pore geometry (Song, 2002). It should also be stressed that the related boundary value problem is not specific to NMR, being applicable to diffusion through permeable membranes, heterogeneous catalysis, electric potentials in electrolytes, etc. [see, for instance, Klafter and Drake (1989); Mendelson (1990); Wilkinson *et al.* (1991); Sapoval (1994, 1996)]. As this problem has been thoroughly considered elsewhere, it is not discussed at length in the review.

H. Non-Gaussian behavior

Neuman's relations were in such good agreement with numerical and experimental observations that the Gaussian phase approximation was often applied for any set of physical parameters.[23] In particular, Stepišnik (1999) gave a phenomenological estimate for the gradient intensity under which the Gaussian phase approximation was supposed to be correct.[24]

Stoller *et al.* (1991) studied the spectral properties of the Bloch-Torrey equation for a constant gradient over

[22]See also Torquato and Avellaneda (1991); Halperin *et al.* (1994); Kleinberg (1994, 1996b); Latour *et al.* (1995).

[23]It is worth noting that the Gaussian phase approximation fails for PGSE experiments at long enough time separation τ between two narrow gradient pulses. For a bounded domain, the propagator in Eq. (15) approaches $1/V$ in the limit $\tau\to\infty$, making the positions $\mathbf{r}$ and $\mathbf{r}'$ independent from each other. Therefore the signal becomes simply the square of the form factor of the domain (the Fourier transform of its indicator function) which does not exhibit a Gaussian-like behavior:

$$E \simeq \left| \frac{1}{V}\int_\Omega d\mathbf{r}\, \exp[i\gamma\delta\mathbf{g}\cdot\mathbf{r}] \right|^2.$$

This failure of the GPA, already known from Tanner and Stejskal (1968), was experimentally observed by Callaghan *et al.* (1991) (see Sec. II.D). This case, however, is rather special since the macroscopic signal turns out to be independent of the diffusive motion at long times. This is a very specific, deliberately introduced feature of the narrow-pulse approximation. In this subsection, we discuss the opposite case when the signal depends on the whole Brownian trajectory of a diffusing spin. The Gaussian character of this motion was believed to ensure the GPA, and its failure was unexpected in this case.

[24]This estimate ($g \leqslant 40$ T/m for gases and $g \leqslant 100$ T/m for liquids) should be taken with caution, as discussed in this subsection.

TABLE I. Summary of spectral characteristics of the Laplace operator in three basic domains. The Fourier boundary condition (10) is written explicitly in L1. The eigenvalues (L2) are determined by the positive roots α_m or α_{nk} of the equation in L3. The normalization constants L5 are defined by condition (35) for the eigenfunctions L4. The vector U is calculated for uniform initial density $\rho_0(\mathbf{r})=1/V$ (L6). The asymptotic behavior of the lowest eigenvalue as $h\to 0$ is shown in L7. The matrix $\mathcal{B}$ (L8) is computed for a linear magnetic-field gradient (the limit of $\mathcal{B}_{m,0}$ as $h\to 0$ is given in L9). The matrix $e^{iq\delta\mathcal{B}}$ is calculated for a linear gradient at $h=0$ (L10). The matrix $\mathcal{B}$ (L11) is found for an isotropic parabolic magnetic field (the limit of $\mathcal{B}_{m,0}$ as $h\to 0$ is given in L12.

	Slab, $\Omega=\{x\in\mathbb{R}:0<x<1\}$ $(V=1)$	Cylinder, $\Omega=\{\mathbf{r}\in\mathbb{R}^2:\lvert\mathbf{r}\rvert<1\}$ $(V=\pi)$	Sphere, $\Omega=\{\mathbf{r}\in\mathbb{R}^3:\lvert\mathbf{r}\rvert<1\}$ $(V=4\pi/3)$
L1	$\left[\frac{\partial u_m}{\partial x}-hu_m\right]_{x=0}=0,\quad \left[\frac{\partial u_m}{\partial x}+hu_m\right]_{x=1}=0$	$\left[\frac{\partial u_{nk}}{\partial r}+hu_{nk}\right]_{r=1}=0$	$\left[\frac{\partial u_{nk}}{\partial r}+hu_{nk}\right]_{r=1}=0$
L2	$\lambda_m=\alpha_m^2,\quad \Lambda_{m,m'}=\delta_{m,m'}\lambda_m$	$\lambda_{nk}=\alpha_{nk}^2,\quad \Lambda_{nk,n'k'}=\delta_{n,n'}\delta_{k,k'}\lambda_{nk}$	$\lambda_{nk}=\alpha_{nk}^2,\quad \Lambda_{nk,n'k'}=\delta_{n,n'}\delta_{k,k'}\lambda_{nk}$
L3	$\frac{\tan(\alpha_m)}{\alpha_m}=\frac{2h}{\alpha_m^2-h^2}$	$\alpha_{nk}J_n'(\alpha_{nk})+hJ_n(\alpha_{nk})=0$	$\alpha_{nk}j_n'(\alpha_{nk})+hj_n(\alpha_{nk})=0$
L4	$u_m(x)=\sqrt{2}\beta_m\left(\cos(\alpha_m x)+\frac{h}{\alpha_m}\sin(\alpha_m x)\right)$	$u_{nk}(r,\varphi)=\frac{\epsilon_n}{\sqrt{\pi}}\frac{\beta_{nk}}{J_n(\alpha_{nk})}J_n(\alpha_{nk}r)\cos(n\varphi)$	$u_{nkl}(r,\theta,\varphi)=\frac{\beta_{nk}}{\sqrt{2\pi}\,j_n(\alpha_{nk})}j_n(\alpha_{nk}r)P_n(\cos\theta)e^{il\varphi}$
	$0\leqslant x\leqslant 1$	$0\leqslant r\leqslant 1,\ 0\leqslant\varphi<2\pi$	$0\leqslant r\leqslant 1,\ 0\leqslant\theta\leqslant\pi,\ 0\leqslant\varphi<2\pi$
		$J_\nu(z)=\frac{z^\nu}{2^\nu}\sum_{k=0}^{\infty}\frac{(-1)^k z^{2k}}{2^{2k}k!\Gamma(\nu+k+1)}$	$j_\nu(z)=(\pi/2z)^{1/2}J_{\nu+1/2}(z)$
L5	$\beta_m=\left(\frac{\lambda_m}{\lambda_m+2h+h^2}\right)^{1/2}\quad(\beta_0\to 1/\sqrt{2})$	$\beta_{nk}=\left(\frac{\lambda_{nk}}{\lambda_{nk}-n^2+h^2}\right)^{1/2}\quad(\beta_{00}\to 1)$	$\beta_{nk}=\left(\frac{(2n+1)\lambda_{nk}}{\lambda_{nk}-n(n+1)+h(h-1)}\right)^{1/2}\quad\left(\beta_{00}\to\sqrt{\frac{3}{2}}\right)$
L6	$U_m=[1+(-1)^m]\frac{\sqrt{2}h}{\sqrt{\lambda_m(\lambda_m+2h+h^2)}}$	$U_{nk}=\delta_{n,0}\frac{2h}{\sqrt{\lambda_{0k}(\lambda_{0k}+h^2)}}$	$U_{nk}=\delta_{n,0}\frac{\sqrt{6}h}{\sqrt{\lambda_{0k}[\lambda_{0k}+h(h-1)]}}$
L7	$\lambda_0=2h-\frac{1}{3}h^2+\frac{2}{45}h^3-\frac{4}{945}h^4+O(h^5)$	$\lambda_{00}=2h-\frac{1}{2}h^2+\frac{1}{12}h^3-\frac{1}{192}h^4+O(h^5)$	$\lambda_{00}=3h-\frac{3}{5}h^2+\frac{12}{175}h^3+O(h^5)$

TABLE I. (*Continued.*)

	Slab, $\Omega=\{x\in\mathbb{R}:0<x<1\}$ $(V=1)$	Cylinder, $\Omega=\{\mathbf{r}\in\mathbb{R}^2:\lvert\mathbf{r}\rvert<1\}$ $(V=\pi)$	Sphere, $\Omega=\{\mathbf{r}\in\mathbb{R}^3:\lvert\mathbf{r}\rvert<1\}$ $(V=4\pi/3)$
	Linear magnetic-field gradient: $B(x)=x$ for a slab, $B(\mathbf{r})=r\cos\varphi$ for a cylinder, and $B(\mathbf{r})=r\cos\theta$ for a sphere		
L8	$\mathcal{B}_{m,m'}=2[(-1)^{m+m'}-1]\beta_m\beta_{m'}\dfrac{\lambda_m+\lambda_{m'}+2h^2}{(\lambda_m-\lambda_{m'})^2}$ and $\mathcal{B}_{m,m}=1/2$	$\mathcal{B}_{nk,n'k'}=\delta_{n,n'\pm1}(1+\delta_{n,0}+\delta_{n',0})^{1/2}\times\beta_{nk}\beta_{n'k'}\dfrac{\lambda_{nk}+\lambda_{n'k'}-2nn'+2h(h-1)}{(\lambda_{nk}-\lambda_{n'k'})^2}$	$\mathcal{B}_{nk,n'k'}=\dfrac{(n+n'+1)\delta_{n,n'\pm1}}{(2n+1)(2n'+1)}\beta_{nk}\beta_{n'k'}\times\dfrac{\lambda_{nk}+\lambda_{n'k'}-n(n'+1)-n'(n+1)+1+2h(h-2)}{(\lambda_{nk}-\lambda_{n'k'})^2}$
L9	$\lim_{h\to0}\mathcal{B}_{0,m}=\begin{cases}\sqrt{2}[(-1)^m-1]/\lambda_m, & m>0\\ 1/2, & m=0\end{cases}$	$\lim_{h\to0}\mathcal{B}_{00,1k}=\dfrac{\sqrt{2}}{\sqrt{\lambda_{1k}(\lambda_{1k}-1)}}$	$\lim_{h\to0}\mathcal{B}_{00,1k}=\dfrac{\sqrt{2}}{\sqrt{\lambda_{1k}(\lambda_{1k}-2)}}$
L10	$[e^{iq\delta\mathcal{B}}]_{0,m}=\dfrac{(-1)^m\epsilon_m q\delta}{(q\delta)^2-(\pi m)^2}\times\{\sin q\delta+i[(-1)^m-\cos q\delta]\}$	$[e^{iq\delta\mathcal{B}}]_{00,nk}=2\epsilon_n\beta_{nk}\dfrac{i^n q\delta J_n'(q\delta)}{\lambda_{nk}-(q\delta)^2}$	$[e^{iq\delta\mathcal{B}}]_{00,nk}=\sqrt{6}\beta_{nk}\dfrac{i^n q\delta j_n'(q\delta)}{\lambda_{nk}-(q\delta)^2}$
	Isotropic parabolic magnetic field: $B(\mathbf{r})=\lvert\mathbf{r}\rvert^2$		
L11	$\mathcal{B}_{m,m'}=4(-1)^{m+m'}\beta_m\beta_{m'}\times\dfrac{\lambda_m+\lambda_{m'}+2h[h+(-1)^{m+m'}+1]}{(\lambda_m-\lambda_{m'})^2}$ $\mathcal{B}_{m,m}=\dfrac{1}{3}\beta_m^2\left(1+\dfrac{3+6h+2h^2}{2\lambda_m}-\dfrac{3h(h+2)}{2\lambda_m^2}\right)$	$\mathcal{B}_{nk,n'k'}=4\delta_{n,n'}\beta_{nk}\beta_{nk'}\times\dfrac{\lambda_{nk}+\lambda_{nk'}-2n^2+2h^2}{(\lambda_{nk}-\lambda_{nk'})^2},\ k\neq k'$ $\mathcal{B}_{nk,n'k}=\dfrac{1}{3}\delta_{n,n'}\beta_{nk}^2\left(1+\dfrac{n^2+h(h+2)}{\lambda_{nk}}-\dfrac{2(n^2-1)(n^2-h^2)}{\lambda_{nk}^2}\right),\ k=k'$	$\mathcal{B}_{nk,n'k'}=4\delta_{n,n'}\beta_{nk}\beta_{nk'}\times\dfrac{\lambda_{nk}+\lambda_{nk'}-2n(n+1)+2h(h-1)}{(\lambda_{nk}-\lambda_{nk'})^2},\ k\neq k'$ $\mathcal{B}_{nk,n'k}=\dfrac{1}{3}\delta_{n,n'}\beta_{nk}^2\left(1+\dfrac{n(n+1)+h(h+1)-1/2}{\lambda_{nk}}-\dfrac{(2n-1)(2n+3)[n(n+1)+h(1-h)]}{2\lambda_{nk}^2}\right),\ k=k'$
L12	$\lim_{h\to0}\mathcal{B}_{0,m}=\begin{cases}2\sqrt{2}(-1)^m/\lambda_m, & m>0\\ 1/3, & m=0\end{cases}$	$\lim_{h\to0}\mathcal{B}_{00,0k}=\begin{cases}4/\lambda_{0k}, & k>0\\ 1/2, & k=0\end{cases}$	$\lim_{h\to0}\mathcal{B}_{00,0k}=\begin{cases}2\sqrt{6}/\lambda_{0k}, & k>0\\ 3/5, & k=0\end{cases}$

an interval that corresponds to restricted diffusion in a slab geometry. For a large gradient intensity g, they demonstrated a *non-Gaussian* stretched-exponential decrease of the macroscopic signal as a function of g. The physical consequences of this new and unexpected behavior were discussed by de Swiet and Sen (1994). This so-called localization regime was experimentally observed for the first time by Hürlimann *et al.* (1995). They studied the restricted diffusion of water molecules between two parallel plates separated by a distance of 0.16 mm. A drastic deviation from the Gaussian g^2 dependence of $\ln E$ was observed at gradient intensities higher than 15 mT/m (see Sec. VI.F and Fig. 9). In this case, the dephasing length $(D/\gamma g)^{1/3}$ over which the spins travel to gain a phase spread in the order of 2π becomes shorter than both the diffusion length $\sqrt{DT}$ and the plate separation L. Consequences of the localization regime for diffusion edge enhancement were experimentally investigated by many authors; see, e.g., de Swiet (1995), Saam *et al.* (1996), and Song *et al.* (1998) (see Sec. II.K). The manifestation of the localization regime for a CPMG sequence was analyzed by Sen *et al.* (1999) and by Zhang and Hirasaki (2003). We continue this discussion in Sec. VI.F.

The discovery of the localization regime forced physicists to revise a common belief in the Gaussian phase approximation and stimulated theoretical research in this field. For instance, Bergman and Dunn (1995) [see also Dunn and Bergman (1995)] developed a formalism to calculate the fourth moment in the case of a periodic porous medium. Some of their ideas will be used in Sec. III to compute the multiple correlation functions of reflected Brownian motion.

I. Studying porous media

In the 1990s, a series of papers[25] was devoted to restricted diffusion in porous media in the short-time limit. Starting from Woessner's qualitative arguments, Mitra *et al.* developed and experimentally checked a quantitative theory to account for the contribution of nuclei whose motion was restricted by boundaries of the confining medium. Using the method of boundary perturbation, they found the effective or apparent diffusion coefficient (ADC) at short times:

$$D_{\rm app} \simeq D\left(1 - \alpha\sqrt{DT}\frac{S}{V}\right), \tag{20}$$

where S/V is the surface-area-to-pore-volume ratio of the confining medium. The numerical prefactor α was analytically computed for steady and pulsed gradient profiles shown in Figs. 2(a) and 2(c) (see Sec. IV.E). The higher-order correction $O(DT)$ was related to the average value of the mean curvature of the boundary and to surface relaxation [see footnote 58 and Mitra *et al.* (1993) for details]. NMR techniques appeared as promising experimental tools to measure the surface-to-volume ratio, the intrinsic characteristic of porous media, which plays an important role in the oil industry and in medical diagnostics alike. The notion of an effective time-dependent diffusion coefficient was applied by Helmer, Dardzinski, *et al.* (1995) to investigate *in vivo* systems and by Mair and co-workers (Mair *et al.*, 1998, 1999; Mair, Rosen, *et al.*, 2002) to the case of granular materials. Zielinski and Hürlimann (2005) proposed the use of the CPMG sequence to probe short length scales in a static gradient. A tutorial about the time-dependent diffusion coefficient and its application to probe geometry was given by Sen (2004). We discuss the result (20) in detail in Sec. IV.

In the limit of long time T, another asymptotic behavior of the apparent diffusion coefficient was found for "open" (or unbounded) geometries

$$D_{\rm app} \simeq D_\infty + \frac{\kappa_1}{T} + \frac{\kappa_{3/2}}{T^{3/2}} + \cdots, \tag{21}$$

where the coefficients κ_1, $\kappa_{3/2}$, … depend on the confining geometry (Haus and Kehr, 1987; Latour *et al.*, 1993; de Swiet and Sen, 1996). In this regime, the free diffusion coefficient D is reduced to D_∞ by a geometrical factor $\mathfrak{T}$ called the tortuosity. This is an important macroscopic characteristic of porous materials and biological tissues. Through the tortuosity, the ADC is connected to many transport properties of fluids confined in porous media: the porosity, permeability, electrical conductivity of electrolytes, and velocity of sound in superfluidic helium [see Bear (1972); Johnson *et al.* (1982)]. Since this review is primarily devoted to closed domains[26] such as isolated pores, we do not consider in detail this tortuosity regime [see, for instance, Sen (2004)].

The role of the connectivity in a material matrix has also been intensively studied. McCall and co-workers[27] investigated magnetization evolution in multiply connected pore systems in the fast-diffusion regime when the coupling between individual pores is important. To have a specific model of a pore system, they chose a hypercubic lattice whose sites and bonds were identified with pores and throats, respectively. A volume and a surface area were assigned to each site, while each bond was characterized by a cross-sectional area and a length. In this coarse-grained model, the evolution of magnetization at each site followed a master equation whose spectral properties were analyzed. Knowledge of restricted diffusion within individual pores (or groups of pores) may provide a better coarse graining for such models.

[25] See Mitra *et al.* (1992, 1993); Latour *et al.* (1993); de Swiet and Sen (1994); Helmer, Dardzinski, *et al.* (1995); Helmer, Hürlimann, *et al.* (1995); Sen (2004); and references therein.

[26] As discussed in Sec. VI.I, the mathematical methods developed originally for closed systems can still be applied, to some extent, to investigate open systems.

[27] McCall *et al.* (1991, 1993); Guyer (1993). See also Cohen and Mendelson (1982).

J. Nonlinear magnetic fields

While the investigation of restricted diffusion in a linear magnetic-field gradient reveals hundreds of works, a much smaller number of theoretical publications have been devoted to nonlinear magnetic fields. This situation may seem a bit surprising since the difference in magnetic susceptibilities of porous matrix and bulk fluid often induces structure-dependent nonlinear internal fields. The role of diffusion through such locally inhomogeneous magnetic fields was pointed out by Packer (1973) and later investigated by many authors. On the other hand, *ex situ* or mobile sensor measurements are in general also realized in nonlinear magnetic fields.

The first theoretical study into the effect of nonlinear magnetic fields on restricted diffusion was proposed by Tarczon and Halperin (1985). In the case of one-dimensional diffusion restricted over a finite interval, an arbitrary spatial profile of the magnetic field was represented by a Fourier series. Its coefficients were shown to determine the second moment of the accumulated phase, and the Gaussian phase approximation gave the macroscopic signal. In particular, Tarczon and Halperin proposed an approximate relation in the short-time limit:

$$E \approx \exp[-D\gamma^2 g_{\rm eff}^2 T^3/12], \tag{22}$$

where $g_{\rm eff}^2=\langle(\nabla B(\mathbf{r}))^2\rangle$ is the spatial average of the squared gradient of the magnetic field. Tarczon and Halperin argued that the signal attenuation in a nonlinear magnetic field $B(\mathbf{r})$ could be characterized by an effective gradient $g_{\rm eff}$. This result was applied by Hürlimann (1998) to consider the effect of susceptibility-induced internal magnetic fields in porous media. In the simple case of a linear gradient $B(\mathbf{r})=\mathbf{g}\cdot\mathbf{r}$ one could get $g_{\rm eff}^2=g^2$ and retrieve the relation (3). Tarczon and Halperin suggested a more accurate result, which is now known as the local gradient approximation:

$$E \simeq \frac{1}{V}\int_\Omega d\mathbf{r}\,\exp\left(-\frac{D\gamma^2T^3}{12}[\nabla B(\mathbf{r})]^2\right). \tag{23}$$

We discuss this result in Sec. IV.

Other theoretical treatments of nonlinear magnetic fields in the whole space (that is, unrestricted diffusion) should be mentioned. The first was given by Majumdar and Gore (1988), who proposed modeling the spatial distribution of susceptibility-induced magnetic-field inhomogeneities as discrete random fields. The effective diffusion coefficient was found to be proportional to the variance of the distribution of the magnetic-field gradients. The case of continuous Gaussian random fields was considered by Mitra and Le Doussal (1991). In the long-time limit, they found an exponential decrease of the macroscopic signal in time T with a power-law correction. The problem of large fluctuations in finite-size systems was discussed.

Le Doussal and Sen (1992) derived an exact solution of the Bloch-Torrey equation in the whole space for a quadratic (or parabolic) magnetic-field profile $B(z)=g_0+g_1z+g_2z^2$. In the short-time limit, the signal attenuation was similar to that of the effective linear gradient, in agreement with the approximate relation (22). In the long-time limit, however, Le Doussal and Sen found that $\ln E$ was proportional to T instead of Hahn's T^3 dependence. A natural length scale $(8D/\gamma g_2)^{1/4}$ was shown to govern the problem. Parabolic magnetic fields were studied experimentally by Bendel (1990).

Zielinski and Sen (2000) reported a numerical solution of the one-dimensional Bloch-Torrey equation with parabolic and cosine spatial profiles of the magnetic field. The evolution of the signal was argued to be largely determined at all times solely by the two moments of the magnetic field, $\langle(\nabla B)^2\rangle$ and $\langle(\int dx\,B(x))^2\rangle$, and not by the details of its local spatial distribution. They also showed that the local gradient approximation holds only in the short-time limit and becomes invalid for longer times. Grebenkov (2007a) applied the multiple correlation function description, presented in Sec. III, to study theoretically the restricted diffusion between parallel planes in a cosine magnetic field. The particular choice of this spatial profile as proportional to an eigenfunction of the related Laplace operator considerably simplified the underlying mathematics and allowed exact and explicit formulas for several high-order moments of the accumulated phase φ to be obtained.

The presence of susceptibility-induced internal magnetic fields was employed by Song *et al.*[28] to obtain the pore size distribution in porous media. Instead of using a uniform initial density and diffusion-sensitizing gradients, the spins can be excited selectively within a narrow frequency range to create a nonuniform magnetization at time $t=0$. Further relaxation to the equilibrium state is governed by the Laplace operator eigenvalues which are related to the characteristic length scales of the domain. For instance, this experimental technique was used to determine multiple length scales in rocks (Song *et al.*, 2000).

K. Diffusive edge enhancement

In this review, we consider restricted diffusion in the whole sample. At the same time, position-encoding gradients can be additionally applied to excite and acquire the spin magnetizations within a small region of the sample. This technique, known as magnetic resonance imaging (MRI), is widely used in medical and materials research as a noninvasive experimental tool. A separate review would be required to list and comment on various imaging methods developed during the last decades.[29] In this subsection, we briefly mention the role

[28]See Song (2000b); Song *et al.* (2000, 2003); Lisitza and Song (2001, 2002); Chen and Song (2002). An excellent review of this decay-due-to-diffusion-in-internal-field method is by Song (2003).

[29]A general review of MRI is given by Wehrli (1995). The concepts of NMR imaging of materials and biological cells are described by Miller (1998) and Ciobanua *et al.* (2003), respec-

of diffusive motion for MRI.

On the one hand, the study of diffusive motion in each of the small regions (called voxels) creates a diffusion-weighted map of the sample, providing useful information about its geometry. For instance, diffusion-weighted proton imaging allows one to detect abnormal modifications in the structure and functionality of the brain.[30] Highly spin-polarized noble gases (like helium-3 or xenon-129) have been used for human lung imaging.[31] Gas diffusion was also recognized as a powerful experimental tool for imaging of materials (see Song *et al.*, 1995; Mair, Rosen *et al.*, 2002, and references therein) and for dynamical monitoring of temperature gradients (Schmidt *et al.*, 1997).

On the other hand, diffusive motion is known to play an important role in classical MRI, where the image represents the spatial distribution of the signal intensity in different voxels. If diffusion was unrestricted, the attenuation would be the same in different voxels and the signal would be uniform throughout the sample.[32] Different "obstacles" (walls, membranes, grains, etc.) lead to inhomogeneous signal attenuation. Since the motion is more restricted near the boundary, the spins travel smaller distances, resulting in less pronounced dephasing than that of the spins in the bulk. As a consequence, a stronger macroscopic signal near an obstacle would "highlight" its boundary. This effect, known as diffusive edge enhancement, was first predicted in numerical simulations by Hyslop and Lauterbur (1991) and Putz *et al.* (1992). It was later explored experimentally by Barsky *et al.* (1992) and Callaghan *et al.* (1993) using water proton NMR. In particular, Hyslop and Lauterbur (1991) suggested using the effect of diffusion to detect impermeable and semipermeable membranes.

A quantitative theory for the shape of the image distortion in the slow-diffusion and motional-narrowing regimes was proposed by de Swiet (1995). He showed that frequency encoding is preferable to enhance the edges, while pure phase encoding is better to reduce edge enhancement. Song *et al.* (1998) systematically characterized the effects of diffusion on MRI in a one-dimensional (1D) sample using polarized xenon gas. They found that the contrast between the boundaries and the interior of the sample should become more pronounced if sufficient time is allowed for diffusion.

L. Conventional numerical techniques

To fully discuss all numerical aspects of restricted diffusion would require another review, so conventional techniques only are mentioned in this subsection. To calculate the attenuation of the macroscopic signal, either a numerical resolution of the Bloch-Torrey equation or Monte Carlo simulations of reflected Brownian motion are generally employed. In the former case, the bulk of a confining domain is discretized by a regular lattice or a more complicated mesh, so that a discrete version of the Bloch-Torrey equation can be numerically solved by finite-difference or finite-element methods.[33] The distribution of the spin magnetization $\mathfrak{m}(\mathbf{r},t)$ over lattice sites is successively calculated step by step with a small time interval τ. The macroscopic signal is then given as the spatial average of $\mathfrak{m}(\mathbf{r},t)$. In contrast, Monte Carlo techniques are used to simulate diffusive motion and to compute accumulated phase of an individual spin.[34] Brownian trajectories are usually modeled as a sequence of independent random jumps in the bulk with (partial) reflections on the boundary. The jump distance is either fixed or normally distributed with dispersion $\sqrt{2D\tau}$ in each spatial direction.[35] Once the accumulated phase distribution $\mathbb{P}(\varphi)$ is approximately found by launching a large number of particles undergoing a random walk, the signal can be deduced as the expectation of $e^{i\varphi}$. A number of improvements can be introduced to speed up Monte Carlo simulations. For instance, Leibig (1993) suggested performing jumps of variable length depending on the distance between the particle and the boundary.

Aside from these classical methods for diffusive processes, we mention the lattice Boltzmann procedure developed by Guyer and McCall (2000) to numerically simulate the time evolution of magnetization in a porous medium. This technique, based on a coarse-grained picture of the particle system, is well suited to problems in which a flow field is also present. Some other methods were also employed, for instance, neural networks to interpret pulsed-gradient restricted-diffusion data (Lennon and Kuchel, 1994).

---

tively. The clinical impact of the magnetic resonance spectroscopy is analyzed by Smith and Stewart (2002). Medical applications for functional MRI are discussed in Le Bihan (1995).

[30]See Le Bihan (1995, 2003); Darquié *et al.* (2001); Assaf *et al.* (2004); Frahm *et al.* (2004), and references therein.

[31]Among a variety of published results, we mention Albert *et al.* (1994); Bachert *et al.* (1996); Macfall *et al.* (1996); Saam *et al.* (2000); Yablonskiy *et al.* (2002); Bidinosti *et al.* (2003); Swift *et al.* (2005); Fain *et al.* (2006); Shanbhag *et al.* (2006). Further information can be found in reviews by Möller *et al.* (2002); van Beek *et al.* (2004); Kadlecek *et al.* (2005); Conradi *et al.* (2006).

[32]It should be also noticed that diffusion presents one of the main limitations to increase spatial resolution of MRI [e.g., see Brandl and Haase (1994)].

[33]Finite-difference technique was implemented by many authors; see, e.g., Wayne and Cotts (1966); Putz *et al.* (1992); Blees (1994); Sen *et al.* (1999); Zielinski and Sen (2000); Hwang *et al.* (2003), although the list is far from complete.

[34]Among others, see Mendelson (1990); Hyslop and Lauterbur (1991); Balinov *et al.* (1993); Coy and Callaghan (1994); Linse and Söderman (1995); Mitra and Halperin (1995); Kuchel *et al.* (1996); Duh *et al.* (2001); Valckenborg *et al.* (2002); Grebenkov *et al.* (2007).

[35]See Bergman *et al.* (1995) for comparison between a random-walk method and a Fourier series expansion of diffusion eigenmodes for periodic arrangements of spherical grains.

M. Matrix formalisms

Although efficient for some purposes, the above classical techniques present inconveniences and limitations. For instance, the statistical error of Monte Carlo simulations decreases slowly with the number of particles undergoing a random walk. In turn, the study of intensive gradients requires a very fine resolution (or discretization) of the Bloch-Torrey equation. Long-time analysis is generally difficult with both techniques. To overcome these problems, Caprihan *et al.* (1996) proposed an original numerical approach. The idea was to approximate a given temporal gradient profile (or wave form) $\mathbf{g}(t)$ by a large sum of equidistant very narrow gradient pulses at times $k\tau$, τ being a short time interval between two successive pulses. These gradient pulses encode the successive positions $\mathbf{r}_k=\mathbf{r}(k\tau)$ of a diffusing nucleus by factors $e^{i\gamma\delta\mathbf{g}_k\cdot\mathbf{r}_k}$, where $\mathbf{g}_k=\mathbf{g}(k\tau)$. The random displacements of nuclei during the time interval τ is determined by the propagator $G_\tau(\mathbf{r}_k,\mathbf{r}_{k+1})$. To calculate the average over all positions $\mathbf{r}_k$, Caprihan *et al.* used the expansion of this heat kernel over the Laplace operator eigenfunctions (see Appendix D for details). A general but cumbersome expression for the macroscopic signal was derived. As an example, they considered the case of restricted diffusion between two parallel planes.

This approach was reformulated by Callaghan (1997) in a simple and elegant matrix form. He showed that the macroscopic signal can be written within a matrix formalism involving the eigenbasis of the Laplace operator (see Appendix D for details). In practice, the numerical problem of finding the signal attenuation under an arbitrary temporal gradient profile was reduced to symbolic manipulation with two matrices which depend on several physical parameters. Callaghan illustrated the efficiency of this multiple propagator approach by considering restricted diffusion between two parallel planes. In further work, Callaghan and Codd (1998) and Codd and Callaghan (1999) studied restricted diffusion in a cylinder and a sphere and discussed the role of surface relaxation. Price *et al.* (2003) used this technique to check the validity of the narrow-pulse approximation. Grebenkov (2006b) developed a spectral analysis of the underlying matrices to show multiexponential signal attenuation for CPMG sequences.

Callaghan's matrix formalism was reformulated in terms of random walks by Sukstanskii and Yablonskiy (2002). Using the modified approach, they obtained a number of interesting results; in particular, they found a transition between oscillatory and monotonic behaviors of the free induction decay signal as a function of time. The accuracy of the Gaussian phase approximation was also discussed.

Finally, Barzykin (1998, 1999) proposed an equivalent matrix formalism by considering a stepwise approximation of the temporal gradient profile. In his approach, the two matrices determining the macroscopic signal depend solely on the confining geometry. These matrices have thus to be calculated only once for a chosen confining medium (e.g., a sphere), after which the computation of the signal is straightforward and rapid for any set of physical parameters. This was an important improvement of the above matrix techniques and a crucial simplification for numerical analysis.

The different matrix approaches outlined above were intended mainly for numerical computation of the macroscopic signal. Axelrod and Sen (2001) developed a systematic formalism for calculating the magnetization of spins diffusing in a bounded region in the presence of surface relaxation and general magnetic field inhomogeneity. Following an analogy with quantum mechanics, they considered the magnetization $\mathfrak{m}(\mathbf{r},T)$ at time T as a result of application of an evolution operator $\mathcal{U}$ to its initial state $\mathfrak{m}(\mathbf{r},0)$. This operator was obtained by a formal integration of the Bloch-Torrey equation with an arbitrary time-dependent magnetic field $f(t)B(\mathbf{r})$,

$$\mathcal{U}=\mathcal{T}\left\{\exp\left(-\int_0^T dt[D\Delta+i\gamma f(t)\hat{B}]\right)\right\}, \tag{24}$$

where $\mathcal{T}\{\cdots\}$ denotes a time-ordered product and $\hat{B}$ is the operator of multiplication by $B(\mathbf{r})$. A perturbative expansion of this relation in powers of the magnetic field allowed many theoretical results to be derived and extended. Axelrod and Sen gave special emphasis to the CPMG spin echoes.

In the next section, we reformulate[36] their approach using an alternative method (Grebenkov, 2007b). The central focus of our consideration will be reflected Brownian motion and its multiple correction functions, so we shall call it the multiple correlation function (MCF) description. There will be no *a priori* favor given to any particular temporal dependence of the magnetic field. The results for CPMG spin echoes, as well as for many other temporal profiles, will be derived from general relations. Unlike Axelrod and Sen, we introduce the normal modes of the Laplace operator as a natural eigenbasis for this problem from the beginning. From this point of view, the MCF approach can be seen as an extension of Barzykin's numerical technique to tackle the problem of restricted diffusion in an arbitrary magnetic field *theoretically*. Throughout the review, this approach will be applied to retrieve, extend, and critically discuss numerous results briefly presented in the above overview.

III. MULTIPLE CORRELATION FUNCTIONS

In this section, the moments of the random phase accumulated by a diffusing spin are found in a matrix form involving the Laplace operator eigenbasis in a confining domain. The spatial inhomogeneities and time dependence of the magnetic field enter the multiple correla-

[36]The author is thankful to one of the referees for pointing out the article by Axelrod and Sen (2001). The multiple correlation function (MCF) approach developed independently by the author and described below turns out to reproduce many ideas and methods from their work.

tion functions as functionals and weight factors. After formulation for a general case in Sec. III.B, this MCF description is applied to spin echoes in Sec. III.C. Different choices for temporal and spatial profiles of the magnetic field are considered in Secs. III.D and III.E, respectively. In Sec. III.F, the analytical results are derived for restricted diffusion in three simple domains (slab, cylinder, and sphere).

A. Physical assumptions

Before starting the mathematical description, we first specify and comment on the underlying physical assumptions and limitations of this approach.

(i) The system consists of two kinds of matter: a "solid" matrix (rock, grains, bone, tissue, membranes, glass beads, colloids, proteins, etc.) and a "fluid" substance (liquid or gas). The fluid substance undergoes a motion that is confined by a solid matrix (fixed and unchanged). From the geometrical point of view, the fluid substance fills a volume (domain Ω) restricted by the frontier between fluid and solid (boundary $\partial\Omega$). The domain and its boundary remain unchanged during the experiment.[37]

(ii) The fluid substance may be composed of different particles (molecules or atoms), but there is only one kind of particle that bears nuclear spin of 1/2. Their interaction with the magnetic field is described in a classical way [via the accumulated phase (1) or Bloch-Torrey equation (9)]. We neglect the bulk relaxation (spin-spin as well as spin-lattice interactions). Its effect is trivial, and it can be measured and factored out by a NMR sequence without diffusion-weighting magnetic fields. As a result, the signal can be renormalized in such a way as to account for attenuation due to restricted diffusion alone. In contrast, surface relaxation will be taken into account.

(iii) The spin-bearing particles of the fluid substance undergo ordinary Brownian dynamics. This condition excludes stationary flow (convection or advection) and other hydrodynamic effects.[38] Thermal exchange between the liquid and its saturated vapor is neglected.[39] The mean free path of diffusing particles should be much shorter than geometrical features of the confining domain. Moreover, the elementary displacements of each particle are supposed to be (almost) independent. There are no traps in the bulk[40] or other events that may considerably affect the dynamics (except reflections on the boundary; see below). More generally, there is no anomalous diffusion (like Lévy flights).[41] Throughout the review, the Brownian dynamics are assumed to be governed by the Laplace operator, that is, the collisions of the spin-bearing particles can be effectively described by a single free diffusion coefficient D. This coefficient is time independent and uniform over the confining domain (that is, the fluid substance should be isotropic). Note that many results presented below can be extended for more general dynamics governed by a second-order elliptic operator.

(iv) The microscopic structure and physicochemical properties of the frontier between solid matrix and fluid substance are taken into account through the Fourier boundary condition (10) for the magnetization. In particular, surface relaxation may be caused by paramagnetic impurities uniformly distributed over the boundary, absorption, or transfer of the spin-bearing particles through the boundary to the external environment, specific spin-exchange processes, etc. In contrast, there is no "tunneling" effect: the interface separating two distinct compartments of the bulk is supposed to be impenetrable.[42] In other words, the particle trajectory cannot pass across

[37] In many systems, the boundary may vary with time. For instance, breath causes inflation and deflation of the pulmonary acini (i.e., motion of the acinar tissue). Membranes of biological cells may change their shapes under external perturbations. Chemical reactions lead to a time evolution (propagation) of the boundary between the solid grains and water in cements. In all these cases, however, the characteristic time scale for the boundary evolution is much longer than the duration of the NMR experiment so that the boundary can be considered as fixed.

[38] For some experiments, it may be difficult to completely subtract convection in a sample. Unlike the stochastic character of diffusion, a stationary flow yields systematic bias that may considerably affect the results.

[39] The related enhancement of the self-diffusion for a liquid partially filling a porous medium was observed by different groups; for instance, see D'Orazio *et al.* (1989) and Kimmich *et al.* (1994).

[40] The effect of randomly distributed traps on diffusion was thoroughly studied by different authors, e.g., Bixon and Zwanzig (1981); Grassberger and Procaccia (1982); Kirkpatrick (1982); Kayser and Hubbard (1983, 1984).

[41] For a review of anomalous diffusion, see Bouchaud and Georges (1990), Metzler and Klafter (2000), Kimmich (2002), and Zaslavsky (2002). Anomalous diffusion on percolating clusters was analyzed by Gefen *et al.* (1983). The propagator representation and its use in NMR was discussed by Zavada *et al.* (1999). The statistics of Lévy processes and Brownian flights and their role in NMR were studied in Bychuk and O'Shaughnessy (1995), Stapf *et al.* (1995), Shlesinger *et al.* (1999), Levitz (2005), Levitz *et al.* (2006), and Li *et al.* (2006).

[42] This last assumption is not satisfied in most biological cells. On the contrary, the fundamental role of a cellular membrane is to allow such a tunneling, for instance, entry of metabolites or exit of waste [see Alberts *et al.* (1994)]. To some extent, these effects can be taken into account by the surface permeability. In general, one can describe the transport in such systems by considering two (or more) Bloch-Torrey equations with appropriate boundary conditions [see Tanner (1978); Sen (2003); Sukstanskii *et al.* (2004)].

the boundary. If present, surface relaxation is supposed to be time independent and uniform over the whole boundary. When its magnetization is not lost after collision with the boundary, the spin-bearing particle is normally[43] reflected to the bulk to continue its diffusive motion.

(v) The macroscopic signal is formed by the spins diffusing in a bounded region. We suppose that the whole confining domain and its boundary are contained inside this region. It is equivalent to saying that the domain is closed: no particle can enter or escape. Among the various assumptions, the appropriateness of this is probably the most disputable. If the considered bounded region is a part of a bigger system, the diffusing spins can freely enter and escape the bounded region during a NMR experiment. We propose three strategies that could help one to consider this open system in a similar way to the closed one. First, if the bounded region is big enough, the transport processes across the boundary are in general less significant than that in the bulk, so that they can be neglected in a first approximation. Second, if the computation could be performed for the whole (bigger) system, the macroscopic signal from a bounded region would be found by using a nonuniform pickup function in Eq. (12) and related formulas. Third, some kind of a periodic boundary condition can be employed to model the surface exchange between the bounded region and its environment. In this review, we do not focus on these subtle points (see also the discussion in Sec. VI.I).

(vi) In many systems, differences in the magnetic susceptibility between the solid matrix and the fluid substance induce high internal magnetic fields near their frontier. These geometry-dependent fields are, in general, difficult to access and control. In this review, the susceptibility effects are supposed to be either neglected or effectively taken into account through the spatial profile of the magnetic field. Note that the last option would require elaborate models of internal magnetic fields.[44]

(vii) There is no hardware imperfection: one assumes exact Larmor frequency, precise timing, and high homogeneity of the radio-frequency pulses, no eddy currents, etc. The rf pulses are assumed to be very short so that the diffusive motion of the spins during their application can be neglected.

Although these assumptions may appear too restrictive at first sight, many experiments and most theoretical research have been performed under these conditions, as illustrated in Sec. II.

B. General formulation

As a first step, we reformulate the general physical description (1) and (2) of diffusive NMR phenomena in a way that will allow for further theoretical and numerical study. For this purpose, the exponential function in Eq. (2) is expanded in a power series

$$E = \sum_{n=0}^{\infty} \frac{i^n}{n!} \mathbb{E}\{\varphi^n\}, \tag{25}$$

where the moments of the random variable φ are

$$\mathbb{E}\{\varphi^n\} = \gamma^n \mathbb{E}\left\{ \int_0^T dt_1 \cdots \int_0^T dt_n B_{t_1}(\mathbf{r}(t_1)) \cdots B_{t_n}(\mathbf{r}(t_n)) \right\}. \tag{26}$$

The multiple integral of the product of similar functions can be written as an ordered time average,

$$\mathbb{E}\{\varphi^n\} = n!\gamma^n \int_0^T dt_1 \cdots \times \int_{t_{n-1}}^T dt_n \mathbb{E}\{B_{t_1}(\mathbf{r}(t_1)) \cdots B_{t_n}(\mathbf{r}(t_n))\}, \tag{27}$$

where the time moments $t_1, \ldots, t_n$ are now in ascending order. The multiple correlation function $\mathbb{E}\{B_{t_1}(\mathbf{r}(t_1)) \cdots B_{t_n}(\mathbf{r}(t_n))\}$ can be calculated according to its probabilistic meaning:

- the starting position $\mathbf{r}_0$ of the reflected Brownian motion is chosen with a given initial density[45] $\rho_0(\mathbf{r}_0)$;
- the probability density for arriving from this point to a random position $\mathbf{r}_1 = \mathbf{r}(t_1)$ at time t_1 is given by the propagator, heat kernel, or Green's function $G_{t_1}(\mathbf{r}_0, \mathbf{r}_1)$ of the diffusion equation in a bounded domain Ω,

[43] In many thermal systems, particles are reflected in random directions with the cosine distribution of angles (as diffuse reflection of light). On average, however, this microscopic mechanism is equivalent to normal reflections.

[44] See Brown and Fantazzini (1993, 1994); Borgia *et al.* (1995); Sen and Axelrod (1999); Sun and Dunn (2002); Audoly *et al.* (2003). The effect of internal gradients on the time-dependent diffusion coefficient in model porous systems has been measured by different groups, e.g., Zhong *et al.* (1991) and Seland *et al.* (2000); see also Weisskoff *et al.* (1994).

[45] As mentioned in Sec. II.B, the magnetization density at time $t=0$ is proportional to the initial spin density when rf pulses are spatially homogeneous. In some circumstances, however, inhomogeneous rf pulses may be preferred or unavoidable. For instance, Song (2000a) proposed an experimental technique to detect the pore geometry, when the uniformly distributed spins are excited selectively within a narrow frequency range to create a nonuniform magnetization at time $t=0$. As a consequence, the initial magnetization is in general a complex-valued function of $\mathbf{r}_0$. Strictly speaking, such probability density has no meaning. However, one can still use the subsequent matrix formalism to compute the moments of the total dephasing and the resulting macroscopic signal.

$$\left(\frac{\partial}{\partial t} - D\Delta\right) G_t(\mathbf{r},\mathbf{r}') = 0 \quad \text{in } \Omega, \tag{28}$$

with the appropriate Fourier or Neumann boundary condition,

$$\left(D\frac{\partial}{\partial n} + \rho\right) G_t(\mathbf{r},\mathbf{r}') = 0 \quad \text{on } \partial\Omega, \tag{29}$$

and the initial condition

$$G_{t=0}(\mathbf{r},\mathbf{r}') = \delta(\mathbf{r}-\mathbf{r}'),$$

δ being the Dirac distribution (delta function);

- the subsequent positions $\mathbf{r}_2=\mathbf{r}(t_2),\ldots,\mathbf{r}_n=\mathbf{r}(t_n)$ are also distributed according to the corresponding probability densities $G_{t_2-t_1}(\mathbf{r}_1,\mathbf{r}_2),\ldots,G_{t_n-t_{n-1}}(\mathbf{r}_{n-1},\mathbf{r}_n)$.

Since reflected Brownian motion is a Markovian process (without memory), the multiple correlation function is[46]

$$\begin{aligned}\mathbb{E}\{B_{t_1}(\mathbf{r}(t_1))\cdots B_{t_n}(\mathbf{r}(t_n))\} &= \int_\Omega d\mathbf{r}_0 \cdots \int_\Omega d\mathbf{r}_{n+1}\rho_0(\mathbf{r}_0) \\ &\times G_{t_1}(\mathbf{r}_0,\mathbf{r}_1)B_{t_1}(\mathbf{r}_1)G_{t_2-t_1}(\mathbf{r}_1,\mathbf{r}_2)B_{t_2}(\mathbf{r}_2)\cdots \\ &\times G_{t_n-t_{n-1}}(\mathbf{r}_{n-1},\mathbf{r}_n)B_{t_n}(\mathbf{r}_n)G_{T-t_n}(\mathbf{r}_n,\mathbf{r}_{n+1})\tilde{\rho}(\mathbf{r}_{n+1}).\end{aligned} \tag{30}$$

A similar relation was used by Bergman and Dunn (1995) to describe the signal attenuation in periodic porous media.

To proceed, one can use the spectral decomposition of the heat kernel over the eigenfunctions $u_m(\mathbf{r})$ of the Laplace operator (Arfken and Weber, 2001)

$$G_t(\mathbf{r},\mathbf{r}') = \sum_{m=0}^{\infty} u_m(\mathbf{r})u_m^*(\mathbf{r}')\exp[-Dt\lambda_m/L^2], \tag{31}$$

where L is a characteristic dimension of the confining domain Ω (e.g., its diameter), and the asterisk denotes the complex conjugate. The eigenvalues λ_m are defined to be dimensionless:

$$-\Delta u_m(\mathbf{r}) = \left(\frac{\lambda_m}{L^2}\right) u_m(\mathbf{r}) \quad \text{in } \Omega, \tag{32}$$

and the Fourier (or Neumann) boundary condition is imposed according to the physical properties of the interface:

$$\frac{\partial}{\partial n}u_m(\mathbf{r}) + \frac{h}{L}u_m(\mathbf{r}) = 0 \quad \text{on } \partial\Omega, \tag{33}$$

where the dimensionless surface relaxivity h is defined as the ratio between the size L and the surface relaxation length D/ρ, which is the distance a particle should travel near the boundary before surface relaxation effects reduce its expected magnetization:

$$h = \rho L/D. \tag{34}$$

The eigenfunctions $u_m(\mathbf{r})$ are orthonormal in the space $L^2(\Omega)$ of measurable and square integrable functions:

$$\int_\Omega d\mathbf{r}\, u_m(\mathbf{r})u_{m'}^*(\mathbf{r}) = \delta_{m,m'}, \tag{35}$$

where $\delta_{m,m'}$ is the Kronecker symbol.[47] For theoretical analysis, it is convenient to introduce the dimensionless diffusion coefficient

$$p = DT/L^2. \tag{36}$$

The substitution of the spectral decomposition (31) into Eq. (30) for each propagator leads to

$$\begin{aligned}\mathbb{E}\{B_{t_1}(\mathbf{r}(t_1))\cdots B_{t_n}(\mathbf{r}(t_n))\} &= \sum_{m_1=0}^{\infty}\cdots\sum_{m_{n+1}=0}^{\infty} U_{m_1}e^{-p\lambda_{m_1}t_1/T} \\ &\times \mathcal{B}_{m_1,m_2}(t_1)e^{-p\lambda_{m_2}(t_2-t_1)/T}\mathcal{B}_{m_2,m_3}(t_2)\cdots \\ &\times \mathcal{B}_{m_n,m_{n+1}}(t_n)e^{-p\lambda_{m_{n+1}}(T-t_n)/T}\tilde{U}_{m_{n+1}}^*,\end{aligned} \tag{37}$$

where the infinite-dimensional matrix $\mathcal{B}$ and vectors U and $\tilde{U}$ are defined as[48]

[46] Throughout this review the pickup function $\tilde{\rho}(\mathbf{r}_{n+1})$ is considered to be 1. The function $G_{T-t_n}(\mathbf{r}_n,\mathbf{r}_{n+1})$ in Eq. (30) ensures that the spin magnetization survives until the echo time T (otherwise it would not contribute to the macroscopic signal). In the presence of surface relaxation, the omission of this factor would result in some artifacts [see Kuchel *et al.* (1996)]. In contrast, if there is no surface relaxation ($h=0$), the integral over $d\mathbf{r}_{n+1}$ can be omitted, being equal to 1 due to the normalization of the heat kernel.

[47] It may also be useful to mention that each eigenvalue can be expressed through the integrals of the associated eigenfunction:

$$\lambda_m = L^2\int_\Omega d\mathbf{r}\,|\nabla u_m|^2 + hL\int_{\partial\Omega} d\mathbf{r}\,|u_m|^2.$$

In particular, this relation shows that all eigenvalues are positive. In analogy with quantum mechanics or acoustics, these terms can be respectively interpreted as the bulk kinetic energy and the potential energy which is localized in the surface region (Ryu, 2001). Moreover, one can associate to each eigenmode its characteristic length scale according to

$$\ell_m = \int_{\partial\Omega} d\mathbf{r}|u_m|^2 \Big/ \int_\Omega d\mathbf{r}|\nabla u_m|^2.$$

Note that a similar parameter was introduced by Johnson *et al.* (1986) to characterize transport in porous media.

[48] The initial density $\rho_0(\mathbf{r})$ might alternatively be set to the inverse of the domain volume V provided that eigenfunctions $u_m(\mathbf{r})$ are appropriately normalized [see, for example, Barzykin (1999)]. In practice, however, such a normalization is difficult, and the classical expansion (31) for the heat kernel is preferred.

$$\mathcal{B}_{m,m'}(t) = \int_\Omega d\mathbf{r}\, u_m^*(\mathbf{r}) B_t(\mathbf{r}) u_{m'}(\mathbf{r}), \tag{38}$$

$$U_m = V^{1/2} \int_\Omega d\mathbf{r}\, u_m(\mathbf{r}) \rho_0(\mathbf{r}), \tag{39}$$

$$\tilde{U}_m = V^{-1/2} \int_\Omega d\mathbf{r}\, u_m(\mathbf{r}) \tilde{\rho}(\mathbf{r}), \tag{40}$$

V being the volume of the domain Ω. The summation over indices $m_1, \ldots, m_{n+1}$ can be thought of as a matrix product yielding a compact representation of a scalar product for the multiple correlation function,

$$\mathbb{E}\{B_{t_1}(\mathbf{r}(t_1)) \cdots B_{t_n}(\mathbf{r}(t_n))\} = U\left(\left[\prod_{j=1}^{n} e^{-p\Lambda t_j/T} \mathcal{B}(t_j) e^{p\Lambda t_j/T} \right] e^{-p\Lambda} \tilde{U}^* \right), \tag{41}$$

with the diagonal infinite-dimensional matrix Λ:

$$\Lambda_{m,m'} = \delta_{m,m'} \lambda_m. \tag{42}$$

The ordered time average of the above correlation function gives the moment $\mathbb{E}\{\varphi^n\}$ of the random phase φ and determines the nth-order contribution to the signal expansion (25). An unbounded increase of the eigenvalues λ_m with m ensures a rapid convergence in the matrix product (41) and allows one to truncate the matrices $\mathcal{B}$ and Λ to a limited dimension for numerical analysis.

At first thought, one may wonder what is the interest of such a formal approach? The compact and transparent physical description by Eqs. (1) and (2) is "reduced" to a cumbersome mathematical formalism involving the multiple time integration of the product of time-dependent infinite-dimensional matrices. Even for numerical simulations, modeling reflected Brownian motion might seem to be simpler and more efficient. However, this thought is misleading. The deceptive simplicity of Eqs. (1) and (2) relies on the fact that the diversity of diffusive NMR phenomena is hidden in a very complex behavior of reflected Brownian motion. The stochastic character of diffusive motion is entangled as with particular properties of the confining domain and applied magnetic field. The complexity of these phenomena has made them attractive to physicists since Hahn's seminal paper in 1950 to the present day. The above matrix formalism is in fact a general mathematical basis to study the diffusive motion in any confining geometry under arbitrary magnetic field. In this formal way, the physical problem of finding the macroscopic signal of diffusing spins is entirely reduced to the analysis of the Laplace operator eigenmodes, and is thus solved as a physical problem. In what follows, we show how this mathematical basis can be applied for a theoretical analysis in many cases of particular interest. As the most usual NMR technique, the spin-echo formation will be examined in the next subsection.

C. Application to spin echoes

In the classical Hahn experiment (Hahn, 1950), the second rf pulse is emitted at time $T/2$ to refocus the spin magnetizations. For immobile spins, dephasing during the time interval $[0, T/2]$ is completely compensated by rephasing during the following time interval $[T/2, T]$, if the applied magnetic field satisfies the rephasing condition

$$\int_0^{T/2} dt\, B_t(\mathbf{r}) - \int_{T/2}^{T} dt\, B_t(\mathbf{r}) = 0 \tag{43}$$

at any spin location $\mathbf{r}$ inside Ω. In this case, the accumulated phase φ is strictly zero for all spins (i.e., their magnetizations are in phase at time T), which leads to echo formation at time T. When spins diffuse, rephasing is not complete, and the echo amplitude is decreased. This attenuation can be experimentally measured to study the spin motion.

In a typical situation, the magnetic field $B_t(\mathbf{r})$ is composed of a constant field B_0 generated by a static magnet, and a time-dependent diffusion-sensitizing inhomogeneous field $\beta F(t) B(\mathbf{r})$ of maximum intensity β. The temporal and spatial profiles $F(t)$ and $B(\mathbf{r})$ are defined to be dimensionless and normalized to 1. For mathematical convenience, the temporal profile is supposed to be a piecewise-smooth function on the interval $[0, T]$, while the spatial profile is a smooth function in the bulk (domain Ω). These formal assumptions are satisfied in practice.

Throughout this review, the application of the 180° rf pulse will be taken into account by inverting the sign of the function $F(t)$ for $t > T/2$. The above rephasing condition is reformulated for such an effective temporal profile of the magnetic field as

$$\int_0^T dt\, F(t) = 0. \tag{44}$$

Since the contribution of a constant field vanishes after rephasing, the total phase φ, accumulated during the time T, can be written in the same form as before, with $B_t(\mathbf{r}) = \beta F(t) B(\mathbf{r})$:

$$\varphi = \gamma \int_0^T dt\, \beta F(t) B(\mathbf{r}(t)). \tag{45}$$

The time dependence of the matrix $\mathcal{B}(t)$ in Eq. (38) can thus be factored out,

$$\mathcal{B}(t) = F(t)\mathcal{B}, \tag{46}$$

where

$$\mathcal{B}_{m,m'} = \int_\Omega d\mathbf{r}\, u_m^*(\mathbf{r}) B(\mathbf{r}) u_{m'}(\mathbf{r}). \tag{47}$$

For convenience, the integral variable t can be replaced by a dimensionless parameter t/T:

$$\varphi = \gamma\beta T \int_0^1 dt\, f(t) B(X_t), \tag{48}$$

where

$$X_t \equiv \mathbf{r}(tT) \quad \text{and} \quad f(t) \equiv F(tT) \tag{49}$$

correspond to the time rescaling of reflected Brownian motion and the effective temporal profile. In the remainder of this paper, t will denote the dimensionless time ranging between 0 and 1. In particular, the rephasing condition (44) reads as

$$\int_0^1 dt\, f(t) = 0. \tag{50}$$

The dimensionless parameter

$$q = \gamma\beta T \tag{51}$$

quantifies the effective dephasing of spins with gyromagnetic ratio γ in a magnetic field of strength β applied over time T.[49] The presence of three *independent* dimensionless parameters p, q, and h will result in different NMR regimes for restricted diffusion.

According to Eq. (48), the physical phase φ is proportional to the random variable

$$\phi = \int_0^1 dt\, f(t) B(X_t), \tag{52}$$

which we still call the "phase."[50] Relation (2) shows that the macroscopic signal E is in fact a characteristic function of this variable:

$$E = \mathbb{E}\{e^{iq\phi}\}. \tag{53}$$

Since the phase ϕ is a bounded random variable, its characteristic function is analytic (Feller, 1971). In particular, its series expansion

$$E = \sum_{n=0}^{\infty} \frac{(iq)^n}{n!} \mathbb{E}\{\phi^n\} \tag{54}$$

absolutely converges for any q. The moments $\mathbb{E}\{\phi^n\}$ may be straightforwardly deduced from the results of Sec. III.B:

$$\mathbb{E}\left\{\frac{\phi^n}{n!}\right\} = \langle \mathbb{E}\{B(X_{t_1}) \cdots B(X_{t_n})\}\rangle_n, \tag{55}$$

where $\langle \cdots \rangle_n$ denotes the f-weighted (ordered) time average, with the effective temporal profile $f(t)$. For any function $h(t_1, \ldots, t_n)$ of time variables $t_1, \ldots, t_n$, this average is defined as

$$\langle h(t_1, \ldots, t_n)\rangle_n = \int_0^1 dt_1 \cdots \int_{t_{n-1}}^1 dt_n f(t_1) \cdots f(t_n) h(t_1, \ldots, t_n). \tag{56}$$

For example, one has

$$\langle (t_1 - t_2)\rangle_2 = \int_0^1 dt_1 f(t_1) \int_{t_1}^1 dt_2 f(t_2)(t_1 - t_2). \tag{57}$$

Note that a similar concept of the ordered time average has been used by Axelrod and Sen (2001), with special emphasis on the CPMG spin echoes.

The multiple correlation function $\mathbb{E}\{B(X_{t_1}) \cdots B(X_{t_n})\}$ represents the spatial average of reflected Brownian motion, weighted by the magnetic field profile $B(\mathbf{r})$. It can be written according to Eq. (41) in the matrix form

$$\mathbb{E}\{B(X_{t_1}) \cdots B(X_{t_n})\} = U\left(\left[\prod_{j=1}^{n} e^{-p\Lambda t_j} \mathcal{B} e^{p\Lambda t_j}\right] e^{-p\Lambda} \tilde{U}^*\right). \tag{58}$$

The multiple correlation function does not depend on the temporal profile $f(t)$ of the magnetic field. The crucial advantage of the last relation in comparison with Eq. (41) is that the temporal and spatial averages can now be calculated separately. First, the matrix $\mathcal{B}$ is constructed for a given domain Ω and spatial profile $B(\mathbf{r})$, independently of the function $f(t)$. Second, the f-weighted time average of the multiple correlation function is calculated. This is a significant simplification for the theoretical analysis and numerical computation.

In the case of the Neumann boundary condition (11), there is no loss of magnetization at the interface, so that its steady-state distribution does exist and has to be uniform. This means that

- for any geometry of the domain Ω, the ground eigenmode corresponds to the constant eigenfunction $u_0(\mathbf{r}) = V^{-1/2}$, with eigenvalue $\lambda_0 = 0$;
- the initial density of spins is typically uniform,[51] $\rho_0(\mathbf{r}) = 1/V$.

[49] The dimensionless variable q should not be confused with the q-space parameter $\gamma g \delta / 2\pi$ introduced in the literature in the pulsed gradient spin-echo technique and the related narrow-pulse approximation (Callaghan, 1991), where δ is the duration of the narrow gradient pulses. Note that both parameters quantify the strength of the magnetic-field inhomogeneity. For instance, a linear gradient g over a characteristic length L yields a magnetic-field variation $\beta = gL$, giving $q = \gamma g T L$ (instead of $\gamma g \delta / 2\pi$). The dimensionless variable q can thus be seen as an extension of the q-space parameter for arbitrary temporal and spatial profiles of the magnetic field.

[50] For given temporal and spatial profiles $f(t)$ and $B(\mathbf{r})$, ϕ is a functional of the reflected Brownian motion X_t. In mathematical literature, similar integral forms are sometimes called "Kac functionals," while the relation between their characteristic functions and partial differential equations is known as Feynman-Kac formula (Kac, 1949, 1951; Freidlin, 1985; Majumdar, 2005).

[51] At thermal equilibrium, the initial spin density $\rho_0(\mathbf{r})$ is uniform for reflecting boundaries so that the magnetization $\mathfrak{m}(\mathbf{r}, t=0)$ is uniform too. If this is not the case (see footnote

In this case, the orthogonality of the eigenfunctions implies $U_m=\tilde{U}_m=\delta_{m,0}$ according to the definitions (39) and (40) of the vectors U and $\tilde{U}$. Moreover, the first diagonal element of the matrices $e^{-p\Lambda t_1}$ and $e^{-p\Lambda(1-t_n)}$ in Eq. (58) is equal to 1, independently of p, t_1, and t_n. All these simplifications lead to the following expression for the multiple correlation functions in the case of reflecting boundaries:

$$\mathbb{E}\{B(X_{t_1})\cdots B(X_{t_n})\} = [\mathcal{B}e^{-p(t_2-t_1)\Lambda}\mathcal{B}e^{-p(t_3-t_2)\Lambda}\mathcal{B}\cdots\mathcal{B}e^{-p(t_n-t_{n-1})\Lambda}\mathcal{B}]_{0,0}, \tag{59}$$

where the subscript 0,0 denotes the first diagonal element of the matrix product in brackets. In the next sections, we show how this representation can be applied to derive different NMR regimes of restricted diffusion. For the sake of clarity, we focus our attention on the reflecting boundary condition, bearing in mind that taking into account surface relaxation is in general straightforward but more cumbersome.

D. Temporal profiles of the magnetic field

1. Simple spin echo

The application of two identical linear gradients of duration $\delta \leqslant 1/2$ before and after the 180° rf pulse is probably the most common way to encode the diffusive motion. The temporal profile of these pulses (i.e., their "shape") is typically trapezoidal in an experiment [Fig. 4(d)] and rectangular for theoretical analysis [Fig. 4(c)]:

$$f(t) = \Theta(t) - \Theta(t-\delta) - \Theta(t-1/2) + \Theta(t-\delta-1/2), \tag{60}$$

where $\Theta(t)$ is the Heaviside step function, $\Theta(t)=1$ for $t>0$, and 0 otherwise. Two specific cases have been particularly favored by theoreticians. These are the steady profile ($\delta=1/2$) employed in the first spin-echo experiment by Hahn (1950) and the narrow-pulse profile ($\delta \ll 1/2$) first introduced by Tanner and Stejskal (1968). Whatever the value of δ, the function (60) will be called the Stejskal-Tanner temporal profile.

2. CPMG spin echoes

A train of k 180° rf pulses at times $t_j=(2j-1)/2k$, $j=1,\ldots,k$, yields the successive refocusing of spin magnetizations (i.e., echo formation) at times $\tilde{t}_j=j/k$. Due to its relatively simple implementation, this Carr-Purcell-Meiboom-Gill (CPMG) sequence is commonly used in experiments to study restricted diffusion. Its effective temporal profile can be represented as a shifted periodic repetition of the rectangular template $f_0(t)$ in Eq. (60) with $\delta=1/2$:

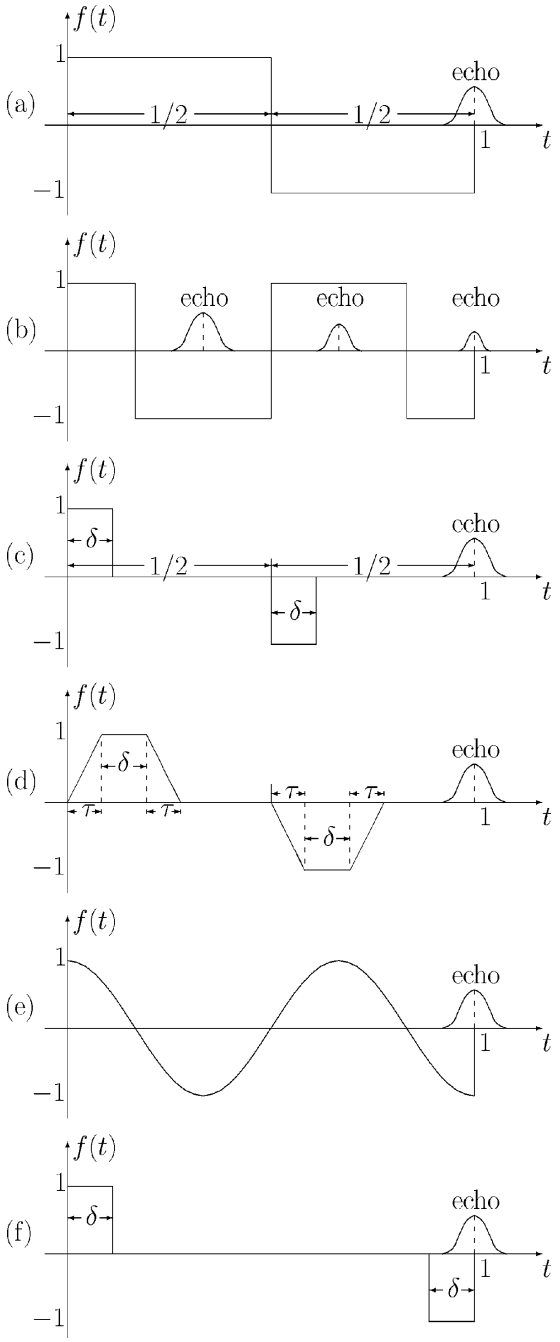

FIG. 4. Several effective temporal profiles $f(t)$: (a) steady, (b) CPMG, (c) Stejskal-Tanner rectangular, (d) trapezoidal, (e) periodic, and (f) stimulated echo. Profiles (a)–(c) correspond to the gradient shapes shown in Fig. 2 [for convenience, the rectangular profile (c) was shifted to the left]. The case (e) is related to a frequency modulated magnetic field. The 180° rf pulse is already taken into account for (a)–(e) by changing the sign of the effective profile. The stimulated echo profile (f) represents a steady gradient with three 90° rf pulses applied at times 0, δ, and $1-\delta$. In this case, the echo shown corresponds to the coherence pathway $\{1,0,-1\}$.

$$f(t) = \sum_{j=0}^{k-1} f_0(kt/2 - j + 1/4). \tag{61}$$

Its example for $k=3$ is shown in Fig. 4(b).

45), the given magnetization $\mathfrak{m}(\mathbf{r},t=0)$ can be inserted through the vector U.

3. Oscillating profile

Another interesting situation occurs when the magnetic field is applied periodically with time. In this case, one samples molecular dynamics in the frequency domain rather than in the time domain. Callaghan and Stepišnik (1995, 1996) showed that such frequency-modulated gradient spin-echo measurements provide access to much shorter time scales than that of the traditional Stejskal-Tanner profile. We consider the sine and cosine temporal profiles $f(t)=\sin(2\pi kt)$ and $f(t)=\cos(2\pi kt)$, where k is the number of periods until echo formation at time $t=1$ [Fig. 4(e)].

4. Arbitrary coherence pathway

A repetition of 180° rf pulses in a CPMG sequence is only one example among many other pulse sequences employed in current NMR experiments. In general, one can use a sequence of k rf pulses applied at times t_j. Each of them rotates a fraction of the magnetization into the transverse plane xy and a fraction into the longitudinal z direction. These fractions are determined by a flip angle α that is proportional to the duration τ and the amplitude B_1 of the rf pulse: $\alpha=\gamma B_1\tau$. Since the transverse and longitudinal components of the magnetization evolve differently in time, the subsequent pulse splits them again into transverse and longitudinal components, and so on. Each branch of this splitting cascade is called a coherence pathway and represents the history of a magnetization component over the entire pulse sequence. Since the rotation by the rf pulse is a linear transformation, the total magnetization is the sum over the various coherence pathways. This concept was first introduced by Kaiser *et al.* (1974) and further developed by others [see McDonald (1997); Hürlimann (2001); Song (2002), and references therein]. A general approach to this problem was developed by Zielinski and Sen (2003b) and Zielinski and Hürlimann (2004) who generalized the Bloch-Torrey equation to account for a chosen coherence pathway. In the case of a time-independent magnetic field, a set of coherences $\{c_j\}$ can be incorporated through the effective temporal profile $f(t)$:

$$f(t)=\sum_{j=1}^{k} c_j[\Theta(t-t_j)-\Theta(t-t_{j+1})]$$

(here $t_{k+1}=1$). If the magnetic field itself evolves in time, its temporal profile should be multiplied by the right-hand side of the above relation. For example, a typical stimulated echo sequence is formed by three 90° rf pulses at times $t_1=0$, $t_2=\delta$, and $t_3=1-\delta$, with $c_1=1$, $c_2=0$, and $c_3=-1$. The corresponding temporal profile is shown in Fig. 4(f).

It is important to stress that the signal attenuation due to restricted diffusion for arbitrary pulse sequences can be studied by the same theoretical and numerical tools as used for simple spin echoes. The only difference with respect to Hahn or CPMG echoes is that one needs to compute the transverse magnetizations for each coherence pathway and then average them with the appropriate geometrical factors [see Zielinski and Sen (2003a) for further details].

E. Spatial profiles of the magnetic field

1. Linear gradient

A linear magnetic-field gradient covers the majority of theoretical, numerical, and experimental NMR studies of the diffusive motion. If nonlinear effects can be neglected, the magnetic field of a linear gradient g is proportional to the projection of the coordinate vector $\mathbf{r}$ onto the gradient direction $\mathbf{e}_g$, i.e., $\beta=gL$ and

$$B(\mathbf{r})=(\mathbf{e}_g\cdot\mathbf{r})/L. \tag{62}$$

The dimensionless magnetic-field strength q is then

$$q=\gamma gTL. \tag{63}$$

Substitution of the linear magnetic-field gradient (62) into Eq. (47) leads to the matrix $\mathcal{B}$ which was first introduced by Robertson (1966) and then extended by Barzykin (1998, 1999) to describe signal attenuation due to restricted diffusion.

2. Parabolic magnetic field

As mentioned in Sec. II.J, nonlinear magnetic fields may have different origins such as hardware device features or susceptibility effects. In this review, the normalized isotropic parabolic magnetic field

$$B(\mathbf{r})=\mathbf{r}^2/L^2 \tag{64}$$

is considered as a paradigm for nonlinear fields. Its intensity g_2 determines the dimensionless magnetic-field strength q:

$$q=\gamma g_2TL^2. \tag{65}$$

Note that parabolic magnetic fields can also be experimentally generated (Bendel, 1990).

Other choices for the spatial profile of magnetic field can be straightforwardly implemented, at least at the numerical level. In particular, Zielinski and Sen (2000) and later Grebenkov (2007a) paid special attention to the cosine profile of the magnetic field in the one-dimensional case because it can be thought of as a crude model for microscopic field inhomogeneities induced by susceptibility differences.

F. Basic confining domains

Before proceeding with the analysis of the moments $\mathbb{E}\{\phi^n\}$, we give three examples of confining media for which the Laplace operator eigenbasis is explicitly known (Carslaw and Jaeger, 1959; Crank, 1975). Many theoretical studies of restricted diffusion are actually focused on these basic domains. Although their shapes are quite simple, the use of these structures to mimic a geometrical confinement considerably helped to comprehend the diffusive motion in more realistic media.

1. Slab

Restricted diffusion between two parallel infinite planes separated by a unit distance is the most studied case. This problem is equivalent to one-dimensional diffusion on the interval (0,1) with reflections at end points 0 and 1. The eigenbasis of the Laplace operator with Neumann boundary condition (11) is simple and well known:

$$\lambda_m = \pi^2 m^2, \quad u_m(x) = \epsilon_m \cos(\pi m x), \tag{66}$$

where $\epsilon_m = \sqrt{2}$ for $m > 0$ and $\epsilon_0 = 1$ to normalize the eigenfunctions $u_m(x)$. The eigenvalues λ_m directly give the elements of the matrix Λ.

The elements of the matrix $\mathcal{B}$ depend on the choice of the spatial profile $B(x)$ of the magnetic field. In the case of a linear gradient applied in the direction normal to the planes, $B(x) = x$, one calculates[52]

$$\mathcal{B}_{m,m'} = \frac{\epsilon_m \epsilon_{m'}}{\pi^2}[(-1)^{m+m'} - 1]\frac{m^2 + m'^2}{(m^2 - m'^2)^2} \tag{67}$$

for $m \neq m'$, and $\mathcal{B}_{m,m} = 1/2$. In particular, one gets for $m > 0$

$$\mathcal{B}_{0,m} = \sqrt{2}[(-1)^m - 1]\lambda_m^{-1}. \tag{68}$$

For the parabolic magnetic field (64), one finds

$$\mathcal{B}_{m,m'} = \begin{cases} \dfrac{2\epsilon_m \epsilon_{m'}(-1)^{m+m'}(m^2 + m'^2)}{\pi^2 (m^2 - m'^2)^2}, & m \neq m' \\ \dfrac{1}{3} + \dfrac{1}{2\pi^2 m^2}, & m = m' > 0, \end{cases} \tag{69}$$

and $\mathcal{B}_{0,0} = 1/3$. In particular, one has for $m > 0$

$$\mathcal{B}_{0,m} = 2\sqrt{2}(-1)^m \lambda_m^{-1}. \tag{70}$$

If the surface relaxation is significant, the Neumann boundary condition (11) should be replaced by a more general Fourier boundary condition (10). The eigenvalues and eigenfunctions of the Laplace operator have to be recalculated (see Table I). Although the expressions become more cumbersome and less transparent, the same concept is applied. We should mention, however, two differences with respect to the reflecting boundary condition. First, one has to use the general relation (58) for the multiple correlation functions instead of its simpler form (59). In particular, computation of the vectors U and $\tilde{U}$ is required (see Table I). Second, the matrices $\mathcal{B}$ and Λ depend on the dimensionless surface relaxivity h. If this value is fixed, there is no conceptual difference with respect to the case $h = 0$. Alternatively, if one studies the dependence of the signal (or correlation functions) on this parameter, the matrices $\mathcal{B}$ and Λ have to be recalculated for each value of h. Although their numerical computation is very rapid, theoretical analysis of the dependence on h is more difficult since the eigenvalues and eigenfunctions of the Laplace operator vary with this parameter in a complex manner.

2. Cylinder

For an infinite cylinder of unit[53] radius (or a disk), the classical representation of the eigenfunctions involves two positive indices n and k,

$$u_{nk}(r,\varphi) = \frac{\epsilon_n}{\sqrt{\pi}} \frac{\beta_{nk}}{J_n(\alpha_{nk})} J_n(\alpha_{nk} r)\cos(n\varphi), \tag{71}$$

where $J_n(z)$ are the Bessel functions of the first kind. The normalization constants β_{nk} and the positive roots α_{nk} are defined in Table I. In our notation, the pair of indices n and k can still be thought of as a single index m. For numerical implementation, one has to sort the eigenvalues $\lambda_{nk} = \alpha_{nk}^2$ in ascending order to truncate the infinite-dimensional matrices $\mathcal{B}$ and Λ. The position of the eigenmode in such a sequence can be used for its single index m.

The matrix $\mathcal{B}$ for a linear magnetic-field gradient in a cylinder was first considered by Barzykin (1999) who wrote its elements as the integrals involving the Bessel functions. In Table I, we give the explicit representation for the matrix $\mathcal{B}$ and vector U in terms of the eigenvalues λ_{nk} for linear gradient and parabolic magnetic fields.[54] Finding these eigenvalues (or roots α_{nk}) requires a numerical computation that is simple and has to be

[52] The matrix $\mathcal{B}$ was calculated for a linear magnetic-field gradient in basic domains by Barzykin (1999). This computation is elementary for a slab geometry since the eigenbasis is formed by sine and cosine functions. Note that the relations presented here correspond to restricted diffusion in an interval (0,1), while Barzykin considered a centered interval $(-1/2, 1/2)$.

[53] The physical radius L will reappear in dimensionless coefficients p, q, and h. At this point, we stress that the term "characteristic dimension of the confining medium" is somewhat ambiguous. For example, if one considers restricted diffusion in a long thin tube, the motion is essentially confined along the transverse direction (perpendicular to the axis of the tube). In this case, the characteristic dimension means the width and not the height of the tube. The situation is more complicated still in porous media when different length scales are present. We shall not discuss these subtle points here, maintaining a formal position in which L can be thought of as an appropriate length scale to get dimensionless parameters p, q, and h (their definitions are conventional as well, up to a constant factor). For a slab, L will always be the separation width of the parallel plates (length of an interval). For a cylinder and a sphere, L will be the radius.

[54] Quite surprisingly, the elements of the matrix $\mathcal{B}$ are fully determined by eigenvalues in all considered cases: for three different confining domains (slab, cylinder, and sphere) and two choices of the spatial profile (linear gradient and parabolic magnetic fields). This means that the matrix $\mathcal{B}$ (representing perturbative interaction in quantum-mechanics language) does not bring new information about these geometries with respect to the matrix Λ (unperturbed Hamiltonian of a free particle).

performed only once[55] for a chosen spatial profile of the magnetic field. The stored matrices $\mathcal{B}$ and Λ can then be used to study restricted diffusion. Note that the dimensionless surface relaxivity h is still defined by Eq. (34), where L is the physical radius of the cylinder.

3. Sphere

For a sphere of unit radius, the eigenfunctions are

$$u_{nkl}(r,\theta,\varphi) = \frac{1}{\sqrt{2\pi}} \frac{\beta_{nk}}{j_n(\alpha_{nk})} j_n(\alpha_{nk} r) P_n(\cos\theta) e^{il\varphi}, \qquad (72)$$

where $P_n(x)$ are the Legendre polynomials and $j_n(z)$ the spherical Bessel functions. The normalization constants β_{nk} and the positive roots α_{nk} are defined in Table I. Although the eigenfunctions are formally enumerated by triple index $\{n,k,l\}$, the last index l will be omitted throughout this paper since the polar coordinate φ is not involved in the following analysis. In particular, the integration over φ will simply give a factor 2π. If the spatial profile of the magnetic field was dependent on φ, this coordinate would be taken into account.

For a linear magnetic-field gradient in a sphere, Barzykin (1999) expressed the elements of the matrix $\mathcal{B}$ as integrals involving the spherical Bessel functions. In Table I, we give the explicit representation for the matrix $\mathcal{B}$ and vector U in terms of the eigenvalues λ_{nk} for linear gradient and parabolic magnetic fields. As mentioned previously, the elements of the matrices $\mathcal{B}$ and Λ have to be numerically computed only once, and then their stored values can be used for further analysis of restricted diffusion in a sphere. In what follows, we focus mainly on the reflecting boundary condition, while the accounting for surface relaxation is straightforward but more cumbersome.

IV. SLOW-DIFFUSION REGIME ($p \ll 1$)

Now we show how many classical results on diffusive NMR phenomena can be retrieved within the MCF description. We start with the analysis of the moments $\mathbb{E}\{\phi^n\}$ in the slow-diffusion regime, when the dimensionless diffusion coefficient p goes down to 0. This regime is also known as the short-time limit since $T \to 0$ implies $p \to 0$. We first calculate the leading term of the second moment and conjecture its general form for the higher-order moments. Then corrections to the leading term are discussed. Throughout this section, the surface relaxation is neglected ($h=0$).

A. Leading term of the second moment

According to the general relation (59), the second moment of the random phase ϕ can be written as

$$\mathbb{E}\left\{\frac{\phi^2}{2}\right\} = \langle [\mathcal{B} e^{-p(t_2-t_1)\Lambda} \mathcal{B}]_{0,0} \rangle_2. \qquad (73)$$

In the limit $p \to 0$, one can formally expand the exponential function in a power series up to the first order:

$$\mathbb{E}\left\{\frac{\phi^2}{2}\right\} = \langle 1 \rangle_2 \tilde{\zeta}_0 - p \langle t_2 - t_1 \rangle_2 \zeta_1 + \cdots, \qquad (74)$$

where the f-weighted time averages $\langle 1 \rangle_2$ and $\langle t_2 - t_1 \rangle_2$ are defined by Eq. (56), while the coefficients ζ_k denote the following spatial averages:

$$\zeta_k = \sum_{m=1}^{\infty} \mathcal{B}_{0,m} \lambda_m^k \mathcal{B}_{m,0} \quad (\text{for } k \leqslant 1) \qquad (75)$$

and

$$\tilde{\zeta}_0 = \zeta_0 + (\mathcal{B}_{0,0})^2. \qquad (76)$$

Note that the above expansion is formal since higher-order terms $(\mathcal{B}\Lambda^2\mathcal{B}, \mathcal{B}\Lambda^3\mathcal{B}, \ldots)$ diverge, strictly speaking (this divergence can be renormalized as discussed in the next subsections).

The coefficients $\tilde{\zeta}_0$ and ζ_1 can be further simplified by considering the spatial averages $[\mathcal{B}^2]_{0,0}$ and $[\mathcal{B}\Lambda\mathcal{B}]_{0,0}$ using a field theory technique. Indeed, the matrix $\mathcal{B}$ contains and represents a scalar field $B(\mathbf{r})$, while the matrix Λ acts like a field operator: one can replace the combination $\lambda_m u_m(\mathbf{r})$ by $-L^2 \Delta u_m(\mathbf{r})$, and then apply the second Green's formula[56] to transpose the Laplace operator to the adjacent field $B(\mathbf{r})$. For example, one starts from the definition

$$\tilde{\zeta}_0 = \frac{1}{V} \sum_{m=0}^{\infty} \int_\Omega d\mathbf{r}\, u_m(\mathbf{r}) B(\mathbf{r}) \int_\Omega d\mathbf{r}'\, u_m^*(\mathbf{r}') B(\mathbf{r}') \qquad (77)$$

[where $u_0(\mathbf{r}) = V^{-1/2}$ is substituted] and obtains

$$\tilde{\zeta}_0 = \frac{1}{V} \int_\Omega d\mathbf{r}\, B^2(\mathbf{r}), \qquad (78)$$

since there is no matrix Λ to act on the field $B(\mathbf{r})$, while the summation over m gives $\delta(\mathbf{r}-\mathbf{r}')$. For the reflecting boundary condition, this coefficient is equal to the expectation of the squared field[57]

[55] If one considers the dependence on the dimensionless surface relaxivity h, α_{nk} have to be recalculated for each value of h.

[56] If u and v are twice continuously differentiable functions in Ω, then

$$\int_\Omega d\mathbf{r}(u\Delta v - v\Delta u) = \int_{\partial\Omega} d\mathbf{r} \left(u \frac{\partial v}{\partial n} - v \frac{\partial u}{\partial n} \right).$$

[57] As a consequence, the second correlation function $\mathbb{E}\{B(X_{t_1})B(X_{t_2})\}$ can be written as

$$\mathbb{E}\{B(X_{t_1})B(X_{t_2})\} = \tilde{\zeta}_0 - \tfrac{1}{2}\mathbb{E}\{[B(X_{t_1}) - B(X_{t_2})]^2\},$$

where the second term is referred to as the field scattering kernel and quantifies the amount of field inhomogeneity experienced by diffusing spins between times t_1 and t_2 (Zielinski and Sen, 2003a; Zielinski, 2004). For a linear magnetic-field gradient, the field scattering kernel is reduced to the time-

$$\mathbb{E}\{B(X_t)^2\} = \tilde{\zeta}_0. \tag{79}$$

Note that the coefficient $\tilde{\zeta}_0$ does not contribute to the second moment since the f-weighted time average of a constant vanishes due to the rephasing condition (50).

In a similar way, one writes the definition of the coefficient ζ_1 and obtains by the second Green's formula

$$\zeta_1 = \frac{L^2}{V}\sum_{m=1}^{\infty}\left(\int_\Omega d\mathbf{r}\, u_m(\mathbf{r})\Delta B(\mathbf{r}) - \int_{\partial\Omega} d\mathbf{r}\, u_m(\mathbf{r})\frac{\partial B}{\partial n}\right) \times \int_\Omega d\mathbf{r}' u_m^*(\mathbf{r}')B(\mathbf{r}'), \tag{80}$$

where the boundary condition $\partial u_m(\mathbf{r})/\partial n = 0$ canceled another integral over the boundary $\partial\Omega$. The summation over m gives $\delta(\mathbf{r}-\mathbf{r}') - 1/V$ yielding

$$\zeta_1 = \frac{L^2}{V}\int_\Omega d\mathbf{r}\, |\nabla B(\mathbf{r})|^2, \tag{81}$$

where $\nabla B(\mathbf{r})$ is the gradient of the magnetic field $B(\mathbf{r})$. In particular, for the linear gradient profile (62), the spatial average ζ_1 is equal to 1 for any confining geometry.

The leading term of the second moment is then

$$\mathbb{E}\left\{\frac{\phi^2}{2}\right\} \simeq p\langle t_1 - t_2\rangle_2\left(\frac{L^2}{V}\int_\Omega d\mathbf{r}\, |\nabla B(\mathbf{r})|^2\right). \tag{82}$$

We stress that this slow-diffusion behavior is valid for arbitrary temporal and spatial profiles of the magnetic field. In the particular case of a Stejskal-Tanner temporal profile (60), one has

$$\langle t_1 - t_2\rangle_2 = \delta^2(1/2 - \delta/3), \tag{83}$$

and Eq. (82) is reduced to the result of Tarczon and Halperin (1985) derived for the restricted diffusion between two parallel planes by Fourier expansion of the magnetic field.

B. Higher-order moments

A similar analysis can in principle be applied to calculate the leading terms for higher moments of even orders. However, the computation becomes much more cumbersome, since a large number of particular cases have to be carefully considered. Moreover, the unbounded increase of the elements $\Lambda_{m,m}$ when $m \to \infty$ requires a renormalization procedure. From a direct computation of the fourth moment in Appendix A, we conjecture a general form of the leading terms for even order moments in the slow-diffusion regime:

$$\mathbb{E}\left\{\frac{\phi^{2n}}{(2n)!}\right\} \simeq \frac{p^n}{n!}(\langle t_1 - t_2\rangle_2)^n \frac{L^{2n}}{V}\int_\Omega d\mathbf{r}\, |\nabla B(\mathbf{r})|^{2n}. \tag{84}$$

A systematic computational technique to rigorously demonstrate this relation would be of great interest.

In the particular case of a linear magnetic-field gradient, one has $L^{2n}|\nabla B(\mathbf{r})|^{2n} = 1$, and

$$\mathbb{E}\left\{\frac{\phi^{2n}}{(2n)!}\right\} \simeq \frac{1}{n!}\left(\mathbb{E}\left\{\frac{\phi^2}{2}\right\}\right)^n, \tag{85}$$

where the leading term of the second moment is simply

$$\mathbb{E}\left\{\frac{\phi^2}{2}\right\} \simeq p\langle t_1 - t_2\rangle_2. \tag{86}$$

Substituting the leading terms (85) into the series expansion (54), one finds a compact form of the Stejskal-Tanner formula (7),

$$E \simeq \exp[-q^2 p\langle t_1 - t_2\rangle_2], \tag{87}$$

where the f-weighted time average $\langle t_1 - t_2\rangle_2$ can be written in the standard manner as

$$\langle t_1 - t_2\rangle_2 = \int_0^1 dt\left(\int_0^t dt' f(t')\right)^2. \tag{88}$$

For example, it is equal to $1/12$ for a steady temporal profile, leading to a widely used expression (3).

Interestingly, the relation (85) becomes exact in the free- (or unrestricted-)diffusion limit, when the characteristic dimension L of the confining domain goes to infinity. In this case, the dimensionless diffusion coefficient p tends to 0 while the dimensionless magnetic-field strength q diverges, but their combination q^2p remains constant. Since the moment $\mathbb{E}\{\phi^{2n}\}$ appears in front of q^{2n}, its leading term of order p^n gives a nontrivial contribution, while the correction terms of order higher than p^n vanish. As a consequence, the Gaussian form (87) is exact for a linear magnetic-field gradient in the free-diffusion limit. It is worth noting that the passage from restricted to unrestricted diffusion is in general more delicate than presented here (see Sec. VI.I).

We stress that there is a significant difference between the slow- and free-diffusion regimes, although in both cases p goes to 0. In the free-diffusion limit ($L \to \infty$ and $q \to \infty$), each combination $(q^2p)^n$ provides a nontrivial contribution, while the correction terms for each moment vanish. Brought together, these contributions lead to the Gaussian form (87). In contrast, L and q are kept fixed in the slow-diffusion limit. The second moment, being of the order of p, thus gives a major contribution, while the other moments of higher orders appear as its vanishing corrections. Consequently, the series expansion (54) of the signal becomes

$$E \simeq 1 - q^2\mathbb{E}\{\phi^2/2\} \tag{89}$$

or, with the same accuracy,

dependent diffusion coefficient measuring the average displacement of diffusing spins between times t_1 and t_2 along the gradient direction (see Sec. VI.D).

TABLE II. Several coefficients ζ_k for a slab, a cylinder, and a sphere under linear gradient and parabolic magnetic fields. Coefficients $\tilde{\zeta}_0$ and ζ_1 are directly obtained by Eqs. (78) and (81). The values of ζ_{-1} and ζ_{-2} were calculated by Robertson and Neuman for a magnetic field with a linear gradient profile. The case of the parabolic magnetic field, as well as the computation of the coefficients $\zeta_{3/2}$, ζ_2, and $\zeta_{5/2}$, is considered in Appendix B.

		Slab	Cylinder	Sphere
Linear gradient	$\zeta_{5/2}$	0	$-1/(15\sqrt{\pi})$	0
	ζ_2	0	$-1/4$	$-1/2$
	$\zeta_{3/2}$	$8/(3\sqrt{\pi})$	$4/(3\sqrt{\pi})$	$4/(3\sqrt{\pi})$
	ζ_1	1	1	1
	ζ_0	1/12	1/4	1/5
	$\tilde{\zeta}_0$	1/3	1/4	1/5
	ζ_{-1}	1/120	7/96	8/175
	ζ_{-2}	17/20160	11/512	83/7875
Parabolic field	$\zeta_{5/2}$	0	$8/(5\sqrt{\pi})$	$32/(5\sqrt{\pi})$
	ζ_2	2	6	12
	$\zeta_{3/2}$	$16/(3\sqrt{\pi})$	$32/(3\sqrt{\pi})$	$48/(3\sqrt{\pi})$
	ζ_1	4/3	2	12/5
	ζ_0	4/45	1/12	12/175
	$\tilde{\zeta}_0$	1/5	1/3	3/7
	ζ_{-1}	8/945	1/192	8/2625
	ζ_{-2}	4/4725	1/2880	148/1010625

$$E \simeq \exp[-q^2\mathbb{E}\{\phi^2/2\}]. \tag{90}$$

Although one retrieves again the Gaussian form (87), this relation is just a convenient representation of the first-order approximation (89). In the literature, there is much speculation about the slow-diffusion approximation (90). The same relation can be written in the limit $q \to 0$ with a fixed p. In both cases, its applicability is limited to relatively small values of q and p. A potential extension of its validity is called the Gaussian phase approximation. In contrast, the very same relation (87) is exact in the free-diffusion limit for any values of p and q. The confusion between the free- and slow-diffusion regimes is quite common and may be misleading. Extending the confining domain is not equivalent to reducing the diffusion length due to the presence of a nonuniform magnetic field.

For nonlinear magnetic fields, the substitution of the moments (84) in the series expansion (54) gives

$$E \simeq \frac{1}{V}\int_\Omega d\mathbf{r}\, \exp[-q^2 p\langle t_1 - t_2\rangle_2 L^2 |\nabla B(\mathbf{r})|^2]. \tag{91}$$

This relation can be seen as an extension of the local gradient approximation (23) by Tarczon and Halperin (1985) to an arbitrary temporal profile $f(t)$. Moreover, the present derivation is not restricted to the one-dimensional case [but it is based on the conjectural expression (84)]. Note that the relation (91) remains an approximation involving only the leading terms of all even moments in the slow-diffusion regime. So the free-diffusion limit ($L \to \infty$) of Eq. (91) in the case of nonlinear magnetic fields may not exist (or be trivial).

C. Correction term to the second moment

A careful revision of the derivation in Sec. IV.A reveals a gross defect. As mentioned at the beginning of this section, the series expansion of the exponential function in Eq. (73) is not mathematically allowed since the terms $\mathcal{B}\Lambda^2\mathcal{B}$, $\mathcal{B}\Lambda^3\mathcal{B}$,… are divergent due to an unbounded increase of the elements $\Lambda_{m,m}$ with m. At the same time, this very increase ensures a rapid convergence of the exponential function $\exp[-p(t_2-t_1)\Lambda]$ itself. Some renormalization procedure must therefore be introduced.

Consider again the second moment and expand the exponential function in a power series:

$$\mathbb{E}\left\{\frac{\phi^2}{2}\right\} = \sum_{m=0}^{\infty} \mathcal{B}_{0,m}\mathcal{B}_{m,0} \sum_{n=0}^{\infty} \frac{(-p)^n}{n!}\lambda_m^n \langle (t_2-t_1)^n\rangle_2. \tag{92}$$

To extract the coefficient in front of p^n, one has to exchange the order of summation. However, this operation is not allowed since it would lead to a divergent series. As we see below, this difficulty can be formally overcome by taking the sum over m up to a large but finite cutoff M:

$$\mathbb{E}\left\{\frac{\phi^2}{2}\right\} \simeq \sum_{n=0}^{\infty} \frac{(-p)^n}{n!}\langle (t_2-t_1)^n\rangle_2 \left[\sum_{m=0}^{M} \mathcal{B}_{0,m}\mathcal{B}_{m,0}\lambda_m^n\right]. \tag{93}$$

As we have already seen, the zeroth term ($n=0$) vanishes after we take the f-weighted time average, while the first term ($n=1$) converges as M goes to infinity and provides the leading contribution of order p. In contrast, higher-order terms ($n \geqslant 2$) are divergent in the limit $M \to \infty$. For three basic domains and two choices of the magnetic-field spatial profile considered above, the asymptotic behavior of the divergent sum at large M is

$$\sum_{m=0}^{M} \mathcal{B}_{0,m}\mathcal{B}_{m,0}\lambda_m^n \propto c_{\mathcal{B}}\pi^{2n-4}\frac{M^{2n-3}}{n-3/2}, \tag{94}$$

where $c_{\mathcal{B}}$ is a geometry-dependent constant (see below). The correction term is then

$$c_{\mathcal{B}}\pi^{-4}M^{-3}\sum_{n=2}^{\infty}\frac{[-p(t_2-t_1)\pi^2M^2]^n}{n!(n-3/2)}. \tag{95}$$

This series can be calculated explicitly with the help of the identity

$$\sum_{n=2}^{\infty}\frac{(-x)^n}{n!}\frac{1}{n-3/2} = x^{3/2}\int_0^x d\alpha(e^{-\alpha}-1+\alpha)\alpha^{-5/2}.$$

The substitution of $x=p(t_2-t_1)\pi^2M^2$ leads to the correction

$$c_{\mathcal{B}} p^{3/2} (t_2 - t_1)^{3/2} \pi^{-1} \Gamma(-3/2), \tag{96}$$

where the integral over α was replaced by its limit $\Gamma(-3/2) = 4\sqrt{\pi}/3$ for M (or x) going to infinity. The complete expression for the second moment is then

$$\mathbb{E}\left\{\frac{\phi^2}{2}\right\} \simeq p\zeta_1 \langle (t_1 - t_2)\rangle_2 + p^{3/2}\zeta_{3/2}\langle (t_2 - t_1)^{3/2}\rangle_2, \tag{97}$$

where

$$\zeta_{3/2} = \frac{4}{3\sqrt{\pi}} c_{\mathcal{B}}. \tag{98}$$

Note that a similar form of Eq. (97) was derived by Axelrod and Sen (2001). In Appendix B, the Laplace transform summation technique is used to obtain, in a more rigorous way, the $p^{3/2}$ dependence and higher-order correction terms for restricted diffusion in three basic domains under linear gradient and parabolic magnetic fields (see also Table II). Unlike the coefficients ζ_k with $k \leqslant 1$, the new coefficient $\zeta_{3/2}$ is not defined by Eq. (75), which is divergent for $k \geqslant 3/2$, at least for linear gradient and parabolic magnetic fields. When $k \geqslant 3/2$, the coefficients ζ_k can be defined by series expansion of the second moment in powers of p:

$$\mathbb{E}\{\phi^2/2\} = \sum_{k=2}^{\infty} (-1)^k p^{k/2} \langle -(t_2 - t_1)^{k/2}\rangle_2 \zeta_{k/2}. \tag{99}$$

Note that this expansion may contain a finite number of terms with exponentially small corrections as in the case of restricted diffusion in a slab (see Appendix B for details).

As shown in Sec. IV.A, the coefficients $\tilde{\zeta}_0$ and ζ_1 are related to the spatial averages of $B^2(\mathbf{r})$ and $|\nabla B(\mathbf{r})|^2$ over the confining domain. Axelrod and Sen (2001) adapted the heat content asymptotics for operators of Laplace type[58] to give

[58]The integral representations for coefficients $\zeta_{3/2}$, ζ_2, and $\zeta_{5/2}$, including Eq. (100), are based on results by Desjardins and Gilkey (1994) [see also Branson and Gilkey (1990); McAvity and Osborn (1991); McAvity (1992); van den Berg and Gilkey (1994)]. In our notation, one has

$$\zeta_2 = -\frac{L^4}{V}\left\{\frac{1}{2}\int_{\Omega} d\mathbf{r}\, |\Delta B|^2 + \int_{\partial\Omega} d\mathbf{r}\left[-(\Delta B)\frac{\partial B}{\partial n} + \frac{1}{2\mathcal{R}}\left(\frac{\partial B}{\partial n}\right)^2\right]\right\},$$

with the mean curvature of the boundary $\mathcal{R}^{-1} = (1/\mathcal{R}_1 + 1/\mathcal{R}_2)/2$, where $\mathcal{R}_1, \mathcal{R}_2$ are the radii of its principal curvatures. In general, $\mathcal{R}$ is a function of the boundary point $\mathbf{r}$. For a linear gradient in direction $\mathbf{e}_g$, one gets

$$\zeta_2 = -\frac{L^2}{2V}\int_{\partial\Omega} d\mathbf{r}\frac{1}{\mathcal{R}(\mathbf{r})}[\mathbf{n}(\mathbf{r})\cdot\mathbf{e}_g]^2,$$

where $\mathbf{n}$ is the unit normal to the boundary at $\mathbf{r}$. In this case, the coefficient ζ_2 is proportional to the average of the mean curvature weighted by $\cos^2(\theta)$, θ being the angle between $\mathbf{n}$ and $\mathbf{e}_g$. A microroughness of the boundary may increase this coefficient. There is a more cumbersome expression for $\zeta_{5/2}$,

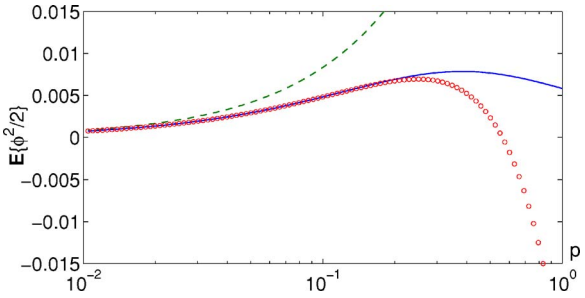

FIG. 5. (Color online) The second moment $\mathbb{E}\{\phi^2/2\}$ (solid line) as a function of p for the restricted diffusion between two parallel planes (in a slab) under a steady linear magnetic-field gradient. For small p, this moment is compared to its leading term in the slow diffusion regime with (circles) and without (dashed line) the correction term in Eq. (97). One clearly sees the importance of this correction.

$$\zeta_{3/2} = \frac{4}{3\sqrt{\pi}}\frac{L^3}{V}\int_{\partial\Omega} d\mathbf{r}\left(\frac{\partial B}{\partial n}\right)^2. \tag{100}$$

As a consequence, the coefficient $c_{\mathcal{B}}$ characterizing the asymptotic decrease of the elements $\mathcal{B}_{0,m}\mathcal{B}_{m,0}$ as $m \to \infty$ is proportional to the above integral. For example, in the case of restricted diffusion in a slab under a linear gradient, the boundary $\partial\Omega$ consists of two end points, and hence the integral is simply equal to 2 (see Table II). While the leading term is determined by the bulk average of the squared magnetic-field gradient $|\nabla B|^2$ (coefficient ζ_1), the surface average of this squared gradient is taken into account through the correction $\zeta_{3/2}$. Axelrod and Sen (2001) pointed out the physical importance of the appearance of the surface gradient $\partial B/\partial n$. In fact, the presence of paramagnetic impurities near pore boundaries or a susceptibility contrast between the wall and the bulk often make the field at the pore wall considerably different from that in the interior. These internal fields, which are in general difficult to control, may enhance the contribution of the $p^{3/2}$ correction and lead to erroneous determination of the surface-to-volume ratio (see below). On the other hand, the coefficient $\zeta_{3/2}$ may vanish for specific spatial profiles of the magnetic field for which $\partial B/\partial n = 0$ [e.g., the cosine field $\cos(\pi\kappa x)$ with a positive integer κ in a slab considered by Grebenkov (2007a)].

Although the correction of order $p^{3/2}$ vanishes in the limit $p \to 0$ faster than p, it is significant for practical applications (see Fig. 5). This correction is related to restriction of spins in the neighborhood of the interface,

$$\zeta_{5/2} = \frac{2}{15\sqrt{\pi}}\frac{L^5}{V}\int_{\partial\Omega} d\mathbf{r}\left[8\frac{\partial(\Delta B)}{\partial n}\frac{\partial B}{\partial n} - 2\left(\frac{\partial}{\partial\xi_1}\frac{\partial B}{\partial n}\right)^2 - 2\left(\frac{\partial}{\partial\xi_2}\frac{\partial B}{\partial n}\right)^2 + (2\mathcal{R}^{-2} + \mathcal{R}_1^{-2} + \mathcal{R}_2^{-2})\left(\frac{\partial B}{\partial n}\right)^2\right],$$

where ξ_1 and ξ_2 are the local boundary coordinates [for further details, see Desjardins and Gilkey (1994)].

within the diffusion length $(DT)^{1/2}$. These spins are more confined than those of the bulk, resulting in less pronounced dephasing. The fraction of these spins can be estimated as $(DT)^{1/2}/L$, explaining the additional factor $p^{1/2}$ in the $p^{3/2}$ dependence. The numerical prefactor $\zeta_{3/2}$ accounts for the specific geometry of the confining medium and for the spatial profile of the magnetic field, while the f-weighted time average $\langle(t_2-t_1)^{3/2}\rangle_2$ assesses the choice of the temporal profile $f(t)$. In this way, Eq. (97) is an extension of the results by Mitra *et al.* (1992) and by de Swiet and Sen (1994) to the general case of arbitrary temporal[59] and spatial profiles of the magnetic field (see discussion in Sec. IV.E).

D. Several temporal profiles

For the Stejskal-Tanner temporal profile $f(t)$ shown in Fig. 4(c) (two rectangular pulses of duration δ), the f-weighted time average of the function $(t_2-t_1)^\alpha$ for any positive power α can be found explicitly:

$$\langle(t_2-t_1)^\alpha\rangle_2 = \frac{2\delta^{\alpha+2}+2(1/2)^{\alpha+2}-(1/2+\delta)^{\alpha+2}-(1/2-\delta)^{\alpha+2}}{(\alpha+1)(\alpha+2)}. \tag{101}$$

Note that a similar relation was derived by Kärger *et al.* (1988) in the context of anomalous diffusion. For a steady profile [$\delta=1/2$, Fig. 4(a)], the above relation is reduced to

$$\langle(t_2-t_1)^\alpha\rangle_2 = \frac{2^{-\alpha}-1}{(\alpha+1)(\alpha+2)}. \tag{102}$$

The other case of particular interest is the narrow-pulse approximation ($\delta\to 0$), for which one derives for $\alpha>0$

$$\langle(t_2-t_1)^\alpha\rangle_2 \simeq -(1/2)^\alpha\delta^2. \tag{103}$$

The analytical computation of the f-weighted time average of the function $(t_2-t_1)^\alpha$ for arbitrary α is more difficult for other profiles, but its numerical realization is simple and straightforward. The most important case $\alpha=1$ can still be tackled theoretically. For instance, one retrieves a classical expression for the trapezoidal Stejskal-Tanner profile shown in Fig. 4(d):

$$\langle(t_1-t_2)\rangle_2 = \tfrac{1}{2}\tau^2+\tau\delta+\tfrac{1}{2}\delta^2-\tfrac{7}{15}\tau^3-\tfrac{7}{6}\tau^2\delta-\tau\delta^2-\tfrac{1}{3}\delta^3. \tag{104}$$

If the ramp time τ is equal to 0, the trapezoidal profile is replaced by the rectangular one, while the above relation is reduced to Eq. (83).

For a CPMG sequence, the 180° rf pulse is repeatedly applied to generate a train of spin echoes. The corresponding effective temporal profile $f(t)$ is a shifted periodic repetition of a chosen template $f_0(t)$ [see Fig. 4(b)]. For the classical case of a rectangular pulse $f_0(t)$, a tedious but elementary combinatorial computation gives[60]

$$\langle(t_2-t_1)^\alpha\rangle_2 = \frac{(1/2k)^{\alpha+2}}{(\alpha+1)(\alpha+2)}\left((-1)^k(2k)^{\alpha+2} - 4\sum_{j=1}^{k}(-1)^j(2j-1)^{\alpha+2} - 4\sum_{j=1}^{k-1}(-1)^j(k-j)(2j)^{\alpha+2}\right). \tag{105}$$

It is easy to check that this expression reduces to Eq. (102) for $k=1$. The computation for a general shape of the repeated pulse $f_0(t)$ can be performed numerically. In the particular case $\alpha=1$, the representation (88) allows one to show that the f-weighted time average $\langle(t_2-t_1)\rangle_2$ for a CPMG profile $f(t)$ with k echoes is k^2 times smaller than the f_0-weighted time average $\langle(t_1-t_2)\rangle_2$. For example, if one repeats k times the rectangular Stejskal-Tanner profile shown in Fig. 4(c), the corresponding time average for this CPMG sequence is

$$\langle(t_1-t_2)\rangle_2 = \frac{\delta^2(1/2-\delta/3)}{k^2}. \tag{106}$$

For $\delta=1/2$, one retrieves the Carr-Purcell relation (4).

Finally, a simple calculation of the f-weighted time average $\langle(t_1-t_2)\rangle_2$ for the sine and cosine profiles $f(t)=\sin(2\pi kt)$ and $f(t)=\cos(2\pi kt)$ gives $3/(8\pi^2k^2)$ and $1/(8\pi^2k^2)$, respectively.

E. Discussion of the correction term

As mentioned above, Eq. (97) is an extension of the results by Mitra *et al.* (1992, 1993), de Swiet and Sen (1994), and Sen *et al.* (1994). To compare the two approaches, consider restricted diffusion under a linear magnetic-field gradient, for which the Eq. (97) becomes

$$\mathbb{E}\left\{\frac{\phi^2}{2}\right\} \simeq p\langle(t_1-t_2)\rangle_2\left(1-\zeta_{3/2}p^{1/2}\frac{\langle(t_2-t_1)^{3/2}\rangle_2}{\langle(t_2-t_1)\rangle_2}\right). \tag{107}$$

Two particular choices of the temporal profiles have been discussed in the literature.

- In the narrow-pulse approximation ($\delta\to 0$), one uses Eq. (103) to write

[59] A similar kind of time dependence in the case of multiple-pulse PGSE diffusion measurements was proposed by Fordham *et al.* (1996).

[60] This temporal average for a CPMG sequence was considered by Axelrod and Sen (2001) who computed it for several values of k and α. Their results can be directly deduced from our general relation (105). To this end, Eq. (105) should be multiplied by the factor $(2k)^{\alpha+2}$ coming from a difference in notations.

$$\mathbb{E}\left\{\frac{\phi^2}{2}\right\} \simeq (p/2)\delta^2(1-\zeta_{3/2}(p/2)^{1/2}). \tag{108}$$

Taking the value $\zeta_{3/2}=8/(3\sqrt{\pi})$ for the slab geometry, one obtains

$$\mathbb{E}\left\{\frac{\phi^2}{2}\right\} \simeq (p/2)\delta^2\left(1-\frac{4}{3\sqrt{\pi}}\sqrt{DT/2}\frac{2}{L}\right), \tag{109}$$

where the definition of p was explicitly used in parentheses. In this relation, the factor $2/L$ can be associated with the surface-to-volume ratio of the slab. For a cylinder and a sphere, the value of $\zeta_{3/2}$ is twice smaller than for the slab (see Table II), so that the last factor will be $1/L$, where L is the radius. An elementary calculation shows that $1/L$ is equal to S/Vd for both cases, where d is the spatial dimension. Consequently, the above relation can be written in a unique form for three basic domains as

$$\mathbb{E}\left\{\frac{\phi^2}{2}\right\} \simeq (p/2)\delta^2\left(1-\frac{4}{3\sqrt{\pi}}\sqrt{DT/2}\frac{S}{Vd}\right). \tag{110}$$

This result was derived by Mitra *et al.* (1992) using the properties of Green's functions near a flat reflecting boundary. Equation (110) was argued to be valid for any geometry, providing a way to measure the surface-to-volume ratio of the confining medium.

- A steady magnetic-field gradient ($\delta=1/2$) is another commonly considered choice for the temporal profile. In this case, one finds

$$\langle(t_1-t_2)\rangle_2=\frac{1}{12}, \quad \frac{\langle(t_2-t_1)^{3/2}\rangle_2}{\langle(t_2-t_1)\rangle_2}=\frac{12(4-\sqrt{2})}{35}. \tag{111}$$

For a sphere, the relation (107) can be reduced to

$$\mathbb{E}\left\{\frac{\phi^2}{2}\right\} \simeq \frac{p}{12}\left(1-\sqrt{DT/2}\frac{32(2\sqrt{2}-1)}{105\sqrt{\pi}}\frac{S}{V}\right), \tag{112}$$

where $3/L$ was replaced by the surface-to-volume ratio of a sphere. One retrieves the result by de Swiet and Sen (1994), which was argued to be valid for any statistically isotropic confining medium. A similar expression can be obtained for a slab geometry,

$$\mathbb{E}\left\{\frac{\phi^2}{2}\right\} \simeq \frac{p}{12}\left(1-3\sqrt{DT/2}\frac{32(2\sqrt{2}-1)}{105\sqrt{\pi}}\frac{2}{L}\right), \tag{113}$$

where the factor $2/L$ can again be associated with the surface-to-volume ratio of the slab. Since this geometry is not isotropic, Eq. (112) can be applied only after averaging over all spatial orientations of the confining domain. This operation would suppress the additional prefactor 3 which appeared in Eq. (113). If one considers a fixed slab, the spatial orientation is not applicable, and the prefactor 3 should be taken into account. The case of a cylinder can be similarly treated.

Although the shapes of the basic domains are different, the leading and correction terms are the same for all three cases. This is a characteristic feature of the slow-diffusion regime when the signal attenuation is essentially independent of the particular confining domain geometry. One can expect that a similar relation will hold for more realistic structures in porous materials or biological tissues. Numerical studies of more complicated domains would be useful to clarify this point.

The dependence of the correction term on the surface-to-volume ratio was considered by Mitra *et al.* as a way to determine this important characteristic of porous materials by NMR. In this perspective, the extension (97) to the arbitrary temporal profile $f(t)$ of the magnetic field may become valuable. On the one hand, it allows calculation of this correction for specific gradient profiles used in experiment. On the other hand, one can attempt to optimize the temporal profile $f(t)$ in order to enhance the contribution of the correction term in a way that facilitates the determination of the surface-to-volume ratio.

At the same time, we stress a certain ambiguity of this notion in the present context. The surface-to-volume ratio naturally appears in Eq. (113) as the fraction of spins in the neighborhood of the interface, within the diffusion length $\sqrt{DT}$, with respect to the total number of spins (proportional to the volume). However, depending on the orientation with respect to the linear gradient, various regions of the boundary provide different contributions. To illustrate this point, consider restricted diffusion in a parallelepiped of size $L\times H\times H$. If the linear magnetic-field gradient is applied along the x axis, the presence of restrictive walls along the y and z directions does not change the signal attenuation. This is a simple consequence of the fact that the three components (or coordinates) of Brownian motion with normal reflections on the boundary are independent in this geometry. As a result, two planes orthogonal to the gradient direction give $2/L$ as for the slab, while the other four planes do not contribute at all. In general, the contribution of each boundary point is weighted, according to Eq. (100), by projection of the gradient direction onto the normal vector at this point. For spatially isotropic media, this weighting can be taken into account effectively by averaging over all spatial directions, which gives the supplementary prefactor $1/3$ in three dimensions. However, this averaging is not applicable to anisotropic porous systems. If we consider again the above parallelepiped, one gets Eq. (113) with ratio $2/L$, while the surface-to-volume ratio is $(2H^2+4HL)/H^2L=2/L+4/H$. By changing the dimension H of this domain, one can vary this ratio between $2/L$ and infinity. In this case, there is no apparent relationship between the geometrical surface-to-volume ratio and its physical counterpart from Eq. (113). A more profound analysis of this problem is required, especially in view of applications to systems with anisotropic internal structure like, for example, pulmonary acinus. The MCF description appears to be an efficient theoretical and numerical tool for investigating the correction terms for various confining geometries.

V. MOTIONAL-NARROWING REGIME ($p \gg 1$)

When the diffusion length $\sqrt{DT}$ exceeds the characteristic dimension L ($p \gg 1$), the diffusing spins explore the whole domain several times during their motion.[61] This regime is often called motional narrowing or motional averaging since magnetic-field inhomogeneities are averaged out by diffusion, yielding a Gaussian distribution of the accumulated phase. As this motion is strongly restricted, the geometrical properties of the confining domain become significant. In this section, we first obtain the leading terms and then discuss their corrections. As previously, the surface relaxation is neglected ($h=0$).

A. Leading terms

As with the slow-diffusion regime, we first calculate the leading term of the second moment:

$$\mathbb{E}\left\{\frac{\phi^2}{2}\right\} = \sum_{m=1}^{\infty} \mathcal{B}_{0,m} \langle e^{-p(t_2-t_1)\lambda_m}\rangle_2 \mathcal{B}_{m,0}, \tag{114}$$

where the constant term with $m=0$ (for which $\lambda_0=0$) vanished due to the rephasing condition. In the limit $p\to\infty$, the exponential function in Eq. (114) converges to a delta function allowing it to be replaced by $(p\lambda_m)^{-1}\delta(t_2-t_1)$ in a first approximation.[62] One gets

$$\mathbb{E}\left\{\frac{\phi^2}{2}\right\} \simeq p^{-1}\langle \delta(t_2-t_1)\rangle_2 \sum_{m=1}^{\infty} \mathcal{B}_{0,m}\lambda_m^{-1}\mathcal{B}_{m,0}. \tag{115}$$

The f-weighted time average of the delta function is

$$\langle \delta(t_2-t_1)\rangle_2 = \int_0^1 dt\, f^2(t). \tag{116}$$

The sum over m, denoted as ζ_{-1} according to Eq. (75), depends on the confining geometry and the spatial profile $B(\mathbf{r})$ of the magnetic field. In the next subsection, this constant will be calculated explicitly for basic confining domains and different spatial profiles.

The leading term of the second moment in the motional narrowing regime is then

$$\mathbb{E}\left\{\frac{\phi^2}{2}\right\} \simeq p^{-1}\zeta_{-1}\int_0^1 dt\, f^2(t). \tag{117}$$

In a similar way, one can compute the leading terms for higher-order moments. From a direct computation of the fourth moment in Appendix C, we conjecture their general form for even orders:

$$\mathbb{E}\left\{\frac{\phi^{2n}}{(2n)!}\right\} \simeq \frac{p^{-n}}{n!}\zeta_{-1}^n\left(\int_0^1 dt\, f^2(t)\right)^n, \tag{118}$$

but a systematic computational technique is required for a rigorous demonstration of this relation. Bringing together the leading terms of even moments, one derives an extension of the classical result for the motional-narrowing regime:

$$E \simeq \exp\left(-\frac{q^2}{p}\zeta_{-1}\int_0^1 dt\, f^2(t)\right). \tag{119}$$

The dependence of $\ln E$ as a function of q^2/p was first outlined by Robertson (1966) for one-dimensional diffusion under a steady linear gradient, and then extended to the case of a cylinder and a sphere by Neuman (1974). In fact, Neuman's approach might be directly applied to any confining domain.

B. Corrections to the leading term

While the leading asymptotic behavior in Eqs. (117) and (118) is general for any (non-narrow) temporal profile $f(t)$, the correction terms strongly depend on the particular choice of the function $f(t)$. To illustrate this point, we calculate the correction to the leading term of the second moment for two typical profiles used in NMR experiments.

1. Stejskal-Tanner temporal profile

Once the temporal profile $f(t)$ is chosen, the f-weighted time average of the exponential function in Eq. (114) can be calculated explicitly. In particular, for the two rectangular pulses shown in Fig. 4(c), one gets

$$\langle e^{-p\lambda_m(t_2-t_1)}\rangle_2 = \frac{2\delta}{p\lambda_m} - \frac{2+e^{-p\lambda_m(1/2+\delta)}+e^{-p\lambda_m(1/2-\delta)}-2e^{-p\lambda_m/2}-2e^{-p\lambda_m\delta}}{p^2\lambda_m^2}. \tag{120}$$

The right-hand side of this relation was proposed by Murday and Cotts (1968) to calculate the self-diffusion coefficient of confined liquid lithium within a spherical restriction.

The spatial average of this function with $\mathcal{B}_{0,m}\mathcal{B}_{m,0}$ (summation over m from 1 to infinity) gives the second

[61] To avoid possible ambiguity, we stress again that the confining domain is considered here to be bounded. This situation is significantly different with respect to a commonly used open model of porous structure, e.g., in rocks (Hürlimann *et al.*, 1994; Latour *et al.*, 1995). In the latter case, diffusion of nuclei is restricted within small cavities that are interconnected, forming an infinite pore network. In the long-time limit, nuclei can travel between several pores, but they never explore the whole structure. The results of this section are not applicable to such pore networks (for further discussion, see Sec. VI.I).

[62] This approximation is applicable for *non-narrow* temporal profiles. On the opposite, the specific properties of a *narrow* profile formed by very short-time gradient pulses can be employed to calculate the time averages. For instance, for Stejskal-Tanner rectangular profile with $\delta\to 0$, one has

$$\langle e^{-p\lambda_m(t_2-t_1)}\rangle_2 \simeq \delta^2[1-e^{-p\lambda_m/2}].$$

In this case, there is no p^{-1} behavior. Since the results for narrow profiles are easier to obtain using the narrow-pulse approximation, we do not consider them in this section.

moment $\mathbb{E}\{\phi^2/2\}$. If p is large enough, the exponential functions in Eq. (120) rapidly vanish since the eigenvalues λ_m progressively increase. For $\delta<1/2$, one obtains the second moment to a very good approximation:

$$\mathbb{E}\left\{\frac{\phi^2}{2}\right\} \simeq \zeta_{-1}(2\delta)p^{-1} - 2\zeta_{-2}p^{-2}, \tag{121}$$

where both coefficients ζ_{-1} and ζ_{-2} are defined by Eq. (75). In addition, one can recognize the factor 2δ as the integral of the squared temporal profile (60) in this case:

$$\int_0^1 dt\, f^2(t) = 2\delta. \tag{122}$$

One sees that, for the second moment in the motional-narrowing regime with the Stejskal-Tanner temporal profile (60), all the possible complexity of the confining geometry and the magnetic-field spatial distribution is represented via the two constants ζ_{-1} and ζ_{-2} only. Moreover, if q is small or p is relatively large, the second moment gives the most significant contribution to the signal, so that one can use the first-order approximation

$$E \simeq \exp\left[-\frac{q^2}{p}[\zeta_{-1}(2\delta) - 2\zeta_{-2}p^{-1}]\right]. \tag{123}$$

For the particular case of a steady profile ($\delta=1/2$), the exponential function $e^{-p\lambda_m(1/2-\delta)}$ in Eq. (120) is constant, and one has

$$\mathbb{E}\left\{\frac{\phi^2}{2}\right\} = \sum_{m=1}^{\infty} \mathcal{B}_{0,m}\mathcal{B}_{m,0}\left(\frac{1}{p\lambda_m} - \frac{e^{-p\lambda_m} - 4e^{-1/2p\lambda_m} + 3}{p^2\lambda_m^2}\right). \tag{124}$$

This very same structure of the second moment was given by Robertson [compare to Eq. (18) taking λ_m and $\mathcal{B}_{0,m}$ from Eqs. (66) and (68)], and then reproduced by others. For large enough p, one gets

$$\mathbb{E}\left\{\frac{\phi^2}{2}\right\} \simeq \zeta_{-1}p^{-1} - 3\zeta_{-2}p^{-2}. \tag{125}$$

In this case, the integral of the squared temporal profile is equal to 1. Comparison between this asymptotic result and the precise numerical computation of the second moment is shown in Fig. 6. One can see that Eq. (125) is applicable even for p around 1, where the motional-narrowing regime was not expected to be valid.

Interestingly, Eq. (124) can already be recognized in the paper of Tarczon and Halperin (1985) where there was no sign of the Laplace operator eigenbasis. In that work, restricted diffusion over an interval was considered for a steady magnetic field of arbitrary spatial profile periodically extended over the coordinate axis. The elements $\mathcal{B}_{0,m}$ then appeared as Fourier coefficients of the spatial profile $B(\mathbf{r})$, while the time average (120) was derived by a specific and cumbersome technique. Similarly, Eq. (81) for ζ_1 was also found in the one-dimensional case by Tarczon and Halperin (1985).

Both coefficients ζ_{-1} and ζ_{-2} in the case of a linear magnetic-field gradient were found by Robertson (1966) for a slab and by Neuman (1974) for a cylinder and a sphere. Their values are reproduced in Table II.[63] The calculation for the parabolic magnetic field (64) can be performed in a similar way. In the case of a slab geometry, one uses the explicit formulas (66) and (70) for λ_m and $\mathcal{B}_{0,m}$ to get

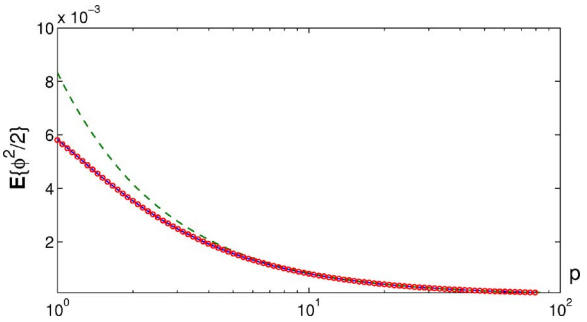

FIG. 6. (Color online) The second moment $\mathbb{E}\{\phi^2/2\}$ (solid line) as a function of p for the restricted diffusion between two parallel planes (in a slab) under steady linear magnetic-field gradient. For large p, the second moment is compared to its leading term in the motional narrowing regime with (circles) and without (dashed line) correction term in Eq. (125).

$$\zeta_{-1} = \frac{8}{\pi^6}\sum_{m=1}^{\infty}\frac{1}{m^6} = \frac{8}{945},$$

$$\zeta_{-2} = \frac{8}{\pi^8}\sum_{m=1}^{\infty}\frac{1}{m^8} = \frac{4}{4725}. \tag{126}$$

Note that the above value of the coefficient ζ_{-1} for the parabolic magnetic field was found by Zielinski and Sen (2000). A general technique to compute these coefficients is presented in Appendix B (the values found are shown in Table II).

2. CPMG temporal profile

Similar results can be deduced for a CPMG sequence producing a train of k echoes, for which the effective temporal profile is given by Eq. (61). Brown and Fantazzini (1993) computed the signal attenuation by assuming a given form of the time correlation function, while Axelrod and Sen (2001) explicitly calculated the temporal average of the exponential function. In our notations, their result reads as

$$\langle e^{-p\lambda_m(t_2-t_1)}\rangle_2 = \frac{1}{p\lambda_m} - \frac{1}{p^2\lambda_m^2}\left[2k\tanh(p\lambda_m/2k) + [1-(-1)^k e^{-p\lambda_m}]\times\left(1-\frac{1}{\cosh(p\lambda_m/2k)}\right)^2\right]. \tag{127}$$

In the limit $p\to\infty$, the only remaining terms are

[63] Note a typographical error in Neuman (1974): for a cylinder, the coefficient ζ_{-1} was misprinted as 7/296 instead of 7/96.

$$\langle e^{-p\lambda_m(t_2-t_1)}\rangle_2 \simeq \frac{1}{p\lambda_m} - \frac{2k+1}{p^2\lambda_m^2}, \tag{128}$$

yielding

$$\mathbb{E}\left\{\frac{\phi^2}{2}\right\} \simeq \zeta_{-1}p^{-1} - (2k+1)\zeta_{-2}p^{-2}. \tag{129}$$

To avoid possible ambiguity, it is useful to remember that the time T was defined as the moment of signal acquisition. Here T is the moment of the last kth echo. For CPMG experiments, however, it is natural to express formulas in terms of the echo period τ. The substitution of $T=k\tau$ and of p and q from their definitions leads to the following explicit signal attenuation for the case of a linear magnetic-field gradient g (within the GPA):

$$E \simeq \exp\left[-\frac{\gamma^2 g^2 L^4 \tau}{D}\left(k\zeta_{-1} - (2k+1)\zeta_{-2}\frac{L^2}{D\tau}\right)\right].$$

Further discussion of this behavior can be found in Sen *et al.* (1999).

3. Oscillating temporal profile

In the case of the sine temporal profile $f(t)=\sin(2\pi kt)$, one gets

$$\langle e^{-p\lambda_m(t_2-t_1)}\rangle_2 = \frac{1}{2}\frac{p^3\lambda_m^3 + 4\pi^2k^2p\lambda_m + 8\pi^2k^2}{(p^2\lambda_m^2+4\pi^2k^2)^2} - \frac{4\pi^2k^2e^{-p\lambda_m}}{(p^2\lambda_m^2+4\pi^2k^2)^2}. \tag{130}$$

The second term vanishes rapidly in the limit $p\to\infty$, while the first term can be expanded into a series in powers of p^{-1}:

$$\langle e^{-p\lambda_m(t_2-t_1)}\rangle_2 = \tfrac{1}{2}p^{-1}\lambda_m^{-1} - 2\pi^2k^2p^{-3}\lambda_m^{-3} + O(p^{-4}). \tag{131}$$

The prefactor $1/2$ in front of p^{-1} is indeed equal to the integral of the squared temporal profile $f(t)$ as required. In contrast to the case of the Stejskal-Tanner profile, the correction terms start from p^{-3} and contain higher orders in a series expansion.

A similar analysis for a cosine temporal profile $f(t)=\cos(2\pi kt)$ leads to a different result:

$$\langle e^{-p\lambda_m(t_2-t_1)}\rangle_2 = \frac{1}{2}\frac{p\lambda_m(p^2\lambda_m^2 - 2p\lambda_m + 4\pi^2k^2)}{(p^2\lambda_m^2+4\pi^2k^2)^2} - \frac{p^2e^{-p\lambda_m}}{(p^2\lambda_m^2+4\pi^2k^2)^2}. \tag{132}$$

In the limit $p\to\infty$, one gets

$$\langle e^{-p\lambda_m(t_2-t_1)}\rangle_2 = \tfrac{1}{2}p^{-1}\lambda_m^{-1} - p^{-2}\lambda_m^{-2} - 2\pi^2k^2p^{-3}\lambda_m^{-3} + O(p^{-4}), \tag{133}$$

where the first correction to the leading term p^{-1} is of order p^{-2}. While the leading term is always of order $1/p$, independently of the temporal profile, the form of correction terms strongly depends on a particular choice of $f(t)$.

VI. DISCUSSION

In the two previous sections, the MCF description has been applied to retrieve, extend, and reinterpret many classical results on diffusive NMR phenomena. After a sketch of the numerical implementation of this approach, we discuss some related issues as well as open or poorly understood questions which can now be better investigated.

A. Numerical implementation

The implementation of the MCF description for a numerical analysis is straightforward and simple for the basic domains: a slab, a cylinder, and a sphere. The matrices $\mathcal{B}$ and Λ, determining all moments $\mathbb{E}\{\phi^n\}$, have to be computed numerically only once for a chosen confining geometry and spatial profile of the magnetic field. The signal can then be found through the series expansion (54).

Interestingly, the numerical computation of the signal can be performed in a much simpler way. The technique that we summarize was developed by Robertson and further extended by Barzykin (1998, 1999) to study restricted diffusion under a linear magnetic field gradient. To illustrate the idea, consider the Bloch-Torrey equation (9) with time-independent magnetic field $\beta B(\mathbf{r})$:

$$\left(\frac{\partial}{\partial t} - D\Delta + i\gamma\beta B(\mathbf{r})\right)\mathfrak{m}(\mathbf{r},t) = 0. \tag{134}$$

In general, the Fourier boundary condition (10) is imposed.[64] The magnetization $\mathfrak{m}(\mathbf{r},t)$ can be expanded over the Laplace operator eigenbasis:

$$\mathfrak{m}(\mathbf{r},t) = \sum_{m'=0}^{\infty} c_{m'}(t)u_{m'}(\mathbf{r}). \tag{135}$$

The macroscopic signal E is then obtained by integrating $\mathfrak{m}(\mathbf{r},T)$ over the domain Ω with a given pickup function $\tilde{\rho}(\mathbf{r})$:

$$E = \sum_{m'=0}^{\infty} c_{m'}(T)\int_\Omega d\mathbf{r}\, u_{m'}(\mathbf{r})\tilde{\rho}(\mathbf{r}) = V^{1/2}\sum_{m'=0}^{\infty} c_{m'}(T)\tilde{U}_{m'}, \tag{136}$$

where the infinite-dimensional vector $\tilde{U}$ was defined by Eq. (40).

[64] We recall a formal analogy with quantum mechanics, when the Laplace operator can be interpreted as a Hamiltonian of a free particle, while the last term represents a perturbative interaction.

To find the unknown coefficients $c_{m'}(T)$, one substitutes the expansion (135) into the Bloch-Torrey equation (134), multiplies it by the eigenfunction $u_m^*(\mathbf{r})$, and integrates over Ω. These operations lead to a set of ordinary differential equations

$$\frac{d}{dt}c_m(t) + \frac{D\lambda_m}{L^2}c_m(t) + i\gamma\beta\sum_{m'=0}^{\infty}\mathcal{B}_{m,m'}c_{m'}(t) = 0, \quad (137)$$

where the matrix $\mathcal{B}$ is defined by Eq. (47).[65] The initial condition $\mathfrak{m}(\mathbf{r},t=0)=\rho_0(\mathbf{r})$ implies that

$$c_m(0) = \int_\Omega d\mathbf{r}\,\rho_0(\mathbf{r})u_m^*(\mathbf{r}) = V^{-1/2}U_m^*, \quad (138)$$

where the definition (39) of the vector U was used.

The coefficients $c_m(t)$ can be thought of as components of an infinite-dimensional vector $C(t)$, and the above set of equations become

$$T\frac{d}{dt}C(t) = -(p\Lambda + iq\mathcal{B})C(t), \quad (139)$$

where the matrix Λ is defined by Eq. (42). The solution of this differential equation is simply

$$C(t) = \exp[-(p\Lambda + iq\mathcal{B})t/T]C(0). \quad (140)$$

Bringing together the above relations, one can write the macroscopic signal in the compact form of a scalar product[66]

$$E = (\tilde{U}\exp[-(p\Lambda + iq\mathcal{B})]U^*). \quad (141)$$

A particular simplification can be achieved for the Neumann boundary condition. Since the initial density is uniform [and $\tilde{\rho}(\mathbf{r})=1$], one gets $U_m=\tilde{U}_m=\delta_{m,0}$. In this case, the macroscopic signal is simply equal to the first diagonal element of the exponential matrix:

$$E = [e^{-p\Lambda - iq\mathcal{B}}]_{0,0}. \quad (142)$$

We stress that Eqs. (141) and (142) are exact for any time-independent magnetic field.

In fact, this result can be applied to numerically compute the signal for a given time-dependent profile $f(t)$. For this purpose, the time interval [0,1] is divided into a large number K of subintervals of duration $\tau=1/K$. On the kth subinterval, the function $f(t)$ is approximated by a constant $f(k\tau)$. The signal can be numerically found with[67]

$$E \simeq \left(\tilde{U}\left[\prod_{k=0}^{K}\exp\{-\tau[p\Lambda + iqf(k\tau)\mathcal{B}]\}\right]U^*\right) \quad (143)$$

or, for the Neumann boundary condition, with

$$E \simeq \left(\prod_{k=0}^{K}\exp\{-\tau[p\Lambda + iqf(k\tau)\mathcal{B}]\}\right)_{0,0}. \quad (144)$$

This is an approximate representation of the time-ordered product in Eq. (24). On the other hand, this relation appears as an extension of Barzykin's numerical approach to an arbitrary spatial profile $B(\mathbf{r})$ of the magnetic field.

The efficiency of this numerical technique is based upon an unbounded increase of the eigenvalues λ_m with m: the matrix Λ representing the argument of the exponential function allows one to truncate the infinite-dimensional matrices $\mathcal{B}$ and Λ to moderate sizes. A very rough estimate of the truncation size $\tilde{m}$ could be given by the strong inequality

$$p\lambda_{\tilde{m}} \gg q. \quad (145)$$

It states that the "damping" real part $p\Lambda$ of the exponential function in Eq. (143) or (144) dominates its "oscillating" imaginary part $iq\mathcal{B}$. This inequality shows that the matrices Λ and $\mathcal{B}$ can be truncated to smaller sizes for smaller q and larger p. For instance, many results corresponding to the Gaussian phase approximation (for $q\ll 1$) can be computed with $\tilde{m}\leqslant 10$. In contrast, the study of the localization regime ($q\gg 1$) requires large matrices. Note that this study would be much easier for a slab than for a cylinder or a sphere. In fact, Weyl's asymptotics for eigenvalues states that $\lambda_m \propto m^{2/d}$, where d is the dimension of the space [see, for instance, Lapidus (1991)]. As a consequence, the condition (145) is easier to satisfy in dimension $d=1$ (smaller $\tilde{m}$ is needed).

Once the matrices $\mathcal{B}$ and Λ are constructed, computation of the matrix product in Eq. (143) or (144) with the help of mathematical softwares such as MATLAB, MAPLE, or MATHEMATICA is rapid and very accurate. This technique can be readily implemented for basic domains for which the matrices $\mathcal{B}$ and Λ are explicitly known.[68] The surface relaxivity h can also be included.[69] When the

[65] In the language of quantum mechanics, $\mathcal{B}_{m,m'}$ are nothing else than the matrix elements of the interaction $B(\mathbf{r})$ in the unperturbed basis $\{u_m(\mathbf{r})\}$ of the Hamiltonian of a free particle.

[66] The surface relaxation attenuates the signal even in the case when no diffusion-sensitizing magnetic field is applied ($q=0$). It is then convenient to normalize the signal with $q>0$ by the signal at $q=0$,

$$E_{\text{norm}} = \frac{(\tilde{U}\exp[-(p\Lambda + iq\mathcal{B})]U^*)}{(\tilde{U}\exp[-p\Lambda]U^*)}.$$

This normalization is not needed for the Neumann boundary condition, for which $(\tilde{U}\exp[-p\Lambda]U^*)=1$.

[67] It is worth noting that the matrices $\mathcal{B}$ and Λ do not commute, so that the product in Eq. (143) cannot be reduced to

$$\exp\left[-\tau\sum_{k=0}^{K}[p\Lambda + iqf(k\tau)\mathcal{B}]\right].$$

[68] This technique has been implemented for MATLAB software and called the Multiple Correlation Function Approach Library (MCFAL). This library is freely available at http://pmc.polytechnique.fr/pagesperso/dg/MCF/MCF_e.htm

[69] It is worth noting that the eigenvalues λ_m with increasing m become less dependent on the surface relaxivity h. This is il-

geometry of the confining domain Ω is more complex, one needs first to compute the eigenbasis of the Laplace operator in order to build $\mathcal{B}$ and Λ. This is a classical problem in applied mathematics for which a number of numerical algorithms have been developed.[70] As for the basic domains, one needs only a relatively small number of eigenmodes.

Note that the general matrix representation (59) of the moments $\mathbb{E}\{\phi^n\}$ could be derived from Eq. (144) in the limit $\tau \to 0$ and $K \to \infty$. The main steps of this derivation for a similar case of the multiple propagator approach are shown in Appendix D.

B. Odd-order moments

The series expansion (54) of the signal E involves, in general, both even and odd moments $\mathbb{E}\{\phi^n\}$ of the random phase ϕ. In the literature, the odd moments forming the imaginary part of the signal somehow disappear: some authors proposed heuristic arguments or specific assumptions to neglect them (e.g., inversion symmetry of the confining domain), and others simply ignored them. In this subsection, we discuss why the odd moments do not contribute, at least for typical cases considered in the literature. At the same time, several counterexamples will be given to illustrate possible deviations from this common belief.

1. First moment

Although the results of this subsection could be derived directly from Eq. (59), we first provide an intuitive explanation for why odd moments may or may not disappear under certain conditions. For the sake of simplicity, we consider the case without surface relaxation, when the density $\rho_0(\mathbf{r})$ is uniform. The first moment $\mathbb{E}\{\phi\}$ is equal to the f-weighted time average of the expectation $\mathbb{E}\{B(X_t)\}$. Here the magnetic-field spatial profile $B(\mathbf{r})$ is averaged over all possible trajectories of reflected Brownian motion starting from a uniformly distributed initial position. In other words, the expectation $\mathbb{E}\{B(X_t)\}$ can be written as

$$\mathbb{E}\{B(X_t)\} = \frac{1}{V}\int_\Omega d\mathbf{r}\, v(\mathbf{r},t), \tag{146}$$

where $v(\mathbf{r},t)$ is the expectation for the reflected Brownian motion starting from a fixed point $\mathbf{r}$:

$$v(\mathbf{r},t) = \mathbb{E}\{B(X_t)|X_0 = \mathbf{r}\}. \tag{147}$$

This function is a solution of the diffusion equation

$$\left(\frac{\partial}{\partial t} - D\Delta\right) v(\mathbf{r},t) = 0, \tag{148}$$

with the Neumann boundary condition and $v(\mathbf{r},t=0) = B(\mathbf{r})$. Therefore the function $v(\mathbf{r},t)$ can be interpreted as a density of some kind of pseudoparticles diffusing in domain Ω with a reflecting boundary. The magnetic field $B(\mathbf{r})$ formally appears as the initial density of these pseudoparticles, while the expectation $\mathbb{E}\{B(X_t)\}$ gives the total number of pseudoparticles at time t. Note that this is only a formal illustration since the magnetic field $B(\mathbf{r})$ can be negative. Since the boundary is reflecting, there is no loss of these pseudoparticles, and $\mathbb{E}\{B(X_t)\}$ is constant for any t:

$$\mathbb{E}\{B(X_t)\} = \mathbb{E}\{B(X_0)\} = \frac{1}{V}\int_\Omega d\mathbf{r}\, B(\mathbf{r}). \tag{149}$$

This result could be derived directly from Eq. (59) for $n=1$:

$$\mathbb{E}\{B(X_t)\} = [\mathcal{B}]_{0,0} = \frac{1}{V}\int_\Omega d\mathbf{r}\, B(\mathbf{r}). \tag{150}$$

From this point, different situations can be considered:

(i) If the magnetic field $B(\mathbf{r})$ is such that its integral over domain Ω is equal to 0, then the first moment $\mathbb{E}\{\phi\}$ is zero for any temporal profile $f(t)$. This is the case for a linear gradient $B(\mathbf{r}) = r\cos\theta$ in a cylinder and a sphere. However, this condition is limited to symmetric domains and linear gradients. For example, it is impossible to satisfy this condition for a linear gradient in a nonsymmetric domain or for a parabolic magnetic field.[71]

(ii) If the temporal profile $f(t)$ satisfies the rephasing condition (50), the constant expectation $\mathbb{E}\{B(X_t)\}$ vanishes for any spatial profile $B(\mathbf{r})$ of the magnetic field, leading to $\mathbb{E}\{\phi\}=0$.

(iii) If none of the above conditions are satisfied, the first moment $\mathbb{E}\{\phi\}$ is not zero, providing a nontrivial contribution to the imaginary part of the signal E.

Nontrivial contribution from the first moment can also be expected for the Fourier boundary condition in non-

lustrated by the first relation in footnote 47. Since the eigenfunctions u_m oscillate more rapidly with increasing m, the contribution of the first integral with $|\nabla u_m|^2$ becomes dominant on the second integral with $|u_m|^2$, and the dependence on h vanishes. This property may be useful for theoretical and numerical analysis.

[70] Investigation of the Laplace operator eigenbasis is a vast domain ranging from rigorous analysis of partial differential equations to approximate schemes and practical applications. Depending on the specific problem at hand, different numerical methods can be used, from sparse matrix techniques to variational principles. For this reason, it is difficult to give a thorough list of references. In addition to classical books on numerical methods, one may see Ciarlet (1987); Wesseling (1991); Saad (1992); Trottenberg *et al.* (2001); Buhmann (2003); Heuveline (2003); Platte and Driscoll (2004).

[71] Of course, the averaged magnetic field in Eq. (150) can always be made 0 by adding a constant to the spatial profile $B(\mathbf{r})$. But the contribution of this constant vanishes only under the rephasing condition that brings us to the second item.

symmetric domains. In this case, $\mathbb{E}\{B(X_t)\}$ can still be interpreted as the total number of pseudoparticles which, in turn, decreases in time due to surface relaxation. As a consequence, its f-weighted time average (i.e., the first moment) may contribute.

These examples show that the situation with odd moments is not as simple as is commonly believed. Moreover, the above analysis cannot be directly applied to higher-order moments. For instance, the zero integral of the magnetic-field spatial profile ($\mathcal{B}_{0,0}=0$) is not sufficient to cancel higher odd moments since $\mathcal{B}_{m,m}$ are not necessarily zero for $m>0$. On the other hand, their cancellation due to the rephasing condition (50) remains an open question. In the next subsection, we give the proof in one case, as more detailed analysis, which would clarify the role of these moments, is beyond the scope of this review.

2. Antisymmetric temporal profiles

The most interesting situation corresponds to a cancellation of odd moments for an arbitrary spatial profile of the magnetic field due to the rephasing condition. However, its derivation is much more difficult and would require a more profound study of the f-weighted time averages. Here we focus on a specific case when the temporal profile is antisymmetric with respect to the point 1/2:

$$f(1-t) = -f(t). \tag{151}$$

A simple algebraic proof is based on the approximate relation of Sec. VI.A. Initially, the matrix product in Eq. (144) can be separated into two parts: the first $K/2$ factors remain unchanged, while the next $K/2$ factors are modified according to a simple matrix identity $XY=(Y^*X^*)^*$:

$$E \simeq \left[\prod_{k=0}^{K/2} e^{-\tau[p\Lambda + iq\mathcal{B}f(k\tau)]} \left(\prod_{k=0}^{K/2} e^{-\tau[p\Lambda - iq\mathcal{B}f((K-k)\tau)]} \right)^* \right]_{0,0}. \tag{152}$$

In the second product, one uses $f((K-k)\tau)=-f(k\tau)$ to obtain

$$E \simeq \left[\left(\prod_{k=0}^{K/2} e^{-\tau[p\Lambda + iq\mathcal{B}f(k\tau)]} \right) \left(\prod_{k=0}^{K/2} e^{-\tau[p\Lambda + iq\mathcal{B}f(k\tau)]} \right)^* \right]_{0,0}. \tag{153}$$

It is clear now that the matrix in large square brackets is real valued as the product of two matrices, one of them being the complex conjugate of the other. Consequently, the imaginary part of the signal E is zero, so that all odd moments vanish. To complete the derivation, one takes the limit $\tau \to 0$ (and $K \to \infty$).

Another demonstration of the odd moment cancellation for antisymmetric temporal profiles was given by Bergman and Dunn (1995). It is based on the fact that any possible trajectory X_t is as probable as the time reversed trajectory $\tilde{X}_t \equiv X_{1-t}$ when $h=0$. This property follows from the symmetry of the propagator, $G_t(\mathbf{r},\mathbf{r}') = G_t(\mathbf{r}',\mathbf{r})$, and the Markovian nature of Brownian motion. For the antisymmetric function $f(t)$, contributions of any trajectory X_t and its time reversed counterpart $\tilde{X}_t$ to the total phase ϕ differ only by the sign. As a result, these contributions compensate each other for odd moments.

Since the usual temporal profiles (Stejskal-Tanner, sine, etc.) satisfy the condition (151) or its variations, the problem of the odd moments in such typical cases is now solved. We conjecture that the rephasing condition (50) is generally sufficient for cancellation of the odd moments. Its mathematical demonstration remains an interesting open problem.

C. Cumulant expansion

Knowledge of the even moments of the random phase ϕ gives the macroscopic signal in the form of a series expansion (54). The basic properties of the exponential function allow one to find the series representation of the logarithm of the signal, which is known as the cumulant expansion:

$$\ln E = \sum_{n=1}^{\infty} \frac{(-q^2)^n}{(2n)!} < \phi^{2n} >_c. \tag{154}$$

Here $<\phi^{2n}>_c$ denote so-called cumulants or cumulant moments which can be expressed through the ordinary moments, for example,

$$\begin{aligned} <\phi^2>_c &= \mathbb{E}\{\phi^2\}, \\ <\phi^4>_c &= \mathbb{E}\{\phi^4\} - 3(\mathbb{E}\{\phi^2\})^2 \end{aligned} \tag{155}$$

(under the condition that odd moments are zero). The characteristic feature of the cumulant expansion is that fourth- and higher-order cumulant moments are exactly zero for a Gaussian phase ϕ. In this case, the cumulant expansion is naturally truncated to the second moment, and one obviously retrieves the Gaussian form of the signal. If the phase is not Gaussian, the cumulant expansion provides higher-order corrections to the Gaussian behavior. The fourth- and higher-cumulant moments indicate to which extent the Gaussian phase approximation remains valid. For this reason, the cumulant expansion has been preferred by some to the ordinary expansion. At the same time, it should be clear that both representations contain exactly the same information about the signal E.

In spite of an apparent convenience of the cumulant expansion, Frøhlich *et al.* (2006) pointed out its mathematical "defect": a limited convergence radius. This means that the series expansion (154) converges only inside a certain disk in the complex plane of values q. In other words, there exists a critical value q_c such that the above relation is divergent for $q \geqslant q_c$ [see Frøhlich *et al.* (2006) for a more detailed discussion on this topic]. At the same time, the ordinary expansion (54) is absolutely convergent for any value of q.

D. Apparent diffusion coefficient

Under a weak diffusion-sensitizing magnetic field ($q \ll 1$), the signal is mainly determined by the second moment $\mathbb{E}\{\phi^2/2\}$, while higher-order moments can be neglected,

$$E \simeq 1 - q^2\mathbb{E}\{\phi^2/2\} \simeq \exp[-q^2\mathbb{E}\{\phi^2/2\}], \tag{156}$$

whatever the magnitude of the dimensionless diffusion coefficient p. In the limit $p \to 0$, the second moment $\mathbb{E}\{\phi^2/2\}$ is proportional to p according to Eq. (82), yielding $-\ln E \propto q^2 p \propto D$. When p increases, the second moment is not necessarily dominated by its leading term, and $\ln E$ is not proportional to the free diffusion coefficient D any more. This deviation was experimentally observed by Woessner (1963) and traditionally characterized by effective or apparent diffusion coefficients (ADCs).[72] In our notation, the ADC can be defined as

$$\frac{D_{\rm app}}{D} = \frac{\mathbb{E}\{\phi^2/2\}}{p\zeta_1\langle(t_1 - t_2)\rangle_2}. \tag{157}$$

In the limit $p \to \infty$, the ratio $D_{\rm app}/D$ goes to 0 for the closed systems considered in this review. For open systems, the inverse of this ratio was shown to converge to the tortuosity (Haus and Kehr, 1987; de Swiet and Sen, 1996); see Sec. II.I.

The apparent diffusion coefficient shows how diffusion of spins is effectively slowed down by the presence of restrictive boundaries. In other words, unrestricted diffusion of spins with the apparent diffusion coefficient $D_{\rm app}$ is supposed to represent restricted diffusion of spins with their free diffusion coefficient D. Of course, this qualitative picture is just a simplified interpretation of restricted diffusion. Nonetheless, the apparent diffusion coefficient was used for a long time as a convenient characteristic for the confining geometry of porous materials or biological tissues. For example, human lung diseases like emphysema were suggested to be identified by an increase of the ADC due to enlargement or partial destruction of the alveolar tissue (Saam *et al.*, 2000; Möller *et al.*, 2002; Yablonskiy *et al.*, 2002; van Beek *et al.*, 2004). In spite of numerous applications of the ADC in different branches of the NMR industry, this notion remains limited to the first-order approximation (156) of the general series expansion (54).

The apparent diffusion coefficient is directly related to another widely used concept of b value or b coefficient. To find the ADC in experiment, one measures the macroscopic signal as a function of the parameters of the applied magnetic field (typically, gradient intensity g or duration T). The substitution of the second moment, expressed from Eq. (156) as $\mathbb{E}\{\phi^2/2\} \simeq -\ln E/q^2$, to Eq. (157) leads to

$$D_{\rm app} \simeq \frac{-\ln E}{b}, \tag{158}$$

where the b value is defined as

$$b = \frac{q^2 p}{D}\langle(t_1 - t_2)\rangle_2 \left(\frac{L^2}{V}\int_\Omega d\mathbf{r}\,|\nabla B(\mathbf{r})|^2\right). \tag{159}$$

This is an extension of the classical definition $b = \gamma^2 g^2 T^3/12$ to the case of an arbitrary spatial and temporal profile of the magnetic field. Equation (158) is often written as

$$E \simeq \exp[-bD_{\rm app}]. \tag{160}$$

While the ADC is intended to represent the effect of the confining geometry, the b value holds all information about the applied magnetic field. The fact that a single parameter might be used to describe the whole experimental setup was widely employed in practical applications, particularly in medical imaging. For example, some have given the b value without even mentioning the gradient intensity, duration, or temporal profile. It should, however, be clear that such a simplification is exaggerated. Since diffusive NMR phenomena are governed by at least two independent parameters p and q (assuming $h=0$), the b value alone cannot capture the whole picture. We stress that the b value is only a useful notation for the combination of different parameters in Eq. (159). We illustrate this point with the following example.

For the slow-diffusion regime ($p \ll 1$), the second moment $\mathbb{E}\{\phi^2/2\}$ is given by Eq. (97), yielding

$$D_{\rm app} \simeq D\left(1 - \sqrt{p}\frac{\zeta_{3/2}}{\zeta_1}\frac{\langle(t_2 - t_1)^{3/2}\rangle_2}{\langle(t_2 - t_1)\rangle_2}\right). \tag{161}$$

For a linear magnetic-field gradient, one retrieves the results by Mitra *et al.* (1992) and de Swiet and Sen (1994) for narrow-pulse and steady temporal profiles, respectively:

$$\frac{D_{\rm app}}{D} \simeq 1 - \frac{4}{3\sqrt{\pi}}\sqrt{DT/2}\frac{S}{Vd}, \tag{162}$$

[72] We should note that this NMR definition is not equivalent to the dynamical definition, when the time-dependent diffusion coefficient $D(t)$ appears as a measure of the mean-square displacements in time t,

$$\mathbb{E}\{[\mathbf{r}(t) - \mathbf{r}(0)]^2\} = 2dD(t)t.$$

As a dynamical characteristic of reflected Brownian motion, $D(t)$ is totally independent of the applied magnetic field, while the NMR diffusion coefficient (ADC) is sensitive to its temporal and spatial profiles. In our notation, the dynamical diffusion coefficient can be written as

$$D(p) = D(2pd)^{-1}\mathbb{E}\{[B(X_1) - B(X_0)]^2\},$$

where $B(\mathbf{r}) = \mathbf{r}/L$. For a reflecting boundary, one obtains a compact matrix form

$$D(p) = D(pd)^{-1}[\mathcal{B}(I - e^{-p\Lambda})\mathcal{B}]_{0,0}.$$

In the limit $p \to 0$, one retrieves $D(p) \to D$ as required. A similar relation, written in the form of a series expansion, has been recognized by Mitra *et al.* (1993), where it was derived for a sphere with reflecting boundary. In the remainder of this review, we consider the NMR diffusion coefficient only.

$$\frac{D_{\rm app}}{D} \simeq 1 - \frac{32(2\sqrt{2}-1)}{105\sqrt{\pi}}\sqrt{DT/2}\frac{S}{V}, \tag{163}$$

where Eqs. (110) and (112) were used. Equation (161) does not depend at all on dimensionless gradient intensity q. Consequently, the parameters q and p can be changed in such a way that $D_{\rm app}$ would be substantially modified according to Eq. (161), while the b value is kept fixed. This simple example shows that two experiments with the same b value can give very different values of the ADC. Knowledge of the b value alone is thus not sufficient to compare different medical measurements presented in the literature (e.g., ADC maps of the lungs). At this point, it is important to recall that the notion of the ADC and Eqs. (158) and (160) are applicable only when the Gaussian phase approximation is valid.

In the motional-narrowing regime ($p \gg 1$), one gets the second moment from Eq. (117) so that

$$D_{\rm app} \simeq D(p_0/p)^2, \tag{164}$$

where

$$p_0^2 = \frac{\zeta_{-1}}{\langle (t_1 - t_2)\rangle_2}\int_0^1 dt\, f^2(t). \tag{165}$$

The coefficient p_0^2 represents the relevant information about the temporal and spatial profiles of the magnetic field, as well as about the confining geometry. We propose a simple interpolation formula between very slow diffusion ($D_{\rm app} \simeq D$) and the motional-narrowing regime:[73]

$$D_{\rm app} \simeq \frac{D}{1 + (p/p_0)^2}. \tag{166}$$

Note that this relation does not account for the $p^{3/2}$ correction in the slow-diffusion regime. In the same manner as for the apparent diffusion coefficient itself, this formula may be used only for magnetic fields of relatively small intensity when the Gaussian form of the macroscopic signal is still valid.

To illustrate the use of the theoretical relations (161) and (166), we compare them to the experimental measurement of the apparent diffusion coefficient by Hayden *et al.* (2004). In their setup, a cylindrical borosilicate glass cell of diameter $L=4.82$ cm was filled with helium-3 gas ($\gamma \simeq 2.04\times 10^8$ rad T^{-1} s^{-1}) to a pressure of 1 Torr. The rescaling of the experimental conditions (temperature and pressure) to a reference measurement (Bendt, 1958; Barbé *et al.*, 1974) gave the free-diffusion coefficient $D \simeq 0.14$ m^2/s. The steady linear magnetic-field gradient was applied in a perpendicular direction to the cylinder axis. The apparent diffusion coefficient $D_{\rm app}$ was measured for different echo times T. We recall that, for this particular case, one has $\zeta_{3/2}=4/(3\sqrt{\pi})$ and $\zeta_{-1}=7/96$, while the f-weighted time averages $\langle (t_2-t_1)\rangle_2$ and $\langle (t_2-t_1)^{3/2}\rangle_2$ are given by Eq. (111) for the steady temporal profile. One then finds $p_0^2=7/8$.

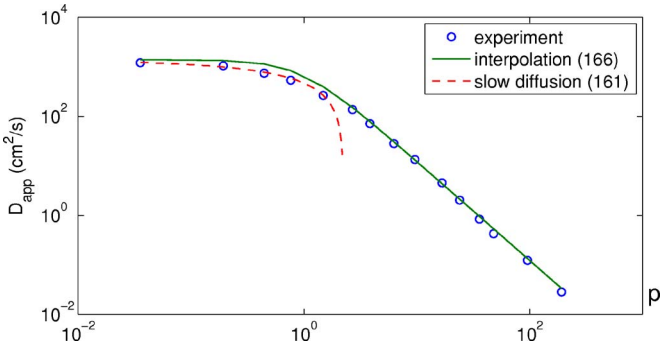

FIG. 7. (Color online) Apparent diffusion coefficient as a function of p for a cylindrical cell. The slow-diffusion correction (161) and the interpolation formula (166) are compared to the spin-echo measurements in a borosilicate glass cell by Hayden *et al.* (2004). Experimental data shown have been provided by Dr. M. E. Hayden.

Comparison between the experimental data and theoretical relations is shown in Fig. 7. For the slow-diffusion regime (small p), Eq. (161) remains in good agreement with experiment, until the correction term exceeds unity. From this point, the apparent diffusion coefficient is negative, and the slow-diffusion regime becomes invalid. In the motional-narrowing regime (large p), one observes the expected behavior p^{-2}. The use of the interpolation formula (166) allows one to avoid an unphysical divergence when p becomes smaller. Note that this formula provides good results even for very small p, when the motional-narrowing regime is not formally applicable. In this region, small deviation from the experimental data is related to the slow-diffusion correction term which was not taken into account in Eq. (166). In summary, one can see that both theoretical relations are in good agreement with experimental measurements over four orders of magnitude. This result may appear more exciting if one recalls that there are no adjustable parameters in the theoretical relations.

E. Narrow-pulse approximation

The Stejskal-Tanner profile (60) in the limit of vanishing pulse duration δ, known as the narrow-pulse approximation, has been applied for a long time to study

[73] This interpolation formula should not be confused with the two-point Padé approximation suggested by Latour *et al.* (1993) to fit ADCs between short- and long-time regimes in open systems:

$$\frac{D_{\rm app}}{D} = 1 - \alpha\frac{c\sqrt{T} + \alpha T/T_0}{\alpha + c\sqrt{T} + \alpha T/T_0},$$

where $c=(4/9\sqrt{\pi})(S/V)\sqrt{D}$, $\alpha = 1 - 1/\mathfrak{T}$ (here $\mathfrak{T}$ is the tortuosity), and $T_0 = \kappa_1/\alpha$ to give the first-order correction κ_1/T in Eq. (21).

restricted diffusion.[74] Its main advantage is that diffusive motion during these short pulses can be neglected, so that the accumulated phase becomes

$$\phi \simeq \delta B(X_0) - \delta B(X_{1/2}), \tag{167}$$

and one gets the signal in the simple form

$$E = \int_\Omega d\mathbf{r}\, \rho_0(\mathbf{r}) \int_\Omega d\mathbf{r}'\, \exp\{iq\delta[B(\mathbf{r}) - B(\mathbf{r}')]\} \times G_{T/2}(\mathbf{r},\mathbf{r}'), \tag{168}$$

where the time $T/2$ corresponds to the application of the second narrow pulse. The combination $q\delta$ is kept fixed in the limit $\delta \to 0$, so that the magnetic-field strength q must go to infinity. For a linear magnetic-field gradient, the macroscopic signal (168) appears as the Fourier transform of the propagator, as in Eq. (15). A complete separation of the geometrical properties of the confining domain (represented by the propagator) and spatial inhomogeneities of the magnetic field allows a number of important theoretical results to be obtained. This concept of q imaging provides a direct experimental measurement of the propagator (or heat kernel). In particular, one can expect an oscillatory behavior related to the geometrical structure of the confining medium (Callaghan, 1991). To illustrate this effect, one can again expand the heat kernel over the Laplace operator eigenbasis. For uniform initial density $\rho_0(\mathbf{r})$, the macroscopic signal from Eq. (168) takes a simple matrix form:

$$E = [e^{iq\delta\mathcal{B}} e^{-p\Lambda/2} e^{-iq\delta\mathcal{B}}]_{0,0}. \tag{169}$$

The matrix $e^{iq\delta\mathcal{B}}$ can be found using the following property of the Laplace operator eigenbasis: for an analytic function $F(z)$ one has[75]

$$[F(\mathcal{B})]_{m,m'} = \int_\Omega d\mathbf{r}\, u_m^*(\mathbf{r})\, F(B(\mathbf{r}))\, u_{m'}(\mathbf{r}). \tag{170}$$

The elements of the matrix $e^{iq\delta\mathcal{B}}$ for three basic domains are given in Table I. For instance, the calculation for a slab geometry with reflecting boundary reads as[76]

$$[e^{iq\delta\mathcal{B}}]_{m,m'} = \frac{\epsilon_m \epsilon_{m'}}{2} [\psi_{|m-m'|}(q\delta) + \psi_{m+m'}(q\delta)], \tag{171}$$

where

$$\psi_m(q\delta) = \frac{(-1)^m q\delta}{(q\delta)^2 - (\pi m)^2} \{\sin q\delta + i[(-1)^m - \cos q\delta]\}. \tag{172}$$

The substitution of this result into Eq. (169) leads to the classical form of the signal attenuation in a slab geometry within the narrow-pulse approximation (Tanner and Stejskal, 1968):

$$E = \frac{\sin^2(q\delta/2)}{(q\delta/2)^2} + 4(q\delta)^2 \sum_{m=1}^{\infty} e^{-\pi^2 m^2 p/2} \frac{1 - (-1)^m \cos q\delta}{[(q\delta)^2 - (\pi m)^2]^2}. \tag{173}$$

If the echo time T is long enough ($p \gg 2/\pi^2$), the second term can be omitted, and the signal exhibits diffraction-like oscillations. Since the dimensionless parameter q is defined as $\gamma g L T$, the behavior of the macroscopic signal as a function of the gradient intensity g allows one to determine the distance L between parallel plates of a slab geometry.

The applicability of the narrow-pulse approximation has been thoroughly studied (Blees, 1994; Wang *et al.*, 1995; Mair, Sen *et al.*, 2002; Lori *et al.*, 2003; Price *et al.*, 2003; Malmborg *et al.*, 2004, etc.) Its practical application is limited by the assumption that the duration δ of the gradient pulses should be short enough to neglect the diffusion during them, that is $\delta p \ll 1$. If p is too small, the diffraction effects are dumped by a number of terms in the sum. In fact, it can be shown that Eq. (173) is reduced to $E \simeq 1 - q^2 p(\delta^2/2)$ that can be written in a classical Gaussian form

$$E \simeq \exp[-q^2 p \delta^2/2]. \tag{174}$$

In this case, there is no need to use the narrow-pulse approximation. In the opposite limit of large p, the diffraction effects would appear (Fig. 8), but the condition $\delta p \ll 1$ is more difficult to realize experimentally (since the gradient pulse duration δ is limited by instrumental constraints). In spite of this difficulty, the diffusive diffraction was experimentally observed for the first time in a water-saturated, orientationally disordered, loosely packed array of monodisperse polystyrene spheres by Callaghan *et al.* (1991).

The narrow-pulse approximation may also be valuable to give an intuitive feeling how other more sophisticated techniques work. For instance, its use as a simplified temporal profile helps to better understand the properties of the f-weighted time average in the MCF approach. In the limit $\delta \to 0$, the f-weighted time average of a smooth function $F(t_1, \ldots, t_n)$ is reduced to

[74] Tanner and Stejskal (1968); Callaghan (1991); Callaghan *et al.* (1991); Balinov *et al.* (1994); Coy and Callaghan (1994); King *et al.* (1994); Sen *et al.* (1995); Söderman and Jönsson (1995); Kuchel *et al.* (1996). See also references in Sec. II.D.

[75] This relation can also be applied in the opposite sense, especially in one dimension. Once the matrix $\mathcal{B}_x$ is found for a linear gradient $B(x)=x$, its computation for any analytic spatial profile $F(x)$ is direct: $\mathcal{B}=F(\mathcal{B}_x)$. For example, the matrix $\mathcal{B}_{x^2}$ for the parabolic magnetic field might be found as $[\mathcal{B}_x]^2$. Similar relations hold in two and three dimensions, although a more careful analysis is required.

[76] The matrix $e^{iq\delta\mathcal{B}}$ naturally appears in the multiple propagator approach (see Appendix D). For a cylinder and a sphere, its elements $[e^{iq\delta\mathcal{B}}]_{m,m'}$ for any m and m' were obtained by Codd and Callaghan (1999) for the Fourier boundary condition (10). Another representation for the Neumann boundary condition (11) was given by Sukstanskii and Yablonskiy (2002). In both cases, the expressions are cumbersome and have to be computed numerically. However, the calculation of the signal by Eq. (169) requires knowledge of the elements $[e^{iq\delta\mathcal{B}}]_{0,m}$ alone, and their expressions are simpler (see Table I).

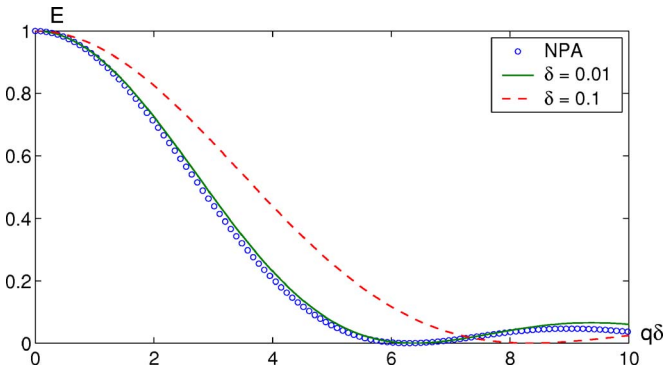

FIG. 8. (Color online) Macroscopic signal as a function of $q\delta$ is found analytically within the narrow-pulse approximation (circles), and numerically by the MCF approach for $\delta=0.01$ (solid line) and $\delta=0.1$ (dashed line). The physical parameters ($D=2.3\times10^{-9}$ m^2/s, $L=1.6\times10^{-5}$ m, $T=0.22$ s) are from Callaghan *et al.* (1991). One sees that the approximate relation (173) is not applicable for $\delta=0.1$ since the condition $\delta p \ll 1$ fails (here $p\simeq 2$).

$$\langle F(t_1,\ldots,t_n)\rangle_n \simeq \frac{\delta^n}{n!}\sum_{k=0}^{n}(-1)^k C_n^k F\Big(0,0,\ldots,\underbrace{\tfrac{1}{2},\tfrac{1}{2}}_{k\ \text{times}}\Big), \tag{175}$$

where C_n^k are the binomial coefficients. For example,

$$\langle F(t_1,t_2)\rangle_2 \simeq \frac{\delta^2}{2}[F(0,0)-2F(0,\tfrac{1}{2})+F(\tfrac{1}{2},\tfrac{1}{2})]. \tag{176}$$

This general result can now be used to write the moments as

$$\mathbb{E}\left\{\frac{\phi^n}{n!}\right\} \simeq \frac{\delta^n}{n!}\Big([1+(-1)^n][\mathcal{B}^n]_{0,0} + \sum_{k=1}^{n-1}(-1)^k C_n^k [\mathcal{B}^k e^{-p\Lambda/2}\mathcal{B}^{n-k}]_{0,0}\Big). \tag{177}$$

Further analysis is significantly simplified using this relation. For instance, one can easily check that all odd moments vanish since $[\mathcal{B}^k e^{-p\Lambda/2}\mathcal{B}^{n-k}]_{0,0}=[\mathcal{B}^{n-k}e^{-p\Lambda/2}\mathcal{B}^k]_{0,0}$. Note that Eq. (177) could be derived directly from Eq. (168) by using the spectral decomposition (31) of the heat kernel within the narrow-pulse approximation.

Another representation for the even moments can be derived by expanding the exponential function in Eq. (168):

$$\mathbb{E}\left\{\frac{\phi^{2n}}{(2n)!}\right\} = \frac{\delta^{2n}}{(2n)!}\int_\Omega d\mathbf{r}_0\rho_0(\mathbf{r}_0)\int_\Omega d\mathbf{r}\, G_{T/2}(\mathbf{r}_0,\mathbf{r}) \times [B(\mathbf{r}_0)-B(\mathbf{r})]^{2n}. \tag{178}$$

The spectral decomposition of the heat kernel allows one to study the dependence of these moments on the parameter p. In particular, one can rigorously obtain their leading terms (see Appendix E for a sketch of this derivation):

$$\mathbb{E}\left\{\frac{\phi^{2n}}{(2n)!}\right\} \simeq \frac{p^n}{n!}(\delta^2/2)^n\left(\frac{L^{2n}}{V}\int_\Omega d\mathbf{r}\,|\nabla B(\mathbf{r})|^{2n}\right). \tag{179}$$

This is a particular form of the general relation (84) for the narrow-pulse profile, for which the f-weighted time average $\langle(t_1-t_2)\rangle_2$ is $\delta^2/2$. While the general result was demonstrated for $n=1,2$ and only conjectured for higher n, Eq. (179) is shown to be valid for any n. This example illustrates the use of the narrow-pulse approximation as an investigation tool.

F. Localization regime

In previous sections, we considered the behavior of the moments $\mathbb{E}\{\phi^{2n}\}$ in two asymptotic limits, when the dimensionless diffusion coefficient p goes to zero or infinity. In both cases, the leading terms could be satisfactory only for very small or large values of p. The use of correction terms significantly improved the quality of the results, but was still insufficient to describe the behavior for intermediate values of p. Moreover, our analysis was essentially focused on the second moment. If the dimensionless magnetic-field strength q is small, this moment provides the most significant contribution to the signal and contains exhaustive information about its attenuation. However, when q increases, a larger number of moments is needed to accurately compute the signal E. One may thus expect to observe a new kind of behavior for sufficiently intense magnetic fields. In fact, if the dephasing length $(D/\gamma g)^{1/3}$ is much smaller than the diffusion length $\sqrt{DT}$ and the characteristic dimension L of the domain, a new localization regime appears (Stoller *et al.*, 1991; de Swiet and Sen, 1994). In this case, the spins of the bulk diffuse over several dephasing lengths so that they have no net contribution to the total magnetization. The macroscopic signal is thus formed by spins close to the interface whose dephasing is less pronounced. In our notation, this situation corresponds to $q\gg p$ and $q^2p\gg 1$.

Stoller *et al.* (1991) gave the first theoretical study of this regime for one-dimensional diffusion. Using an exact resolution of the one-dimensional Bloch-Torrey equation (9) and analyzing of the underlying spectral problem, they showed non-Gaussian stretched-exponential behavior of the signal E:

$$E \simeq C(p/q)^{1/3}\exp\left[-\frac{a_1}{2}(pq^2)^{1/3}\right], \tag{180}$$

where $a_1\simeq 1.0188$ is the absolute value of the first zero of the derivative of the Airy function. The numerical prefactor C was found to be 5.884 for a slab geometry. The dependence (180) and its significance for NMR applications have been discussed (de Swiet and Sen, 1994; Hürlimann *et al.*, 1995; Sen *et al.*, 1999). In particular, the coefficient $a_1/2$ was argued to be independent of the confining geometry.

Four years later, the above theoretical prediction was observed by using the spin-echo technique. An elegant experiment of Hürlimann *et al.* (1995) confirmed the

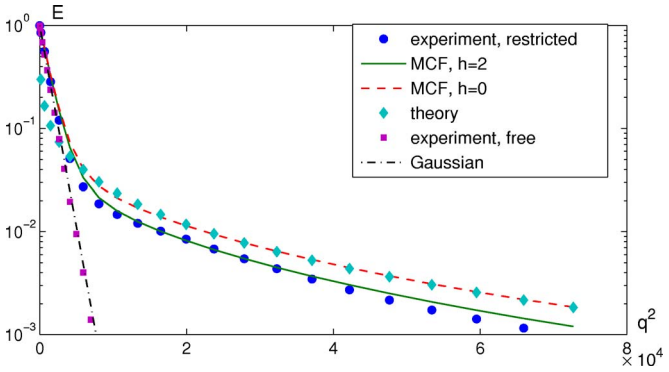

FIG. 9. (Color online) Illustration of a drastic deviation from the Gaussian behavior at high gradient intensity. On a logarithmic scale, experimental data for free diffusion (when the gradient applied along unrestricted direction) fall onto the straight line $-q^2p/12$ as expected. In contrast, experimental data for restricted diffusion follow the theoretical relation (180). A small deviation from this behavior is mainly caused by surface relaxation as confirmed by numerical analysis. Experimental data have been provided by Dr. M. D. Hürlimann.

breakdown of the GPA and the relevance of the localization regime. Hürlimann *et al.* studied restricted diffusion of water molecules ($D \simeq 2.3 \times 10^{-9}$ m^2/s) between two parallel plates at distance $L=0.16$ mm. The signal attenuation was measured as a function of the gradient intensity g. Even for gradient pulses of long duration ($T=120$ ms), the dimensionless diffusion coefficient p was small ($p \simeq 0.01$) so that the slow-diffusion regime, with a Gaussian g^2 dependence, could be expected. This was actually observed for the gradient applied in a longitudinal (unrestricted) direction. Figure 9 shows good agreement between experimental points (squares) and theoretical prediction (dash-dotted line) by the classical relation (3).

The situation becomes completely different when the gradient is turned to the direction perpendicular to the plates (circles in Fig. 9). A spectacular deviation from the Gaussian g^2 dependence of $\ln E$ can be seen clearly at gradient intensities higher than 15 mT/m ($q^2 \geqslant 0.6 \times 10^4$). This behavior can be attributed neither to the slow-diffusion limit nor to the motional-narrowing regime. Neither an apparent diffusion coefficient nor any related concept has meaning in this localization regime.

Figure 9 shows that the experimental data are in qualitative agreement with the predictions by Stoller *et al.* (diamonds). A small deviation from the theoretical relation (180) can be attributed to surface relaxation. To illustrate this point, we have numerically calculated the macroscopic signal by using the MCF approach. The dashed line, corresponding to the Neumann boundary condition (11), confirms the good precision of Eq. (180) when surface relaxation can be neglected ($\rho=0$ or $h=0$). To better fit the experimental points, we calculated the signal for different values of the dimensionless surface relaxivity h. The solid line corresponds to the Fourier boundary condition (10) with $h=2$ (or $\rho \simeq 28.8$ μm/s).[77]

The most exciting feature of the work by Hürlimann *et al.* is that the localization regime is observed under ordinary experimental conditions. In view of the above results, a number of theoretical questions arises. A formal expansion of the exponential function in Eq. (180) leads to a series of *fractional* powers of p and q. This is probably not surprising with respect to p, since we have already seen fractional powers of p in the correction term to the slow-diffusion regime. In contrast, the fractional powers of q would be in contradiction to the fact that the signal E must be an analytic function of q. Of course, Eq. (180) has to be considered as an asymptotic behavior for $pq^2 \gg 1$ so that the above expansion is formally not allowed. Nevertheless, the passage from the general expansion (54) to this asymptotic form is intriguing. The general MCF description may help to shed new light on this interesting problem. Since this description is not restricted to a particular choice of parameters p and q, it can reproduce, at least numerically, any feature of the signal attenuation, including the localization regime (see, for instance, Fig. 9). Its theoretical analysis would require a systematic technique for calculating the moments $\mathbb{E}\{\phi^n\}$ of high orders. Such a technique has been partially implemented for a specific spatial profile of the cosine magnetic field (Grebenkov, 2007a).

At first sight, the problematics of the localization regime may look like a mathematical puzzle of limited practical interest. We believe, however, that better understanding of the nature of this specific non-Gaussian behavior will enrich our knowledge about diffusive NMR phenomena in general. Moreover, some recent research has shown potential importance of the localization regime for restricted diffusion in lungs (Grebenkov *et al.*, 2007).

G. Transition between different regimes

From a mathematical point of view, the breakdown of the GPA always takes place for sufficiently large q. It may happen, however, that the transition between the GPA and the localization regime occurs when the signal is negligible. In such experimental conditions, the localization regime cannot be observed.

To illustrate this statement, a pq diagram of different NMR regimes is depicted in Fig. 10 for restricted diffusion in a slab under two spatial profiles of a steady (bipolar) magnetic field. The signal is attenuated by a factor of 2 at each line separating two adjacent gray-scale regions (appearing as pale and dark stripes). The first

[77] This value of the surface relaxivity ρ is given for illustrative purpose only. Note that typical surface relaxivity of sandstones is of the same order (Sun and Dunn, 2002). A more profound analysis of the localization regime in the presence of surface relaxation is certainly required and will be helpful to determine this characteristic accurately. Some other possible sources of deviation between theory and experiment were discussed by Hürlimann *et al.* (1995).

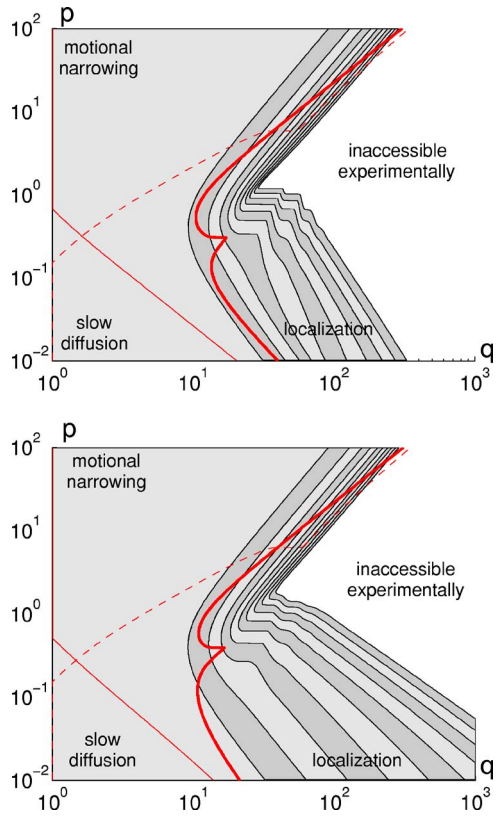

FIG. 10. (Color online) Transition between different regimes of restricted diffusion in a slab under a linear gradient (on the left) and parabolic (on the right) magnetic fields (see description in the text).

large pale region on the left is composed of points (q,p) for which the signal E lies between $1/2$ and 1. The next dark stripe regroups points (q,p) for which $1/4 \leqslant E \leqslant 1/2$, and so on. The white area on the right corresponds to pairs (q,p) for which the signal is below 10^{-3}. Since such a small signal is often comparable to noise, this area is referred to as inaccessible experimentally. On this pq diagram, the bold line delimits the region on the left in which the GPA predictions of the signal attenuation are valid with an accuracy of at least 5%. The thin and dashed lines show the limits of the slow-diffusion and motional-narrowing regimes, in which Eqs. (82) and (117) give results with an accuracy of at least 5%.

For the whole region to the right of the bold line, the Gaussian phase approximation fails to predict accurate results. Apart from the transient region in vicinity of this line, the localization regime is expected for larger q. However, if p is not small enough, the signal attenuation is too strong for large q, driving us to the area inaccessible experimentally. Conversely, the localization regime can be experimentally observed for relatively small p. For instance, Hürlimann *et al.* (1995) performed an experiment for water molecules with p on the order of 0.01.

It is worth noting that the GPA in the slow-diffusion regime ($p \ll 1$) is valid for weakly attenuated signals only (the first pale region). In contrast, the GPA in the motional-narrowing regime describes the signal attenuation in a much wider range. Surprisingly, the GPA based on a rough leading-order approximation (117) seems to better approximate the signal attenuation for large q than that for the precisely computed second moment (in Fig. 10, the dashed line intersects the bold line and goes in a deeper region to the right). This anomalous behavior is caused by the contribution of higher-order moments which become significant for large q.

Comparison of the pq diagrams for two spatial profiles shows that their structures are very similar. One can see that the stripes are thinner for a linear gradient than for the parabolic field. Moreover, similar results can be obtained for a cylinder and a sphere (not shown).[78] Such diagrams can be used in practice to estimate the value of the signal for given parameters p and q. From this plot, one can also determine which kind of restricted diffusion is to be expected, and which formula should be applied to fit experimental data. Note that this information is rather qualitative since the particular location of different regions on the diagram depends on the confining geometry.

H. Inverse spectral problem

The main question we addressed in the review was: How does a geometrical restriction influence Brownian dynamics and the consequent signal attenuation? To give a quantitative answer, we computed the Laplace operator eigenbasis for a given (and thus known) confining domain and then expressed the signal within the MCF description. This analysis is useful to discover new features of diffusive NMR phenomena, to calculate transport characteristics (e.g., ADCs), to explore a wider range of physical parameters, to optimize them for a better realization of experiment, to check and fit acquired data, etc. One may wonder, however, to which extent this knowledge may serve to identify the geometrical restriction from the signal attenuation. More precisely, the new question would be to know which information on the confining geometry is available from measuring the signal attenuation. There is no need to argue neither the practical importance of this inverse problem nor the difficulty of its resolution.[79]

[78] As noted in Sec. VI.A, the numerical computation of the signal for large q and small p is more difficult for a cylinder and a sphere than for a slab. According to the rough estimate (145), one needs $\lambda_{\tilde{m}} \gg 10^5$ to get the signal for $q=10^3$ and $p=0.01$ (right lower corner of the pq diagram). For a slab, this inequality can be safisfied with $\tilde{m} \sim 200$ (in practice, $\tilde{m} \sim 50$ is already sufficient). For a cylinder and a sphere, much bigger matrices are needed. To overcome this difficulty, one can reduce the range of the parameters p and q.

[79] For instance, Zielinski *et al.* (2002) considered the inverse spectral problem for two coupled one-dimensional pores without diffusion-sensitizing gradient. Even in such a simplified model, the identification of individual pores from the spectral features of the diffusion eigenmodes required significant separation of their lengths and moderate coupling.

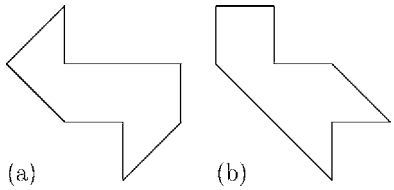

FIG. 11. Example constructed by Gordon *et al.* (1992) of two nonisometric domains with the identical Laplace operator spectra.

This problem goes back to the famous question "Can one hear the shape of a drum?" formulated by Kac (1966). In fact, the drum frequencies that one hears are uniquely determined by the eigenvalues of the Laplace operator for the drum shape. Figuratively speaking, these eigenvalues appear as fingerprints of the geometry, although they may not be sufficient to identify it. This was indeed shown by Gordon *et al.* (1992), who constructed two different (nonisometric) polygons in two dimensions with the identical Laplace operator spectra, for both the Dirichlet and Neumann boundary conditions (Fig. 11). Experimental evidence for this inability to hear the shape of drums was given by Sridhar and Kudrolli (1994).

The situation is slightly different for restricted diffusion in NMR. The macroscopic signal is determined by two matrices Λ and $\mathcal{B}$. If the matrix Λ simply represents the eigenvalues (as for the Kac problem), the matrix $\mathcal{B}$ involves the Laplace operator eigenfunctions and the spatial profile $B(\mathbf{r})$ of the magnetic field. This gives two advantages with respect to the Kac problem. First, more information is encoded in the signal through the matrix $\mathcal{B}$ and might thus be extracted, at least in principle. Second, a voluntary choice of the magnetic field $B(\mathbf{r})$ can also be employed. On the other hand, we have shown that the elements of the matrix $\mathcal{B}$ in the case of a slab, a cylinder, or a sphere are fully expressed in terms of the Laplace operator eigenvalues. This means that the matrix $\mathcal{B}$ does not actually contain more information about these particular geometries than the matrix Λ. The question whether the matrix $\mathcal{B}$ can provide additional information about the confining geometries in general remains open.

For practical applications (e.g., in medicine or the oil industry), there is no way and no need to determine the precise shape of the confining geometry. What one is looking for are rather statistically averaged geometrical characteristics like pore size distribution, surface-to-volume ratio, tortuosity, etc. [see also Ryu (2001); Song (2003); Sen (2004)]. As we have seen above, many of these important characteristics can be determined using NMR.

I. Application to porous media

In spite of the generality of the multiple correlation function description, this review has been focused on three basic shapes: a slab, a cylinder, and a sphere. Particular symmetries of these domains (translational, axial, and rotational) permit reduction of the Laplace equation to separate one-dimensional equations whose solutions can be expressed in terms of known special functions (like Bessel functions for a cylinder). However, even a minor geometrical defect would destroy such a symmetry so that the basic domains appear as useful but very idealized models of confinement. One may thus be curious as to what extent the obtained analytical results can serve in studying more realistic porous media.

Apart from the specific symmetries, the basic domains exhibit another important property: their shapes are characterized by a single relevant geometrical scale L (separation of plates in a slab or the radius for a cylinder and a sphere). Comparison of this scale to the diffusion length $\sqrt{DT}$, the gradient length $(\gamma g T)^{-1}$, and the relaxation length D/ρ naturally brought us to the three dimensionless parameters p, q, and h that determine the signal attenuation. In particular, we observed a transition between the slow-diffusion and motional-narrowing regimes when $\sqrt{DT}$ became comparable to L.

In contrast, multiple length scales are characteristic features of porous media (Sahimi, 1993; Song *et al.*, 2000). For instance, the architecture of sedimentary rocks can be represented by interconnected rough channels with a spread pore size distribution (Kleinberg, 1994; Latour *et al.*, 1995). The diameter of pores is typically between a few and one or several hundreds of microns, while rocks may reach hundreds of meters (of course, much smaller samples are investigated in practice). Human respiratory systems present another example where the characteristic length varies from hundreds of microns (alveoli) to a few decimeters (size of the lungs) (Weibel, 1984). Such broad ranges of geometrical length scales make questionable the use of a single dimensionless diffusion coefficient p.

The microscopic roughness of realistic interfaces may considerably influence the signal attenuation in two different ways. First, irregular boundaries exhibit highly inhomogeneous accessibility for Brownian motion due to diffusional screening.[80] If surface relaxation is high, this effect may yield a considerable deviation between the measured and real surface-to-volume ratios. In the opposite case of a small surface relaxivity, the roughness of the boundary (e.g., its fractal dimension) can be probed

[80]The diffusional screening was originally studied for the Dirichlet boundary condition, when diffusing particles are absorbed (or lose their magnetization) the first time they collide with the interface. Even at an intuitive level, it is clear that most particles are absorbed by a few prominent spikes or irregularities which screen other parts of the boundary. For fractal boundaries, the proportion of the accessible regions with respect to screened ones is negligible. In NMR, the diffusional screening would have a less dramatic effect since surface relaxation is in general small. The interested reader may find more details in Sapoval (1994, 1996); Grebenkov, Lebedev, *et al.* (2005); Grebenkov (2005, 2006c); Grebenkov *et al.* (2006). The role of the diffusional screening for human respiration was discussed by Felici *et al.* (2004, 2005); Grebenkov, Filoche, *et al.* (2005).

(de Gennes, 1982; Banavar *et al.*, 1985; Devreux *et al.*, 1990; Sapoval *et al.*, 1996; Stallmach *et al.*, 2002). Alternatively, the geometrical singularities drastically enhance susceptibility effects that may lead to very high magnetic-field gradients near the boundary. This would bring another source of discrepancy between the observed and real properties of porous media.

In addition, many porous structures may be open, when transport is allowed not only inside the sample, but also to and from the external environment (as for human lungs, for instance). Such structures were often modeled as infinite unbounded systems. In fact, when the size of a sample is much bigger than the pore size and other physical lengths, the sample can be extended to infinity. Roughly speaking, if the majority of diffusing spins cannot reach the frontier of the sample, it does not matter whether this frontier exists or not. In this case, the motion of spins can be modeled as unrestricted diffusion (ordinary Brownian motion in the whole space), which is thought to be simpler for theoretical analysis since the propagator $G_t(\mathbf{r},\mathbf{r}')$ takes an explicit Gaussian form:

$$G_t(\mathbf{r},\mathbf{r}') = (4\pi Dt)^{-d/2} \exp\left[-\frac{(\mathbf{r}-\mathbf{r}')^2}{4Dt}\right], \tag{181}$$

d being the dimension of the space. The presence of paramagnetic impurities, sinks, traps, or other obstacles can be effectively taken into account through an apparent diffusion coefficient or in a more sophisticated way.[81]

It should be noted, however, that unrestricted diffusion causes a number of specific unphysical artifacts like infinite volume of the bulk or unbounded increase of a linear magnetic-field gradient. In some cases, these artifacts do not influence the underlying analysis, but sometimes, they do. For instance, one cannot use a uniform spin density since it would require an infinite amount of spins producing an infinite signal at time $t=0$. As a consequence, the correlation functions $\mathbb{E}\{B(X_{t_1})\cdots B(X_{t_n})\}$ given by Eq. (30) would diverge after integration with a uniform initial density $\rho_0(\mathbf{r}_0)$. Although this divergence can be overcome by some tricks, it makes the application of the MCF description to unrestricted diffusion challenging. Many concepts of this approach might be applied to unbounded domains, but the analysis would become extremely difficult due to the continuous spectrum of the Laplace operator.

In practice, there is no need to follow this sophisticated approach. The same physical argument which supported the modeling of porous media by infinite systems allows one to introduce a fictitious frontier to any unbounded domain. Since the transport occurs in the bulk, the fraction of diffusing spins that saw this frontier and felt its presence can be made negligible by placing it far away. To illustrate this point, consider again the respiratory system. Although the human lungs are connected to the external environment, diffusion of helium-3 nuclei during one second (a long period for *in vivo* experiments) allows them to explore distances no longer than 1 cm. Since the size of the human lungs is a few decimeters, most spins do not feel whether the domain in which they diffuse is bounded or not. In this spirit, even a truly infinite system can be treated, to some extent, as a large but bounded domain, and the MCF description may be a complementary technique to study these systems.

The price to pay for the introduction of a large fictitious frontier is that the numerical analysis may become much more difficult. In particular, the Laplace operator spectrum, albeit still discrete, becomes very dense. A new challenge is now to compute, at least approximately, the governing matrices $\mathcal{B}$ and Λ. For this purpose, some model structures of porous media (like hierarchical morphologies, self-similar fractals, ordered or random packs of spherical beads, etc.) are of great interest. Some kind of statistical averaging may possibly be required to reduce information about irrelevant geometrical details. If this computation is done, further analysis can proceed as described in the previous sections. For instance, the signal attenuation in the slow-diffusion regime should have a Gaussian form (90), in which the second moment is expected to follow Eq. (113) or similar. Here $L=L_{\min}$ would be the size of internal pores, the smallest length scale. In contrast, the motional-narrowing regime is not attainable for open systems since the condition $DT \gg L^2$ is formally forbidden (here $L=L_{\max}$ is the size of the sample, the largest length scale). A broad separation between the smallest and largest geometrical scales leaves space for a number of intermediate regimes. For example, the classical long-time approach to the tortuosity regime (21) in open homogeneous systems is expected to hold for $L_{\min} \ll \sqrt{DT} \ll L_{\max}$. A better understanding of this and other possible regimes presents an exciting area for future research. In particular, a coarse-graining procedure like the regular lattice representation of multiply connected pores considered by McCall *et al.* (1991, 1993) and Guyer (1993) may be the first step along this way.

VII. CONCLUSION

The fascinating properties of Brownian motion have attracted scientists for almost two centuries from its discovery by Brown (1828). Among a variety of related scientific domains, nuclear magnetic resonance provides an efficient experimental tool to survey diffusive motion by a direct measurement of different functionals of this stochastic process. A voluntary choice of the temporal and spatial profiles of applied magnetic field makes possible, in principle, a complete experimental analysis of Brownian trajectories. The presence of a confining boundary makes this problem still more intriguing. On the other hand, the specific properties of reflected Brownian motion are at the origin of the diversity and complexity of diffusive NMR phenomena observed in experiments. In

[81] See, for instance, Grassberger and Procaccia (1982); Majumdar and Gore (1988); Weisskoff *et al.* (1994); de Swiet and Sen (1996); Sukstanskii and Yablonskiy (2003, 2004).

spite of intensive theoretical investigation during the last five decades, a lot of important questions remain unanswered.

The main aim of this review was to show, in a unified way, the progressive development in this field from Hahn's discovery of spin echoes to the present day. For this purpose, the multiple correlation function description was first established and then used to retrieve, extend, and critically discuss a number of classical results. This description allows a theoretical analysis of restricted diffusion in confining media under arbitrary magnetic fields. Its spatial inhomogeneities are naturally included via matrix elements $\mathcal{B}_{m,m'}$ in the Laplace operator eigenbasis. In turn, the dependence on time was taken into account as the f-weighted time average of the multiple correction functions. A thorough analysis of the second- and higher-order moments of the random phase accumulated by a diffusing spin in a magnetic field allowed us to retrieve and extend many classical results. For instance, the slow-diffusion and motional-narrowing regimes were derived for arbitrary temporal and spatial profiles of the magnetic field. A further analysis of high-order moments will help to specify the validity ranges of the Gaussian phase approximation. For this purpose, a systematic computational technique to operate with the temporal and spatial averages for high-order moments will be valuable.[82]

Two simplifications were used to clarify the analysis. First, the computation of the f-weighted time averages was significantly easier due to the rephasing condition which, in turn, was required for echo formation. Second, the Neumann boundary condition involved the spatial averages, for instance, the analytical computation of the coefficients ζ_k. It is important to stress that neither assumption is crucial for the analysis; they were introduced only to lighten the underlying mathematics. For instance, one could derive the coefficients ζ_k in a more general case including surface relaxation. Analytical calculations were performed for three basic domains (slab, cylinder, and sphere), for which the Laplace operator eigenbasis is well known. Even for these idealized cases, the interplay between physics and geometry led to sophisticated diagrams of different restricted-diffusion regimes and highly nontrivial signal attenuation. Systems of practical interest (like rocks or biological tissues) exhibit far more complex, often multiscale, geometries. The theoretical description can still be applied, but the analysis rests on the related computational challenges. An efficient numerical technique to construct the governing matrices $\mathcal{B}$ and Λ would be of great interest. This technique may help to develop many aspects of the transport in porous media. For instance, the respective roles of the whole internal architecture of the confining medium, and of the local boundary properties like microroughness, could be better understood.

The lack of a complete operational theory of restricted diffusion in confining media under arbitrary magnetic fields was probably one of the obstacles in developing experimental NMR techniques with specifically designed temporal and spatial profiles. The use of nonlinear fields beyond simple linear gradients may help to enhance particular geometrical features of a sample. For instance, a spatial profile with local minima at fixed locations or with a local minimum valley would enable one to study the diffusive motion of spins between these locations (since the contribution of other spins would be much more attenuated by higher magnetic field elsewhere). A periodic distribution of $B(\mathbf{r})$ might also be of practical interest to enhance diffusive diffraction. Moreover, susceptibility-induced or even random magnetic fields can now be treated in an efficient theoretical or numerical way. This would be a promising extension for some techniques,[83] developed originally for the whole space, to the more realistic case of confining media. On the other hand, the opportunity to use various temporal profiles of the magnetic field has not yet been explored at length. While the induction of a nonlinear magnetic field presents an experimental challenge in itself, the design of specific temporal profiles is already somewhat accessible. For instance, temporal profile optimization might be useful to increase the contribution of the correction terms in the slow-diffusion regime.

Recent years were marked by rapidly growing interest in development of mobile single-sided NMR sensors[84] and "inside-out" instrumentation for samples that do not fit into the bore of a standard NMR magnet. Such devices are invaluable for well logging, materials tests, and cultural heritage. When the sample is outside the magnet (as in the case of stray field measurements[85]), magnetic fields are inevitably inhomogeneous. An accurate analysis of these effects would require either elaborate models for these fields or their numerical computation. From this perspective, the MCF description would be a mathematical basis for a new branch of computational NMR analysis. Combined with numerical tools in electrodynamics,[86] it would make possible a complete study of diffusive phenomena for these devices. Indeed, if the magnetic field is computed for a chosen setup, its spatial profile can then be used to predict the consequent signal attenuation in NMR experiments. This analysis might also help to design the gradient coils that could generate nonlinear diffusion-sensitizing magnetic

[82]For instance, the choice of a cosine spatial profile of the magnetic field considerably simplifies the structure of the matrix $\mathcal{B}$, allowing one to obtain higher-order moments in an exact and explicit form (Grebenkov, 2007a).

[83]See, for instance, Mitra and Le Doussal (1991); Kiselev and Posse (1998); Kiselev and Novikov (2002); Sukstanskii and Yablonskiy (2003, 2004).

[84]Eidmann *et al.* (1996); Meriles *et al.* (2001); Brill *et al.* (2002); Perlo *et al.* (2005).

[85]McDonald (1997); Hürlimann and Griffin (2000); Hürlimann (2001); Hürlimann and Venkataramanan (2002); Kimmich and Fischer (1994).

[86]For instance, see Bondeson *et al.* (2005); Taflove and Hagness (2005).

fields in order to focus on particular properties of restricted motion.

The scientific interest in diffusive phenomena actually goes far beyond their role in probing porous materials or biological tissues. As we have shown in this review, the close relation to probability theory should make them attractive for mathematicians investigating reflected Brownian motion. A rigorous reformulation of numerous physical results dispersed in the literature should help to bring new ideas to this long-standing field. A number of open mathematical problems were outlined in previous sections. Among them, we should stress a better understanding of the transitions between different diffusion limits, especially the passage to the localization regime. Finally, the inverse problem of determining the confining geometry from knowledge of the signal attenuation is unsolved and of primary practical importance, for instance, to detect the mineral oil in rocky structures or pathological diseases in human organs.

ACKNOWLEDGMENTS

The author is grateful to Dr. G. Guillot, Dr. X. Maître, R. H. Morris, Dr. B. Sapoval, Dr. S. Shadchin, and Dr. P. Tankov for valuable discussions and careful reading of the manuscript. The referees are acknowledged for numerous remarks and suggestions that helped to improve the manuscript. A special acknowledgment is to Dr. M. Hayden and Dr. M. D. Hürlimann for sending to the author a set of experimental data to illustrate different NMR regimes. This work has been supported by EU Network MRTN-CT-2003-504712, the ANR project "MIPOMODIM No. NT05-1-42030," and Ecole Polytechnique (Palaiseau, France).

APPENDIX A: FOURTH MOMENT IN THE SLOW-DIFFUSION REGIME

In the slow-diffusion regime, the leading term of the fourth moment is expected to be of order of p^2. To show this behavior, the exponential functions in Eq. (59) can be formally expanded up to second orders in p. The f-weighted average of a constant (order p^0) vanishes due to the rephasing condition. We first show that there is no contribution of the first order, and then calculate the coefficient in front of p^2.

1. First-order contribution

There are three terms of order p:

$$[\mathcal{B}\Lambda\mathcal{B}^3]_{0,0}\langle(t_2-t_1)\rangle_4+[\mathcal{B}^2\Lambda\mathcal{B}^2]_{0,0}\langle(t_3-t_2)\rangle_4 + [\mathcal{B}^3\Lambda\mathcal{B}]_{0,0}\langle(t_4-t_3)\rangle_4. \tag{A1}$$

The spatial averages are found by a field theory technique briefly outlined in Sec. IV.A:

$$[\mathcal{B}^3\Lambda\mathcal{B}]_{0,0}=[\mathcal{B}\Lambda\mathcal{B}^3]_{0,0}=\frac{3}{4}[\mathcal{B}^2\Lambda\mathcal{B}^2]_{0,0} =\frac{3L^2}{V}\int_\Omega d\mathbf{r}\, B^2(\mathbf{r})|\nabla B(\mathbf{r})|^2. \tag{A2}$$

The f-weighted time averages are

$$\langle(t_2-t_1)\rangle_4=\langle(t_4-t_3)\rangle_4=-\tfrac{2}{3}\langle(t_3-t_2)\rangle_4=-\tfrac{1}{6}F_4, \tag{A3}$$

where

$$F_k=\int_0^1 dt\,[\hat{f}(t)]^k, \tag{A4}$$

and the primitive

$$\hat{f}(t)=\int_0^t dt' f(t') \tag{A5}$$

satisfies $\hat{f}(0)=\hat{f}(1)=0$ due to the rephasing condition (50). Consequently, the sum of the three terms in Eq. (A1) is strictly zero. We have thus shown that there is no contribution of the first order in p.

2. Second-order contribution

The second-order contribution to a formal series expansion is given by the first diagonal element of the matrix

$$\tfrac{1}{2}(t_2-t_1)^2\mathcal{B}\Lambda^2\mathcal{B}^3+\tfrac{1}{2}(t_3-t_2)^2\mathcal{B}^2\Lambda^2\mathcal{B}^2+\tfrac{1}{2}(t_4-t_3)^2\mathcal{B}^3\Lambda^2\mathcal{B} + (t_2-t_1)(t_3-t_2)\mathcal{B}\Lambda\mathcal{B}\Lambda\mathcal{B}^2+(t_2-t_1)(t_4-t_3)\mathcal{B}\Lambda\mathcal{B}^2\Lambda\mathcal{B} + (t_3-t_2)(t_4-t_3)\mathcal{B}^2\Lambda\mathcal{B}\Lambda\mathcal{B}, \tag{A6}$$

where the f-weighted time average has to be taken. The computation of this coefficient in front of p^2 is complicated by the fact that the six individual terms in this expression are divergent (while their combination should converge). One thus need to use a renormalization procedure to regroup these terms in a convergent way.

The computation of the f-weighted time averages is simple:

$$\langle(t_2-t_1)^2\rangle_4=-\tfrac{1}{6}F_1F_3,$$

$$\langle(t_3-t_2)^2\rangle_4=\tfrac{1}{4}F_2^2,$$

$$\langle(t_4-t_3)^2\rangle_4=-\tfrac{1}{6}F_1F_3,$$

$$\langle(t_2-t_1)(t_3-t_2)\rangle_4=\tfrac{1}{4}(F_1F_3-F_2^2),$$

$$\langle(t_2-t_1)(t_4-t_3)\rangle_4=-\tfrac{1}{2}(F_1F_3-F_2^2),$$

$$\langle(t_3-t_2)(t_4-t_3)\rangle_4=\tfrac{1}{4}(F_1F_3-F_2^2). \tag{A7}$$

The field theory technique used in Sec. IV.A to derive Eqs. (78) and (81) can be applied here to calculate the spatial averages. For example, the first diagonal element of the matrix $\mathcal{B}\Lambda^2\mathcal{B}^3$ can be written as

$$\frac{1}{V}\sum_m \int_\Omega d\mathbf{r}_1 \int_\Omega d\mathbf{r}_2 B(\mathbf{r}_1) u_m^*(\mathbf{r}_1)\lambda_m^2 u_m(\mathbf{r}_2) B^3(\mathbf{r}_2), \quad \text{(A8)}$$

where the sum is taken from $m=1$ to a large but finite cutoff. As previously, one replaces $\lambda_m u_m^*(\mathbf{r}_1)$ by $-L^2\Delta u_m^*(\mathbf{r}_1)$ and $\lambda_m u_m(\mathbf{r}_2)$ by $-L^2\Delta u_m(\mathbf{r}_2)$, and then uses the second Green's formula for both integrals. The result can be conveniently represented as

$$[\mathcal{B}\Lambda^2\mathcal{B}^3]_{0,0} = 3\sum_m (2X_m^{(2)} + Y_m^{(2)} - Z_m^{(2)})^*(Y_m^{(0)} - Z_m^{(0)}), \quad \text{(A9)}$$

where the following notations are introduced to lighten the expressions:

$$X_m^{(k)} = \frac{L^2}{V^{1/2}}\int_\Omega d\mathbf{r}\, u_m(\mathbf{r}) B^{k-1}(\mathbf{r})|\nabla B(\mathbf{r})|^2,$$

$$Y_m^{(k)} = \frac{L^2}{V^{1/2}}\int_\Omega d\mathbf{r}\, u_m(\mathbf{r}) B^{k}(\mathbf{r})\Delta B(\mathbf{r}),$$

$$Z_m^{(k)} = \frac{L^2}{V^{1/2}}\int_{\partial\Omega} d\mathbf{r}\, u_m(\mathbf{r}) B^{k}(\mathbf{r})\frac{\partial}{\partial n} B(\mathbf{r}). \quad \text{(A10)}$$

In a similar way, one finds five other spatial averages,

$$[\mathcal{B}^2\Lambda^2\mathcal{B}^2]_{0,0} = 4\sum_m |X_m^{(1)} + Y_m^{(1)} - Z_m^{(1)}|^2,$$

$$[\mathcal{B}^3\Lambda^2\mathcal{B}]_{0,0} = 3\sum_m (2X_m^{(2)} + Y_m^{(2)} - Z_m^{(2)})^*(Y_m^{(0)} - Z_m^{(0)}),$$

$$[\mathcal{B}^2\Lambda\mathcal{B}\Lambda\mathcal{B}]_{0,0} = 2\sum_m (X_m^{(2)} + Y_m^{(2)} - Z_m^{(2)})^*(Y_m^{(0)} - Z_m^{(0)}),$$

$$[\mathcal{B}\Lambda\mathcal{B}^2\Lambda\mathcal{B}]_{0,0} = \sum_m (Y_m^{(2)} - Z_m^{(2)})^*(Y_m^{(0)} - Z_m^{(0)}),$$

$$[\mathcal{B}\Lambda\mathcal{B}\Lambda\mathcal{B}^2]_{0,0} = 2\sum_m (X_m^{(2)} + Y_m^{(2)} - Z_m^{(2)})^*(Y_m^{(0)} - Z_m^{(0)}). \quad \text{(A11)}$$

The substitution of the temporal and spatial averages into Eq. (A6) and further algebraic simplification gives the leading term of the fourth moment as

$$\mathbb{E}\left\{\frac{\phi^4}{4!}\right\} = \tfrac{1}{2}p^2F_2^2\sum_m [|X_m^{(1)} + Y_m^{(1)} - Z_m^{(1)}|^2 - (2X_m^{(2)} + Y_m^{(2)} - Z_m^{(2)})^*(Y_m^{(0)} - Z_m^{(0)})]. \quad \text{(A12)}$$

This expression does not contain divergent terms, so that the sum can be extended up to infinity. One then substitutes the notations (A10) and sums over m to get $\delta(\mathbf{r}_1-\mathbf{r}_2)$. After integration, a number of terms in the above expression vanish. One finally gets the leading terms of the fourth moment:

$$\mathbb{E}\left\{\frac{\phi^4}{4!}\right\} = \frac{1}{2}p^2(\langle(t_1-t_2)\rangle_2)^2\left(\frac{L^4}{V}\int_\Omega d\mathbf{r}\,|\nabla B(\mathbf{r})|^4\right), \quad \text{(A13)}$$

where the f-weighted time average $\langle(t_1-t_2)\rangle_2$ is substituted instead of F_2. A similar analysis could be used to compute higher moments, but a more systematic technique would certainly be helpful.

APPENDIX B: LAPLACE TRANSFORM SUMMATION TECHNIQUE

In Sec. IV.C, the $p^{3/2}$ correction term to the second moment was obtained in the slow-diffusion regime ($p \ll 1$). The use of a renormalization procedure to overcome the formal divergence of the series expansion (92) may appear unsatisfactory from the mathematical point of view. Here we show how the Laplace transform summation technique can be used to study the second-order moment in a more general and rigorous way.[87] In what follows, we are looking for the spatial average

$$[\mathcal{B}e^{-p(t_2-t_1)\Lambda}\mathcal{B}]_{0,0} = (\mathcal{B}_{0,0})^2 + H(p(t_2-t_1))$$

and its dependence on the variable $\tilde{p}=p(t_2-t_1)$, where

$$H(\tilde{p}) = \sum_{m=1}^{\infty} \mathcal{B}_{0,m}e^{-\tilde{p}\lambda_m}\mathcal{B}_{m,0}.$$

For the sake of clarity, we focus on the case of the Neumann boundary condition (11), when $h=0$.

The Laplace transform of the function $H(\tilde{p})$ is simply

$$\mathcal{L}[H](s) = \sum_{m=1}^{\infty}\frac{\mathcal{B}_{0,m}\mathcal{B}_{m,0}}{s+\lambda_m}. \quad \text{(B1)}$$

Note that $\mathcal{L}[H](s)$ appears as the generating function for the coefficients ζ_k defined by Eq. (75):

$$\mathcal{L}[H](s) = \sum_{k=0}^{\infty}(-1)^k\zeta_{-k-1}s^k; \quad \text{(B2)}$$

hence for $k\geq 0$, one gets

$$\zeta_{-k-1} = \frac{(-1)^k}{k!}\left(\frac{\partial^k}{\partial s^k}\mathcal{L}[H](s)\right)_{s=0}. \quad \text{(B3)}$$

Once the function $\mathcal{L}[H](s)$ is found, its inverse Laplace transform provides the spatial average for the second moment. In particular, we shall demonstrate the asymptotic behavior of $H(\tilde{p})$ in the slow-diffusion regime ($\tilde{p}\to 0$)

[87] Note that a similar technique was applied by Mitra *et al.* (1993) to calculate the time-dependent diffusion coefficient for a sphere.

TABLE III. Laplace transform $\mathcal{L}[H](s)$ and related quantities for three basic domains and two spatial profiles of the magnetic field (here $h=0$).

		Slab	Cylinder	Sphere
Linear gradient		$\alpha_m=(2m-1)\pi, \quad y(z)=\cos(z/2)$	$\alpha_m=\alpha_{1m}, \quad y(z)=J_1'(z)$	$\alpha_m=\alpha_{1m}, \quad y(z)=j_1'(z)$
	$\mathcal{L}[H](s)$	$\frac{1}{12}s^{-1}-s^{-2}+\frac{2}{s^2}\frac{\tanh(\sqrt{s}/2)}{\sqrt{s}}$	$\frac{1}{4}s^{-1}-2s^{-2}+\frac{1}{s^2}\left(1+\frac{iJ_1(i\sqrt{s})}{\sqrt{s}J_0(i\sqrt{s})}\right)^{-1}$	$\frac{1}{5}s^{-1}-\frac{3}{2}s^{-2}+\frac{1}{4s}\left(1+s/2-\frac{\sqrt{s}}{\tanh\sqrt{s}}\right)^{-1}$
	$\mathcal{L}[H](s)$ $(s\to 0)$	$\frac{1}{120}-\frac{17}{20160}s+\frac{31}{362880}s^2+O(s^3)$	$\frac{7}{96}-\frac{11}{512}s+\frac{73}{11520}s^2+O(s^3)$	$\frac{8}{175}-\frac{83}{7875}s+\frac{2458}{1010625}s^2+O(s^3)$
	$\mathcal{L}[H](s)$ $(s\to\infty)$	$\frac{1}{12}s^{-1}-s^{-2}+2s^{-5/2}+O(\exp)$	$\frac{1}{4}s^{-1}-s^{-2}+s^{-5/2}+\frac{1}{2}s^{-3}-\frac{1}{8}s^{-7/2}+\cdots$	$\frac{1}{5}s^{-1}-s^{-2}+s^{-5/2}+s^{-3}-\frac{1}{2}s^{-4}+\cdots$
	$H(\tilde{p})$ $(\tilde{p}\to 0)$	$\frac{1}{12}-\tilde{p}+\frac{8}{3\sqrt{\pi}}\tilde{p}^{3/2}+O(\exp)$	$\frac{1}{4}-\tilde{p}+\frac{4}{3\sqrt{\pi}}\tilde{p}^{3/2}+\frac{1}{4}\tilde{p}^2-\frac{1}{15\sqrt{\pi}}\tilde{p}^{5/2}+\cdots$	$\frac{1}{5}-\tilde{p}+\frac{4}{3\sqrt{\pi}}\tilde{p}^{3/2}+\frac{1}{2}\tilde{p}^2-\frac{1}{3}\tilde{p}^3+\cdots$
Parabolic field		$\alpha_m=m\pi, \quad y(z)=\sin(z)$	$\alpha_m=\alpha_{0m}, \quad y(z)=J_0'(z)$	$\alpha_m=\alpha_{0m}, \quad y(z)=j_0'(z)$
	$\mathcal{L}[H](s)$	$\frac{4}{45}s^{-1}-\frac{4}{3}s^{-2}-4s^{-3}+\frac{4}{s^3}\frac{\sqrt{s}}{\tanh\sqrt{s}}$	$\frac{1}{12}s^{-1}-2s^{-2}-16s^{-3}+\frac{8}{s^2}\left(\frac{iJ_0(i\sqrt{s})}{\sqrt{s}J_1(i\sqrt{s})}\right)$	$\frac{12}{175}s^{-1}-\frac{72}{5}s^{-2}-36s^{-3}+\frac{12}{s^2}\left(1-\frac{\tanh\sqrt{s}}{\sqrt{s}}\right)^{-1}$
	$\mathcal{L}[H](s)$ $(s\to 0)$	$\frac{8}{945}-\frac{4}{4725}s+\frac{8}{93555}s^2+O(s^3)$	$\frac{1}{192}-\frac{1}{2880}s+\frac{13}{552960}s^2+O(s^3)$	$\frac{8}{2625}-\frac{148}{1010625}s+\frac{472}{65690625}s^2+O(s^3)$
	$\mathcal{L}[H](s)$ $(s\to\infty)$	$\frac{4}{45}s^{-1}-\frac{4}{3}s^{-2}+4s^{-5/2}-4s^{-3}+O(\exp)$	$\frac{1}{12}s^{-1}-2s^{-2}+8s^{-5/2}-12s^{-3}+3s^{-7/2}+\cdots$	$\frac{12}{175}s^{-1}-\frac{12}{5}s^{-2}+12s^{-5/2}-24s^{-3}+12s^{-7/2}+\cdots$
	$H(\tilde{p})$ $(\tilde{p}\to 0)$	$\frac{4}{45}-\frac{4}{3}\tilde{p}+\frac{16}{3\sqrt{\pi}}\tilde{p}^{3/2}-2\tilde{p}^2+O(\exp)$	$\frac{1}{12}-2\tilde{p}+\frac{32}{3\sqrt{\pi}}\tilde{p}^{3/2}-6\tilde{p}^2+\frac{8}{5\sqrt{\pi}}\tilde{p}^{5/2}+\cdots$	$\frac{12}{175}-\frac{12}{5}\tilde{p}+\frac{48}{3\sqrt{\pi}}\tilde{p}^{3/2}-12\tilde{p}^2+\frac{32}{5\sqrt{\pi}}\tilde{p}^{5/2}+\cdots$

$$H(\tilde{p}) = \zeta_0 - \zeta_1\tilde{p} + \zeta_{3/2}\tilde{p}^{3/2} + O(\tilde{p}^2), \tag{B4}$$

where the values of the coefficients ζ_0, ζ_1, and $\zeta_{3/2}$ are given in Table II for three basic domains and two spatial profiles of the magnetic field.

1. Consequences of the Mittag-Leffler theorem

For basic domains, a rigorous analytical computation of the second moment and related quantities is based on a simple consequence of the Mittag-Leffler theorem in complex analysis (Markushevich, 1965). Let $\{z_n\}$ be a sequence of all zeros (with multiplicities m_n) of an entire function $y(z)$ (i.e., an analytic function in the whole complex plane) so that it can be formally written as

$$y(z) = a_0 \prod_n (z - z_n)^{m_n}$$

(here a_0 is a constant). Taking the derivative and dividing it by $y(z)$, one gets

$$\frac{y'(z)}{y(z)} = \sum_n \frac{m_n}{z - z_n}. \tag{B5}$$

In the case of infinite sequence of simple zeros (with multiplicities $m_n=1$),[88] this relation can be made rigorous by requiring that z_n go to infinity, and

$$\sum_n \frac{1}{|z_n|} = \infty.$$

This relation provides an efficient tool to compute infinite sums involving the Laplace operator eigenvalues λ_m for basic domains, in particular, the function

$$\eta(s) \equiv \sum_{m=1}^{\infty} \frac{1}{s - \lambda_m}. \tag{B6}$$

According to Table I, the eigenvalues λ_m are equal to α_m^2, where α_m are the positive simple zeros of a certain explicit entire function $y(z)$. When the set $\{\pm\alpha_m\}$ contains all zeros of $y(z)$, one can apply the Mittag-Leffler theorem to get

$$\eta(s) = \frac{1}{2\sqrt{s}} \sum_{m=1}^{\infty} \left(\frac{1}{\sqrt{s} - \alpha_m} + \frac{1}{\sqrt{s} + \alpha_m} \right) = \frac{1}{2\sqrt{s}} \frac{y'(\sqrt{s})}{y(\sqrt{s})}. \tag{B7a}$$

If $z=0$ is also a zero of $y(z)$, it should be explicitly subtracted:

$$\eta(s) = \frac{1}{2\sqrt{s}} \left(\frac{y'(\sqrt{s})}{y(\sqrt{s})} - \frac{1}{\sqrt{s}} \right). \tag{B7b}$$

As a consequence, the infinite sum in Eq. (B6) is now expressed in terms of the explicit and known function $y(z)$. Its examples for basic domains and different spatial profiles are given in Table III.

Once $\eta(s)$ is known, one can establish a number of useful results for more complicated sums involving the Laplace operator eigenvalues. For instance, one deduces

$$\sum_{m=1}^{\infty} \frac{1}{(s_1 - \lambda_m)(s_2 - \lambda_m)} = \frac{\eta(s_1) - \eta(s_2)}{s_2 - s_1}. \tag{B8}$$

More generally, one can compute the sum

$$\eta^{(k)}(s_1, \ldots, s_k) \equiv \sum_{m=1}^{\infty} \prod_{j=1}^{k} \frac{1}{s_j - \lambda_m} \tag{B9}$$

iteratively, applying the identity

$$\eta^{(k)}(s_1, \ldots, s_k) = \frac{\eta^{(k-1)}(s_1, \ldots, s_{k-1}) - \eta^{(k-1)}(s_1, \ldots, s_k)}{s_k - s_{k-1}} \tag{B10}$$

with $\eta^{(1)}(s) \equiv \eta(s)$. Multiple differentiation of Eq. (B9) with respect to the variables s_j further extends the set of useful relations for any positive integers $\alpha_1, \ldots, \alpha_k$:

$$\sum_{m=1}^{\infty} \prod_{j=1}^{k} \frac{1}{(s_j - \lambda_m)^{\alpha_j+1}} = \frac{(-1)^{\alpha_1+\cdots+\alpha_k}}{\alpha_1! \cdots \alpha_k!} \frac{\partial^{\alpha_1+\cdots+\alpha_k}}{\partial s_1^{\alpha_1} \cdots \partial s_k^{\alpha_k}} \eta^{(k)}(s_1, \ldots, s_k). \tag{B11}$$

Although cumbersome, these expressions allow one to rigorously compute many sums and related quantities involving the Laplace operator eigenvalues.

2. Example: Slab geometry and parabolic profile

To illustrate the efficiency of the Laplace transform summation technique, we consider restricted diffusion in a slab geometry under a parabolic magnetic field. The substitution of the elements $\mathcal{B}_{0,m}$ from Eq. (70) into Eq. (B1) leads to

$$\mathcal{L}[H](s) = 8 \sum_{m=1}^{\infty} \frac{1}{\lambda_m^2 (s + \lambda_m)}, \tag{B12}$$

where the eigenvalues are simply $\lambda_m = (\pi m)^2$. Since $\{\pm\pi m\}$ are zeros of the entire function $y(z) = \sin z$, Eq. (B7b) yields

$$\eta(s) = \frac{1}{2\sqrt{s}} \left(\frac{\cos\sqrt{s}}{\sin\sqrt{s}} - \frac{1}{\sqrt{s}} \right) \tag{B13}$$

(here the zero $z=0$ is explicitly subtracted). In this case, the sum in Eq. (B12) can be found according to Eq. (B11) as

[88] This mathematical result can be significantly extended as described by Markushevich (1965). Here we do not discuss convergence of the series in the right-hand side of Eq. (B5), especially since the most attention will be focused on the function $\eta(s)$ defined by the convergent series in Eq. (B6).

$$\mathcal{L}[H](s) = 8\left(\frac{\partial}{\partial s_1}\frac{\eta(s_1)-\eta(s_2)}{s_2-s_1}\right)_{s_1=0,s_2=-s}.$$

Substitution of the explicit function $\eta(s)$ from Eq. (B13) into the above relation gives

$$\mathcal{L}[H](s) = \frac{4}{45}s^{-1} - \frac{4}{3}s^{-2} - 4s^{-3} + \frac{4}{s^3}\frac{\sqrt{s}}{\tanh\sqrt{s}}. \qquad \text{(B14)}$$

This is an exact rigorous result. Its series expansion in the limit $s\to 0$ allows determination of the coefficients ζ_{-k} for $k>0$ given in Table II:

$$\mathcal{L}[H](s) = \underset{(\zeta_{-1})}{\frac{8}{945}} - \underset{(\zeta_{-2})}{\frac{4}{4725}}s + \underset{(\zeta_{-3})}{\frac{8}{93555}}s^2 + O(s^3).$$

Although the inverse Laplace transform on the right-hand side of Eq. (B14) cannot be expressed in elementary functions, its numerical computation and series expansion are simple and useful. For instance, the asymptotic behavior of $\mathcal{L}[H](s)$ in the limit $s\to\infty$ describes the spatial average of the second moment in the slow diffusion regime ($\tilde{p}\to 0$). Since $\tanh\sqrt{s}$ in Eq. (B14) exponentially converges to 1 as $s\to\infty$, one finds

$$\mathcal{L}[H](s) \simeq \frac{4}{45}s^{-1} - \frac{4}{3}s^{-2} + 4s^{-5/2} - 4s^{-3}$$

with exponentially small corrections [which are formally denoted in Table III as $O(\exp)$]. Using the identity $\mathcal{L}^{-1}[s^{-\beta}]=\tilde{p}^{\beta-1}/\Gamma(\beta)$, one obtains

$$H(\tilde{p}) \simeq \underset{(\zeta_0)}{\frac{4}{45}} - \underset{(\zeta_1)}{\frac{4}{3}}\tilde{p} + \underset{(\zeta_{3/2})}{\frac{4}{\Gamma(5/2)}}\tilde{p}^{3/2} - \underset{(\zeta_2)}{2\tilde{p}^2} \quad (\text{as } \tilde{p}\to 0).$$

Numerical computation shows that the maximum relative error of this formula is below 1% for $\tilde{p}\leqslant 0.2$. Comparison with Eq. (B4) allows determination of the coefficients ζ_0, ζ_1, $\zeta_{3/2}$, and ζ_2 given in Table II. Note that higher-order polynomial corrections vanish: $\zeta_{5/2}=\zeta_3=\cdots=0$.

In a similar way, one can rigorously calculate $\mathcal{L}[H](s)$ and related quantities for other basic domains and spatial profiles. These results are summarized in Table III. For three basic domains, the function $\eta(s)$ is given by Eqs. (B7a) and (B7b) for a linear gradient and a parabolic magnetic field, respectively. The asymptotic expansion of $\mathcal{L}[H](s)$ as $s\to\infty$ [and of $H(\tilde{p})$ as $\tilde{p}\to 0$] for a slab geometry is cut off after the $p^{3/2}$ correction, that is, $\zeta_2=\zeta_{5/2}=\cdots=0$. This specific feature expains why the only $p^{3/2}$ correction gives very accurate results in the slow-diffusion regime for a slab geometry (Fig. 5). In contrast, similar expansions for a cylinder and a sphere contain an infinite number of terms. As a result, the very same $p^{3/2}$ correction is not accurate enough for a cylinder and a sphere since higher-order polynomial corrections are present.

3. Analogy with the return-to-the-origin probability

For basic domains, the spatial average of the second moment and related quantities appear as infinite sums involving the Laplace operator eigenvalues λ_m alone. This curious fact bridges a number of interesting links to other mathematical fields. For instance, the function

$$\hat{\eta}(s)\equiv -\eta(-s) = \sum_m \frac{1}{s+\lambda_m}$$

turns out to be the Laplace transform of the spectral function

$$H_0(\tilde{p}) = \sum_m e^{-\tilde{p}\lambda_m}$$

over the eigenvalues λ_m that contribute to the second moment. For three basic domains, the following asymptotic behavior holds:[89]

$$\hat{\eta}(s) \simeq \frac{1}{2\sqrt{s}} \quad (\text{as } s\to\infty) \qquad \text{(B15)}$$

which implies the asymptotic behavior of $H_0(\tilde{p})$ in the slow-diffusion regime:

$$H_0(\tilde{p}) \simeq \frac{1}{2\sqrt{\pi}}\frac{1}{\sqrt{\tilde{p}}} \quad (\text{as } \tilde{p}\to 0). \qquad \text{(B16)}$$

At this point, we outline a similarity between this function and the averaged return-to-the-origin probability considered by Mitra *et al.* (1995) and Schwartz *et al.* (1997):

$$P(\tilde{p}) = \int_\Omega d\mathbf{r}\, G_{t_2-t_1}(\mathbf{r},\mathbf{r}) = \sum_{m=0}^{\infty} e^{-\tilde{p}\lambda_m}. \qquad \text{(B17)}$$

The only difference is that the last sum contains all eigenvalues λ_m, while $H_0(\tilde{p})$ is defined for specific eigenmodes, for which $\mathcal{B}_{0,m}\neq 0$. In the limit $\tilde{p}\to 0$, the heat kernel in Eq. (B17) can be roughly approximated by the free-diffusion heat kernel (181), giving $P(\tilde{p})\sim(4\pi\tilde{p})^{-d/2}$. Since $\mathcal{L}[H_0](s)$ contains a smaller number of terms, its convergence as $s\to\infty$ is better, and the behavior of $H_0(\tilde{p})$ as $\tilde{p}\to 0$ is less sharp than for $P(\tilde{p})$. Note that the properties of the function $P(\tilde{p})$ were investigated by Kac (1966) in attempt to answer the famous question: Can one hear the shape of a drum? Although interesting, a further discussion on this topic is beyond the scope of this review.

4. Relation to spectral zeta functions

At the end of this section, we outline the relationship between the coefficients ζ_k defined by Eq. (75) and spec-

[89] The coefficient 1/2 stands in front of $s^{-1/2}$ and $\tilde{p}^{-1/2}$ in Eqs. (B15) and (B16) for all considered cases except slab geometry under a linear gradient, for which the coefficient 1/4 should be used.

tral zeta functions. Consider again the case of slab geometry and parabolic magnetic field. The substitution of Eq. (B12) into Eq. (B3) yields

$$\zeta_{-k} = 8\sum_{m=1}^{\infty} \frac{1}{\lambda_m^{k+2}} = \frac{8}{\pi^{2k+4}} \sum_{m=1}^{\infty} \frac{1}{m^{2k+4}}. \tag{B18}$$

The last sum is the Riemann zeta function

$$\zeta(z) = \sum_{m=1}^{\infty} m^{-z}$$

that is defined for any complex z with $\mathrm{Re}(z)>1$ and has a meromorphic continuation to the whole complex plane. This function found numerous applications in mathematics and physics [see Lapidus and Pomerance (1993); Elizalde (1995); Lapidus and van Frankenhuysen (2000), and references therein]. In turn, the intermediate sum in Eq. (B18) is often referred to as a spectral zeta function since it is formed by eigenvalues of an operator (in our case, this is the Laplace operator). In this light, the coefficients ζ_{-k} for three basic domains under parabolic magnetic field can be considered as spectral zeta functions. For instance, Table I gives for a cylinder

$$\zeta_{-k} = 16\sum_{m} \frac{1}{\lambda_m^{k+2}},$$

where $\lambda_m = \alpha_{0m}^2, \alpha_{0m}$ being the positive roots of $J_0'(z)=0$. We stress again that the above sum is carried out over specific eigenmodes, for which $\mathcal{B}_{0,m} \neq 0$. Finally, the coefficients ζ_{-k} for a linear gradient are slightly more complicated. For example, one has for a cylinder

$$\zeta_{-k} = 2\sum_{m} \frac{1}{(\lambda_m - 1)\lambda_m^{k+1}},$$

which can still be seen as a kind of spectral zeta function. Further discussion of the exciting properties of spectral zeta functions is beyond the scope of the present review.

APPENDIX C: FOURTH MOMENT IN THE MOTIONAL-NARROWING REGIME

As an illustrative example, we calculate the leading term of the fourth moment $\mathbb{E}\{\phi^4\}$ in the motional-narrowing regime. Although the calculation is as elementary as for the second moment, the variety of specific cases makes it cumbersome for higher moments.

Consider the f-weighted time average for the fourth moment:

$$\langle e^{-p\lambda_{m_1}(t_2-t_1)} e^{-p\lambda_{m_2}(t_3-t_2)} e^{-p\lambda_{m_3}(t_4-t_3)} \rangle_4. \tag{C1}$$

As for the second moment, one might simply replace each exponential function by its leading asymptotic term $(p\lambda_{m_i})^{-1}\delta(t_{i+1}-t_i)$ as $p\to\infty$, so that the fourth moment would behave as p^{-3}. However, a more accurate analysis requires one to account for special cases when certain λ_{m_i} are zero. We briefly consider these cases.

- For $m_1=m_2=m_3=0$ (all λ_{m_i} are zero), the f-weighted time average of a constant vanishes.
- When two of three eigenvalues are zero ($m_1=m_2=0$ or $m_1=m_3=0$ or $m_2=m_3=0$), one replaces the remaining exponential function by its leading asymptotic term. The summation over nontrivial eigenvalues gives the same constant for three cases:

$$\sum_{m=1}^{\infty} \lambda_m^{-1} \mathcal{B}_{0,m}\mathcal{B}_{m,0}\mathcal{B}_{0,0}^2 = \mathcal{B}_{0,0}^2 \zeta_{-1}. \tag{C2}$$

Then one calculates the f-weighted time averages of δ functions:

$$2\langle \delta(t_2-t_1)\rangle_4 = 2\langle \delta(t_4-t_3)\rangle_4 = -\langle \delta(t_3-t_2)\rangle_4 = \int_0^1 dt\, f^2(t)\,\hat{f}^2(t), \tag{C3}$$

where the primitive $\hat{f}$ is defined by Eq. (A5). One concludes that the sum of three terms is equal to 0.

- For the cases $m_1=0$ or $m_3=0$, one obtains

$$\langle \delta(t_2-t_1)\delta(t_3-t_2)\rangle_4 = -\int_0^1 dt\, f^3(t)\hat{f}(t),$$

$$\langle \delta(t_3-t_2)\delta(t_4-t_3)\rangle_4 = \int_0^1 dt\, f^3(t)\hat{f}(t), \tag{C4}$$

while the spatial averages are identical, so that these contributions cancel each other.

- The only nontrivial case is $m_2=0$ (with $m_1>0$ and $m_3>0$). One has

$$\langle \delta(t_2-t_1)\delta(t_4-t_3)\rangle_4 = \frac{1}{2}\left(\int_0^1 dt\, f^2(t)\right)^2, \tag{C5}$$

i.e., the time average of these two delta functions is split in two. The same happens for the sums over indices m_1 and m_3,

$$\sum_{m_1,m_3} \lambda_{m_1}^{-1}\mathcal{B}_{0,m_1}\mathcal{B}_{m_1,0}\mathcal{B}_{0,m_3}\mathcal{B}_{m_3,0}\lambda_{m_3}^{-1} = \zeta_{-1}^2. \tag{C6}$$

One finally obtains the leading term of the fourth moment in the motional-narrowing regime in the form (118) with $n=2$.

APPENDIX D: MULTIPLE PROPAGATOR APPROACH

Considerable progress in the numerical analysis of diffusive NMR phenomena was achieved by the multiple propagator approach first proposed by Caprihan *et al.* (1996), further developed by Callaghan (1997), and equivalently reformulated by Sukstanskii and Yablonskiy (2002). Although this approach was intended to study the particular case of a linear magnetic-field gradient, we describe its extension for any spatial profile $B(\mathbf{r})$.

Dividing the time interval [0,1] into K subintervals of duration $\tau=1/K$, one can approximate the integral in Eq. (52) by a finite sum

$$E \simeq \mathbb{E}\left\{ \exp\left[iq\tau \sum_{k=0}^{K} f_k B(X_{k\tau}) \right] \right\}, \tag{D1}$$

where $f_k \equiv f(k\tau)$. To calculate the expectation, all possible values of the random variables $X_{k\tau}$ should be weighted with the corresponding probabilities. Indeed, the starting position $\mathbf{r}_0$ is distributed according to a given initial density $\rho_0(\mathbf{r}_0)$. The probability distribution of the next position $\mathbf{r}_1$ after time τ is given by the propagator $G_\tau(\mathbf{r}_0,\mathbf{r}_1)$, and so on. One thus obtains

$$E \simeq \int_\Omega d\mathbf{r}_0 \int_\Omega d\mathbf{r}_1 \cdots \int_\Omega d\mathbf{r}_K \rho_0(\mathbf{r}_0) e^{iq\tau f_0 B(\mathbf{r}_0)} \times G_\tau(\mathbf{r}_0,\mathbf{r}_1) e^{iq\tau f_1 B(\mathbf{r}_1)} G_\tau(\mathbf{r}_1,\mathbf{r}_2) \cdots e^{iq\tau f_K B(\mathbf{r}_K)}.$$

The spectral expansion (31) of the heat kernel allows the signal E to be written as the scalar product $E=(WH\tilde{W})$, where an infinite-dimensional matrix H is

$$H = RA(f_1)R \cdots A(f_{K-1})R.$$

Two infinite-dimensional matrices R and A and two vectors W and $\tilde{W}$ are defined as

$$A_{m,m'}(f_k) = \int_\Omega d\mathbf{r}\, u_m^*(\mathbf{r}) u_{m'}(\mathbf{r}) \exp[iq\tau f_k B(\mathbf{r})],$$

$$R_{m,m'} = \delta_{m,m'} \exp[-p\tau\lambda_m],$$

$$W_m = V^{1/2} \int_\Omega d\mathbf{r}\, u_m(\mathbf{r}) \rho_0(\mathbf{r}) \exp[iq\tau f_0 B(\mathbf{r})],$$

$$\tilde{W}_m = V^{-1/2} \int_\Omega d\mathbf{r}\, u_m^*(\mathbf{r}) \exp[iq\tau f_K B(\mathbf{r})].$$

Although the multiple propagator approach provided an efficient numerical tool, its use for theoretical analysis has been quite limited since the dependence on the main parameters p and q is hidden in the matrices R and A and the vectors W and $\tilde{W}$. In contrast, the MCF description is given in terms of the matrices $\mathcal{B}$ and Λ that depend only on the confining geometry and the spatial profile of the magnetic field. In addition, the dependence on p and q is explicit and easy to investigate. For this reason, the MCF approach turns out to be more appropiate for theoretical and numerical analysis.

One may wonder what happens with the multiple propagator approach in the limit $\tau\to 0$. To the first order in τ, one has

$$A(f_k) \simeq I + iq\tau f_k \mathcal{B}, \quad R \simeq I - p\tau\Lambda,$$

where the matrices Λ and $\mathcal{B}$ are defined by Eqs. (42) and (47), respectively, and I stands for the identity matrix. For the sake of simplicity, consider the case of reflecting boundaries, for which the elements W_m and $\tilde{W}_m$ can be approximated by $\delta_{m,0}$. The matrix H becomes

$$H \simeq \prod_{k=0}^{K} [I + \tau(iqf_k\mathcal{B} - p\Lambda)],$$

which can be formally expanded as

$$H \simeq I + \tau \sum_{k_1}^{K} (iqf_{k_1}\mathcal{B} - p\Lambda) + \cdots + \tau^n \sum_{k_1<\cdots<k_n}^{K} (iqf_{k_1}\mathcal{B} - p\Lambda) \cdots (iqf_{k_n}\mathcal{B} - p\Lambda) + \cdots. \tag{D2}$$

This expansion contains all possible products of matrices $\mathcal{B}$ and Λ. A general form of the term containing n matrices $\mathcal{B}$ and m matrices Λ can be written as

$$\underbrace{\Lambda\cdots\Lambda}_{\ell_0}\mathcal{B}\underbrace{\Lambda\cdots\Lambda}_{\ell_1}\mathcal{B}\cdots\underbrace{\Lambda\cdots\Lambda}_{\ell_{n-1}}\mathcal{B}\underbrace{\Lambda\cdots\Lambda}_{\ell_n}. \tag{D3}$$

where the positive indices $\ell_0,\ldots,\ell_n$ are such that $\ell_0+\cdots+\ell_n=m$. The coefficient in front of this term is

$$(iq)^n(-p)^m\tau^{n+m} \sum_{k_1<\cdots<k_{n+m}}^{K} F_{k_1}F_{k_2}\cdots F_{k_{n+m}}, \tag{D4}$$

where $F_{k_j}=f_{k_j}$ if the matrix $\mathcal{B}$ stands at the jth place in the sequence (D3), and $F_{k_j}=1$ otherwise. If the subdivision τ is small enough, these coefficients can be considered as integral sums, yielding in the limit $\tau\to 0$

$$(iq)^n(-p)^m \int_0^1 dt_1 \int_{t_1}^1 dt_2 \cdots \int_{t_{n-1}}^1 dt_n \frac{t_1^{\ell_0}}{\ell_0!} f(t_1) \frac{(t_2-t_1)^{\ell_1}}{\ell_1!} \times f(t_2)\cdots\frac{(t_n-t_{n-1})^{\ell_{n-1}}}{\ell_{n-1}!} f(t_n) \frac{(1-t_n)^{\ell_n}}{\ell_n!}.$$

Taking all possible combinations of indices $\ell_0,\ldots,\ell_n$ from 0 to infinity, one obtains the nth-order contribution to the sum (D2) as

$$H_n = (iq)^n \int_0^1 dt_1 \int_{t_1}^1 dt_2 \cdots \int_{t_{n-1}}^1 dt_n f(t_1)\cdots f(t_n) \times e^{-pt_1\Lambda}\mathcal{B}e^{-p(t_2-t_1)\Lambda}\mathcal{B}\cdots\mathcal{B}e^{-p(t_n-t_{n-1})\Lambda}\mathcal{B}e^{-p(1-t_n)\Lambda}.$$

According to Eq. (59), the first diagonal element of the matrix H_n is exactly the f-weighted time average of the correlation function $\mathbb{E}\{B(X_{t_1})\cdots B(X_{t_n})\}$, multiplied by $(iq)^n$. Consequently, we retrieved the series expansion (54) for the signal E. On the one hand, this derivation reveals how the limit $\tau\to 0$ can be taken within the multiple propagator approach. In particular, it justifies the convergence of this method for $\tau\to 0$ which was not proved earlier. On the other hand, the direct relation between the multiple propagator approach and the series expansion may be fruitful for further investigation. Note that a very similar analysis allows one to derive the series expansion (54) from the approximate relation (144) in the limit $\tau\to 0$.

APPENDIX E: EVEN-ORDER MOMENTS IN THE NARROW-PULSE APPROXIMATION

The compact form (179) of the even-order moments can be used to study their dependence on the dimensionless diffusion coefficient p. For this purpose, the heat kernel $G_{T/2}(\mathbf{r}_1,\mathbf{r}_2)$ is represented by the spectral decomposition (31)

$$\mathbb{E}\left\{\frac{\phi^{2n}}{(2n)!}\right\} \simeq \frac{\delta^{2n}}{(2n)!}\sum_{m=0}^{\infty} e^{-p\lambda_m/2}\int_\Omega d\mathbf{r}_1\int_\Omega d\mathbf{r}_2 u_m^*(\mathbf{r}_1) \times u_m(\mathbf{r}_2)[B(\mathbf{r}_1)-B(\mathbf{r}_2)]^{2n}. \quad \text{(E1)}$$

To obtain the leading term, the function $e^{-p\lambda_m/2}$ can be formally developed in a power series up to order n:

$$\mathbb{E}\left\{\frac{\phi^{2n}}{(2n)!}\right\} \simeq \frac{\delta^{2n}}{(2n)!}\sum_{m=0}^{\infty}\sum_{j=0}^{n}\frac{(p/2)^j}{j!}\int_\Omega d\mathbf{r}_1 \times\int_\Omega d\mathbf{r}_2(-1)^j\lambda_m^j u_m^*(\mathbf{r}_1)u_m(\mathbf{r}_2) \times[B(\mathbf{r}_1)-B(\mathbf{r}_2)]^{2n}. \quad \text{(E2)}$$

As earlier, $(-1)^j\lambda_m^j$ can be considered as multiple (j times) application of the Laplace operator to $u_m^*(\mathbf{r}_1)$. Then the Green's formula is used to differentiate by parts. For instance, for $j=1$, one has

$$\Delta_{\mathbf{r}_1}[B(\mathbf{r}_1)-B(\mathbf{r}_2)]^{2n} = 2n(2n-1)[B(\mathbf{r}_1)-B(\mathbf{r}_2)]^{2n-2} \times|\nabla B(\mathbf{r}_1)|^2 + 2n[B(\mathbf{r}_1) - B(\mathbf{r}_2)]^{2n-1}\Delta B(\mathbf{r}_1). \quad \text{(E3)}$$

The summation over m gives $\delta(\mathbf{r}_1-\mathbf{r}_2)$, and the integral vanishes due to the term $[B(\mathbf{r}_1)-B(\mathbf{r}_2)]^{2n-2}$ if $2n-2>0$. In a similar way, all terms vanish for $j<n$. In contrast, the case $j=n$ leads to Eq. (179). A renormalization procedure would of course be required to operate with the divergent terms of orders higher than n and to derive the correction terms.

LIST OF SYMBOLS

B_0	constant magnetic field
$B(\mathbf{r})$	spatial profile of the diffusion-sensitizing magnetic field
$\mathcal{B}_{m,m'}$	matrix elements of the magnetic field in the Laplace operator eigenbasis, Eq. (47)
C_n^k	binomial coefficients, $C_n^k=n!/[(n-k)!k!]$
D	free self-diffusion coefficient
D_{app}	effective or apparent diffusion coefficient
$\mathbb{E}$	expectation
E	macroscopic signal (the notations M and S can be also found in the literature)
$F(t)$	auxiliary notation, $f(t)\equiv F(tT)$
$G_t(\mathbf{r},\mathbf{r}')$	diffusive propagator, heat kernel, or, equivalently, Green's function of diffusion equation in the confining domain
$J_n(z)$	Bessel functions of the first kind
$\mathcal{L}$	Laplace transform
L	characteristic size of the confining domain
$P_n(x)$	Legendre polynomials
$\mathcal{R}_i$	principal radii of curvature
S	total surface area
T	echo time or total gradient duration
$\mathfrak{T}$	tortuosity
U, $\tilde{U}$	infinite-dimensional vectors, Eqs. (39) and (40)
V	volume of the confining domain
X_t	reflected Brownian motion, $X_t\equiv\mathbf{r}(tT)$
b	b value or b coefficient, Sec. VI.D
$c_{\mathcal{B}}$	structure-dependent coefficient, Sec. IV.C
$c_m(t)$	time-dependent coefficients, Eq. (135)
d	dimension of the space ($d=3$ by default)
$f(t)$	effective temporal profile of magnetic field
g, g_1	gradient intensity
g_2	intensity of the parabolic magnetic field
h	dimensionless relaxation rate, Eq. (34)
i	imaginary unity, $i^2=-1$
$j_n(z)$	spherical Bessel functions
$\mathfrak{m}(\mathbf{r},t)$	magnetization, solution of Eq. (9)
p	dimensionless diffusion coefficient, Eq. (36)
q	dimensionless magnetic field intensity, Eq. (51)
r	radial coordinate, radius
$\mathbf{r}(t)$	stochastic trajectory of a diffusing nucleus
t	(dimensionless) time variable
$u_m(\mathbf{r})$	eigenfunctions of the Laplace operator in the confining domain
$\partial\Omega$	boundary of the confining domain
$\partial/\partial n$	normal derivative at the boundary
∇	gradient
$\langle\cdot\rangle_n$	f-weighted time average of a function, Eq. (56)
$<\cdot>_c$	cumulant average, Sec. VI.C
$!$	factorial, $n!=1\times2\times\cdots\times n$
$\Gamma(z)$	Euler gamma function
Δ	Laplace operator, $\Delta=\nabla^2=\partial^2/\partial x_1^2+\cdots+\partial^2/\partial x_d^2$
$\Theta(t)$	Heaviside step function, $\Theta(t)=1$ for $t>0$, and 0 otherwise
Λ	diagonal matrix formed by eigenvalues λ_m
Ω	confining domain
α_m, α_{nk}	positive roots of the equations representing the boundary condition, Table I
β	magnetic-field intensity
β_m, β_{nk}	normalization constants for eigenfunctions, Table I
γ	nuclear gyromagnetic ratio
δ	(normalized) duration of gradient pulses
$\delta_{m,m'}$	Kronecker symbol, $\delta_{m,m}=1$, and 0 otherwise
$\delta(\mathbf{r}-\mathbf{r}')$	Dirac distribution (delta function)
ϵ_m	coefficients, $\epsilon_0=1$ and $\epsilon_m=\sqrt{2}$ for $m>0$
ζ_k	structure-dependent coefficients, Eq. (75)
θ	azimuthal angle, $0\leq\theta\leq\pi$
κ_i	coefficients for tortuosity regime, Eq. (21)
λ_m	dimensionless eigenvalues of the Laplace operator in the confining domain

μ	nuclear magnetic moment
ρ	surface relaxivity or permeability
$\rho_0(\mathbf{r})$	initial density of nuclei
$\tilde{\rho}(\mathbf{r})$	pickup function (assumed to be 1)
τ	small time step
τ	ramp time for the trapezoidal profile, Fig. 4(d)
ϕ	normalized total phase, $\varphi = q\phi$
φ	total phase of a diffusion nucleus, Eq. (1)
φ	polar angle, $0 \leqslant \varphi < 2\pi$

REFERENCES

Abragam, A., 1961, *Principles of Nuclear Magnetism* (Oxford University, Oxford).

Albert, M. S., G. D. Cates, B. Driehuys, W. Happer, B. Saam, C. S. Springer, Jr., and A. Wishnia, 1994, "Biological magnetic resonance imaging using laser-polarized 129-Xe," Nature (London) **370**, 199–201.

Alberts, B., D. Bray, J. Lewis, M. Raff, K. Roberts, and J. D. Watson, 1994, *Molecular Biology of the Cell*, 3rd ed. (Garland, New York).

Ardelean, I., and R. Kimmich, 2003, "Principles and unconventional aspects of NMR diffusometry," Annu. Rep. NMR Spectrosc. **49**, 43–115.

Arfken, G. B., and H. J. Weber, 2001, *Mathematical Methods for Physicists*, 5th ed. (Academic, San Diego).

Armstrong, R. D., and R. A. Burnham, 1976, "The effect of roughness on the impedance of the interface between a solid electrolyte and a blocking electrode," J. Electroanal. Chem. Interfacial Electrochem. **72**, 257–266.

Assaf, Y., R. Z. Freidlin, G. K. Rohde, and P. J. Basser, 2004, "New modeling and experimental framework to characterize hindered and restricted water diffusion in brain white matter," Magn. Reson. Med. **52**, 965–978.

Audoly, B., P. N. Sen, S. Ryu, and Y.-Q. Song, 2003, "Correlation functions for inhomogeneous magnetic field in random media with application to a dense random pack of spheres," J. Magn. Reson. **164**, 154–159.

Axelrod, S., and P. N. Sen, 2001, "Nuclear magnetic resonance spin echoes for restricted diffusion in an inhomogeneous field: Methods and asymptotic regimes," J. Chem. Phys. **114**, 6878–6895.

Bachert, P., L. R. Schad, M. Bock, M. V. Knopp, M. Ebert, T. Grobmann, W. Heil, D. Hofmann, R. Surkau, and E. W. Otten, 1996, "Nuclear magnetic resonance imaging of airways in humans with use of hyperpolarized 3He magnetic resonance in medicine," Magn. Reson. Med. **36**, 192–196.

Balinov, B., B. Jönsson, P. Linse, and O. Söderman, 1993, "The NMR self-diffusion method applied to restricted diffusion. Simulation of echo attenuation from molecules in spheres and between planes," J. Magn. Reson., Ser. A **104**, 17–25; **108**, 130(E) (1994).

Balinov, B., O. Söderman, and J.-C. Ravey, 1994, "Diffraction-like effects observed in the PGSE experiment when applied to a highly concentrated water-oil emulsion," J. Phys. Chem. **98**, 393–395.

Banavar, J. R., M. Lipsicas, and J. F. Willemsen, 1985, "Determination of the random-walk dimension of fractals by means of NMR," Phys. Rev. B **32**, 6066–6066.

Barbé, R., M. Leduc, and F. Lalöe, 1974, "Résonance magnétique en champ de radiofréquence inhomogène 1re partie: Études théorique," J. Phys. (France) **35**, 699–725.

Barrall, G. A., L. Frydman, and G. C. Chingas, 1992, "NMR diffraction and spatial statistics of stationary systems," Science **255**, 714–717.

Barrie, P. J., 2000, "Characterization of porous media using NMR methods," Annu. Rep. NMR Spectrosc. **41**, 265–316.

Barsky, D., B. Pütz, K. Schulten, J. Schoeniger, E. W. Hsu, and S. Blackband, 1992, "Diffusional edge enhancement observed by NMR in thin glass capillaries," Chem. Phys. Lett. **200**, 88–96.

Barzykin, A. V., 1998, "Exact solution of the Torrey-Bloch equation for a spin echo in restricted geometries," Phys. Rev. B **58**, 14171–14174.

Barzykin, A. V., 1999, "Theory of spin echo in restricted geometries under a step-wise gradient pulse sequence," J. Magn. Reson. **139**, 342–353.

Bass, R. F., 1998, *Diffusions and Elliptic Operators* (Springer, New York).

Bear, J., 1972, *Dynamics of Fluids in Porous Media* (Dover, New York).

Bendel, P., 1990, "Spin-echo attenuation by diffusion in nonuniform field gradients," J. Magn. Reson. (1969-1992) **86**, 509–515.

Bendt, P. J., 1958, "Measurements of 3He-4He and H2-D2 gas diffusion coefficients," Phys. Rev. **110**, 85–89.

Bergman, D. J., 1997, "Diffusion eigenstates of a porous medium with interface absorption," Phys. Rev. E **55**, 4235–4244.

Bergman, D. J., and K.-J. Dunn, 1994, "Theory of diffusion in a porous-medium with applications to pulsed-field gradient NMR," Phys. Rev. B **50**, 9153–9156.

Bergman, D. J., and K.-J. Dunn, 1995, "NMR of diffusing atoms in a periodic porous medium in the presence of a nonuniform magnetic field," Phys. Rev. E **52**, 6516–6535.

Bergman, D. J., K.-J. Dunn, L. M. Schwartz, and P. P. Mitra, 1995, "Self-diffusion in a periodic porous medium: A comparison of different approaches," Phys. Rev. E **51**, 3393–3400.

Bidinosti, C. P., J. Choukeife, P.-J. Nacher, and G. Tastevin, 2003, "In vivo NMR of hyperpolarized 3He in the human lung at very low magnetic fields," J. Magn. Reson. **162**, 122–132.

Bishop, M. T., K. H. Langley, and F. E. Karasz, 1986, "Diffusion of a flexible polymer in a random porous material," Phys. Rev. Lett. **57**, 1741–1744.

Bixon, M., and R. Zwanzig, 1981, "Diffusion in a medium with static traps," J. Chem. Phys. **75**, 2354–2356.

Blees, M. H., 1994, "The effect of finite duration of gradient pulses on the pulsed-field-gradient NMR method for studying restricted diffusion," J. Magn. Reson., Ser. A **109**, 203–209.

Bloch, F., 1946, "Nuclear induction," Phys. Rev. **70**, 460–474.

Blümich, B., 2000, *NMR Imaging of Materials* (Clarendon, Oxford).

Bondeson, A., T. Rylander, and P. Ingelström, 2005, *Computational Electromagnetics*, Texts in Applied Mathematics Vol. 51 (Springer, New York).

Borgia, G. C., R. J. S. Brown, and P. Fantazzini, 1995, "Scaling of spin-echo amplitudes with frequency, diffusion coefficient, pore size, and susceptibility difference for the NMR of fluids in porous media and biological tissues," Phys. Rev. E **51**, 2104–2114.

Borodin, A. N., and P. Salminen, 1996, *Handbook of Brownian Motion: Facts and Formulae* (Birkhauser-Verlag, Basel).

Bouchaud, J. P., and A. Georges, 1990, "Anomalous diffusion in disordered media: Statistical mechanisms, models and

physical applications," Phys. Rep. **195**, 127–293.
Brandl, M., and A. Haase, 1994, "Molecular diffusion in NMR microscopy," J. Magn. Reson., Ser. B **103**, 162–167.
Branson, T. P., and P. B. Gilkey, 1990, "The asymptotics of the Laplacian on a manifold with boundary," Commun. Partial Differ. Equ. **15**, 245–272.
Brill, T. M., S. Ryu, R. Gaylor, J. Jundt, D. D. Griffin, Y.-Q. Song, P. N. Sen, and M. D. Hürlimann, 2002, "Nonresonant multiple spin echoes," Science **297**, 369–372.
Brown, R., 1828, "A brief account of microscopical observations made in the months of June, July and August, 1827, on the particles contained in the pollen of plants; and on the general existence of active molecules in organic and inorganic bodies," Edinb. New. Phil. J. **5**, 358–371.
Brown, R. J. S., and P. Fantazzini, 1993, "Conditions for initial quasilinear $1/T_2$ versus τ for Carr-Purcell-Meiboom-Gill NMR with diffusion and susceptibility differences in porous media and tissues," Phys. Rev. B **47**, 14823–14834.
Brown, R. J. S., and P. Fantazzini, 1994, "Taking, processing, and interpreting spin-echo data in porous media and tissues," Magn. Reson. Imaging **12**, 175–178.
Brownstein, K. R., and C. E. Tarr, 1977, "Spin-lattice relaxation in a system governed by diffusion," J. Magn. Reson. (1969-1992) **26**, 17–24.
Brownstein, K. R., and C. E. Tarr, 1979, "Importance of classical diffusion in NMR studies of water in biological cells," Phys. Rev. A **19**, 2446–2453.
Buhmann, M. D., 2003, *Radial Basis Functions* (Cambridge University, Cambridge, UK).
Bychuk, O. V., and B. O'Shaughnessy, 1995, "Anomalous diffusion at liquid surfaces," Phys. Rev. Lett. **74**, 1795–1798.
Callaghan, P. T., 1984, "Pulsed field gradient nuclear magnetic resonance of liquid state molecular organization," Aust. J. Phys. **37**, 359–387.
Callaghan, P. T., 1991, *Principles of Nuclear Magnetic Resonance Microscopy* (Clarendon, Oxford).
Callaghan, P. T., 1995, "Pulsed gradient spin echo NMR for planar, cylindrical and spherical pores under conditions of wall relaxation," J. Magn. Reson., Ser. A **113**, 53–59.
Callaghan, P. T., 1997, "A simple matrix formalism for spin echo analysis of restricted diffusion under generalized gradient waveforms," J. Magn. Reson. **129**, 74–84.
Callaghan, P. T., and S. L. Codd, 1998, "Generalized calculation of NMR imaging edge effects arising from restricted diffusion in porous media," Magn. Reson. Imaging **16**, 471–478.
Callaghan, P. T., S. L. Codd, and J. D. Seymour, 1999, "Spatial coherence phenomena arising from translational spin motion in gradient spin echo experiments," Concepts Magn. Reson. **11**, 181–202.
Callaghan, P. T., A. Coy, L. C. Forde, and C. J. Rofe, 1993, "Diffusive relaxation and edge enhancement in NMR microscopy," J. Magn. Reson., Ser. A **101**, 347–350.
Callaghan, P. T., A. Coy, T. P. J. Halpin, D. MacGowan, K. J. Packer, and F. O. Zelaya, 1992, "Diffusion in porous systems and the influence of pore morphology in pulsed gradient spin-echo nuclear magnetic resonance studies," J. Chem. Phys. **97**, 651–662.
Callaghan, P. T., A. Coy, D. MacGowan, K. J. Packer, and F. O. Zelaya, 1991, "Diffraction-like effects in NMR diffusion studies of fluids in porous solids," Nature (London) **351**, 467–469.
Callaghan, P. T., S. Godefroy, and B. N. Ryland, 2003, "Diffusion-relaxation correlation in simple pore structures," J. Magn. Reson. **162**, 320–327.
Callaghan, P. T., and J. Stepišnik, 1995, "Frequency-domain analysis of spin motion using modulated-gradient NMR," J. Magn. Reson., Ser. A **117**, 118–122.
Callaghan, P. T., and J. Stepišnik, 1996, "Generalized analysis of motions using magnetic field gradients," Adv. Magn. Opt. Reson. **19**, 325–388.
Caprihan, A., L. Z. Wang, and E. Fukushima, 1996, "A multiple-narrow-pulse approximation for restricted diffusion in a time-varying field gradient," J. Magn. Reson., Ser. A **118**, 94–102.
Carr, H. Y., and E. M. Purcell, 1954, "Effects of diffusion on free precession in NMR experiments," Phys. Rev. **94**, 630–638.
Carslaw, H. S., and J. C. Jaeger, 1959, *Conduction of Heat in Solids*, 2nd ed. (Clarendon, Oxford).
Cates, G. D., S. R. Schaefer, and W. Happer, 1988, "Relaxation of spins due to field inhomogeneities in gaseous samples at low magnetic fields and low pressures," Phys. Rev. A **37**, 2877–2885.
Cates, G. D., D. J. White, T.-R. Chien, S. R. Schaefer, and W. Happer, 1988, "Spin relaxation in gases due to inhomogeneous static and oscillating magnetic fields," Phys. Rev. A **38**, 5092–5106.
Chandrasekhar, S., 1943, "Stochastic problems in physics and astronomy," Rev. Mod. Phys. **15**, 1–89.
Chen, Q., and Y.-Q. Song, 2002, "What is the shape of pores in natural rocks," J. Chem. Phys. **116**, 8247–8250.
Ciarlet, P. G., 1987, *The Finite Element Method for Elliptic Problems* (North-Holland, Amsterdam).
Ciobanu, L., A. G. Webb, and C. H. Penningtond, 2003, "Magnetic resonance imaging of biological cells," Prog. Nucl. Magn. Reson. Spectrosc. **42**, 69–93.
Codd, S. L., and P. T. Callaghan, 1999, "Spin echo analysis of restricted diffusion under generalized gradient waveforms: Planar, cylindrical and spherical pores with wall relaxivity," J. Magn. Reson. **137**, 358–372.
Cohen, M. H., and K. S. Mendelson, 1982, "Nuclear magnetic relaxation and the internal geometry of sedimentary rocks," J. Appl. Phys. **53**, 1127–1135.
Conradi, M. S., B. Saam, D. A. Yablonskiy, and J. C. Woods, 2006, "Hyperpolarized 3He and perfluorocarbon gas diffusion MRI of lungs," Prog. Nucl. Magn. Reson. Spectrosc. **48**, 63–83.
Coppens, M.-O., 1999, "The effect of fractal surface roughness on diffusion and reaction in porous catalysts: From fundamentals to practical application," Catal. Today **53**, 225–243.
Cory, D. G., and A. N. Garroway, 1990, "Measurement of translational displacement probabilities by NMR: An indication of compartmentation," Magn. Reson. Med. **14**, 435–444.
Cotts, R. M., 1991, "Diffusion and diffraction," Nature (London) **351**, 443–443.
Coy, A., and P. T. Callaghan, 1994, "Pulsed gradient spin echo nuclear magnetic resonance for molecules diffusing between partially reflecting rectangular barriers," J. Chem. Phys. **101**, 4599–4609.
Crank, J., 1975, *The Mathematics of Diffusion*, 2nd ed. (Clarendon, Oxford).
Darquié, A., J.-B. Poline, C. Poupon, H. Saint-Jalmes, and D. Le Bihan, 2001, "Transient decrease in water diffusion observed in human occipital cortex during visual stimulation," Proc. Natl. Acad. Sci. U.S.A. **98**, 9391–9395.
Das, T. P., and A. K. Saha, 1954, "Mathematical analysis of the Hahn spin-echo experiment," Phys. Rev. **93**, 749–756.

de Gennes, P.-G., 1982, "Transfert d'excitation dans un milieu aléatoire," C. R. Acad. Sci., Ser. 2 **295**, 1061–1064.
de Levie, R., 1965, "The influence of surface roughness of solid electrodes on electrochemical measurements," Electrochim. Acta **10**, 113–130.
de Swiet, T. M., 1995, "Diffusive edge enhancement in imaging," J. Magn. Reson., Ser. B **109**, 12–18.
de Swiet, T. M., and P. N. Sen, 1994, "Decay of nuclear magnetization by bounded diffusion in a constant field gradient," J. Chem. Phys. **100**, 5597–5604.
de Swiet, T. M., and P. N. Sen, 1996, "Time dependent diffusion coefficient in a disordered medium," J. Chem. Phys. **104**, 206–209.
Devreux, F., J.-P. Boilot, F. Chaput, and B. Sapoval, 1990, "NMR determination of the fractal dimension in silica aerogels," Phys. Rev. Lett. **65**, 614–617.
Desjardins, S., and P. B. Gilkey, 1994, "Heat content asymptotics for operators of Laplace type with Neumann boundary conditions," Math. Z. **215**, 251–268.
D'Orazio, F., S. Bhattacharja, W. P. Halperin, and R. Gerhardt, 1989, "Enhanced self-diffusion of water in restricted geometry," Phys. Rev. Lett. **63**, 43–46.
Douglass, D. C., and D. W. McCall, 1958, "Diffusion in paraffin hydrocarbons," J. Phys. Chem. **62**, 1102–1107.
Duh, A., A. Mohorič, and J. Stepišnik, 2001, "Computer simulation of the spin-echo signal distribution in the case of restricted self-diffusion," J. Magn. Reson. **148**, 257–266.
Dullien, F. A. L., 1991, *Porous Media: Fluid Transport and Pore Structure* (Academic, New York).
Dunn, K.-J., and D. J. Bergman, 1995, "Self diffusion of nuclear spins in a porous medium with a periodic microstructure," J. Chem. Phys. **102**, 3041–3054.
Duplantier, B., 2005, "Le mouvement Brownian divers et ondoyant," Semin. Poincare **1**, 155–212.
Eidmann, G., R. Savelsberg, P. Blümler, and B. Blümich, 1996, "The NMR MOUSE, a mobile universal surface explorer," J. Magn. Reson., Ser. A **122**, 104–109.
Elizalde, E., 1995, *Ten Physical Applications of Spectral Zeta Functions* (Springer, Berlin).
Fain, S. B., S. R. Panth, M. D. Evans, A. L. Wentland, J. H. Holmes, F. R. Korosec, M. J. O'Brien, H. Fountaine, and T. M. Grist, 2006, "Early emphysematous changes in asymptomatic smokers: Detection with 3He MR imaging," Radiology **239**, 875–883.
Felici, M., M. Filoche, and B. Sapoval, 2004, "Renormalized random walk study of oxygen absorption in the human lung," Phys. Rev. Lett. **92**, 068101.
Felici, M., M. Filoche, C. Straus, T. Similowski, and B. Sapoval, 2005, "Diffusional screening in real 3D human acini—A theoretical study," Respir. Physiol. Neurbiol. **145**, 279–293.
Feller, W., 1971, *An Introduction to Probability Theory and Its Applications*, 2nd ed. (Wiley, New York), Vols. I and II.
Filoche, M., and B. Sapoval, 1999, "Can one hear the shape of an electrode? II. Theoretical study of the Laplacian transfer," Eur. Phys. J. B **9**, 755–763.
Finkelstein, A., 1987, *Water Movement through Lipid Bilayers, Pores, and Plasma Membranes: Theory and Reality* (Wiley, New York).
Fordham, E. J., P. P. Mitra, and L. L. Latour, 1996, "Effective diffusion times in multiple-pulse PFG diffusion measurements in porous media," J. Magn. Reson., Ser. A **121**, 187–192.
Frahm, J., P. Dechent, J. Baudewig, and K. D. Merboldt, 2004, "Advances in functional MRI of the human brain," Prog. Nucl. Magn. Reson. Spectrosc. **44**, 1–32.
Freidlin, M., 1985, *Functional Integration and Partial Differential Equations*, Annals of Mathematics Studies (Princeton University, Princeton, NJ).
Frey, S., J. Karger, H. Pfeifer, and P. Walther, 1988, "NMR self-diffusion measurements in regions confined by 'absorbing' walls," J. Magn. Reson. (1969-1992) **79**, 336–342.
Frey, E., and K. Kroy, 2005, "Brownian motion: A paradigm of soft matter and biological physics," Ann. Phys. **14**, 20–50.
Frøhlich, A. F., L. Østergaard, and V. G. Kiselev, 2006, "Effect of impermeable boundaries on diffusion-attenuated MR signal," J. Magn. Reson. **179**, 223–233.
Gefen, Y., A. Aharony, and S. Alexander, 1983, "Anomalous diffusion on percolating clusters," Phys. Rev. Lett. **50**, 77–80.
Gibbs, S. J., 1997, "Observations of diffusive diffraction in a cylindrical pore by PFG NMR," J. Magn. Reson. **124**, 223–226.
Gordon, C., D. L. Webb, and S. Wolpert, 1992, "One cannot hear the shape of a drum," Bull., New Ser., Am. Math. Soc. **27**, 134–138.
Grant, D. M., and R. K. Harris 1996, Eds., *Encyclopedia of Nuclear Magnetic Resonance* (Wiley, Chichester).
Grassberger, P., and I. Procaccia, 1982, "The long time properties of diffusion in a medium with static traps," J. Chem. Phys. **77**, 6281–6284.
Grebenkov, D. S., 2005, "What makes a boundary less accessible," Phys. Rev. Lett. **95**, 200602.
Grebenkov, D. S., 2006a, "Partially reflected Brownian motion: A stochastic approach to transport phenomena," in *Focus on Probability Theory*, edited by L. R. Velle (Nova Science, Hauppauge, NY), pp. 135–169.
Grebenkov, D. S., 2006b, "Multiexponential attenuation of the CPMG spin echoes due to a geometrical confinement," J. Magn. Reson. **180**, 118–126.
Grebenkov, D. S., 2006c, "Scaling properties of the spread harmonic measures," Fractals **14**, 231–243.
Grebenkov, D. S., 2007a, "NMR restricted diffusion between parallel planes in a cosine magnetic field: An exactly solvable model," J. Chem. Phys. **126**, 104706.
Grebenkov, D. S., 2007b, "Multiple correlation function approach to study restricted diffusion under arbitrary magnetic field," Magn. Reson. Imaging **25**, 559.
Grebenkov, D. S., M. Filoche, and B. Sapoval, 2003, "Spectral properties of the Brownian self-transport operator," Eur. Phys. J. B **36**, 221–231.
Grebenkov, D. S., M. Filoche, and B. Sapoval, 2006, "Mathematical basis for a general theory of Laplacian transport towards irregular interfaces," Phys. Rev. E **73**, 021103.
Grebenkov, D. S., M. Filoche, B. Sapoval, and M. Felici, 2005, "Diffusion-reaction in branched structures: Theory and application to the lung acinus," Phys. Rev. Lett. **94**, 050602.
Grebenkov, D. S., G. Guillot, and B. Sapoval, 2007, "Restricted diffusion in a model acinar labyrinth by NMR. Theoretical and numerical results," J. Magn. Reson. **184**, 143–156.
Grebenkov, D. S., A. A. Lebedev, M. Filoche, and B. Sapoval, 2005, "Multifractal properties of the harmonic measure on Koch boundaries in two and three dimensions," Phys. Rev. E **71**, 056121.
Güllmar, D., J. Haueisen, and J. R. Reichenbach, 2005, "Analysis of b-value calculations in diffusion weighted and diffusion tensor imaging," Concepts Magn. Reson. **25A**, 53–66.

Guyer, R. A., 1988, "Porosity fluctuations, tortuosity fluctuations, and other types of fluctuations: Long-time tails and localization in porous media," Phys. Rev. B **37**, 5713–5722.

Guyer, R. A., 1993, "Magnetization evolution in connected pore systems. III. Fluid flow," Phys. Rev. B **48**, 6007–6013.

Guyer, R. A., and K. R. McCall, 2000, "Lattice Boltzmann description of magnetization in porous media," Phys. Rev. B **62**, 3674–3688.

Hahn, E. L., 1950, "Spin echoes," Phys. Rev. **80**, 580–594.

Halperin, W. P., J.-Y. Jehng, and Y.-Q. Song, 1994, "Application of spin-spin relaxation to measurement of surface area and pore size distributions in a hydrating cement paste," Magn. Reson. Imaging **12**, 169–173.

Halsey, T. C., and M. Leibig, 1992, "The double layer impedance at a rough surface: Theoretical results," Ann. Phys. (N.Y.) **219**, 109–147.

Haus, J. W., and K. W. Kehr, 1987, "Diffusion in regular and disordered lattices," Phys. Rep. **150**, 263–406.

Havlin, S., and D. ben Avraham, 2002, "Diffusion in disordered media," Adv. Phys. **51**, 187–292.

Hayden, M. E., G. Archibald, K. M. Gilbert, and C. Lei, 2004, "Restricted diffusion within a single pore," J. Magn. Reson. **169**, 313–322.

Helmer, K. G., B. J. Dardzinski, and C. H. Sotak, 1995, "The application of porous-media theory to the investigation of time-dependent diffusion in in vivo systems," NMR Biomed. **8**, 297–306.

Helmer, K. G., M. D. Hürlimann, T. M. de Swiet, P. N. Sen, and C. H. Sotak, 1995, "Determination of ratio of surface area to pore volume from restricted diffusion in a constant field gradient," J. Magn. Reson., Ser. A **115**, 257–259.

Heuveline, V., 2003, "On the computation of a very large number of eigenvalues for selfadjoint elliptic operators by means of multigrid methods," J. Comput. Phys. **184**, 321–337.

Hürlimann, M. D., 1998, "Effective gradients in porous media due to susceptibility differences," J. Magn. Reson. **131**, 232–240.

Hürlimann, M. D., 2001, "Diffusion and relaxation effects in general stray field NMR experiments," J. Magn. Reson. **148**, 367–378.

Hürlimann, M. D., and D. D. Griffin, 2000, "Spin dynamics of Carr-Purcell-Meiboom-Gill-like sequences in grossly inhomogeneous B_0 and B_1 fields and application to NMR well logging," J. Magn. Reson. **143**, 120–135.

Hürlimann, M. D., K. G. Helmer, T. M. de Swiet, P. N. Sen, and C. H. Sotak, 1995, "Spin echoes in a constant gradient and in the presence of simple restriction," J. Magn. Reson., Ser. A **113**, 260–264.

Hürlimann, M. D., K. G. Helmer, L. L. Latour, and C. H. Sotak, 1994, "Restricted diffusion in sedimentary rocks. Determination of surface-area-to-volume ratio and surface relaxivity," J. Magn. Reson., Ser. A **111**, 169–178.

Hürlimann, M. D., and L. Venkataramanan, 2002, "Quantitative measurement of two-dimensional distribution functions of diffusion and relaxation in grossly inhomogeneous fields," J. Magn. Reson. **157**, 31–42.

Hwang, S. N., C.-L. Chin, F. W. Wehrli, and D. B. Hackney, 2003, "An image-based finite difference model for simulating restricted diffusion," Magn. Reson. Med. **50**, 373–382.

Hyslop, W. B., and P. C. Lauterbur, 1991, "Effects on restricted diffusion on microscopic NMR imaging," J. Magn. Reson. (1969-1992) **94**, 501–510.

Itô, K., and H. P. McKean, 1965, *Diffusion Processes and Their Sample Paths* (Springer-Verlag, Berlin).

Johnson, D. L., J. Koplik, and L. M. Schwartz, 1986, "New pore-size parameter characterizing transport in porous media," Phys. Rev. Lett. **57**, 2564–2567.

Johnson, D. L., T. J. Plona, C. Scala, F. Pasierb, and H. Kojima, 1982, "Tortuosity and acoustic slow waves," Phys. Rev. Lett. **49**, 1840–1844.

Kac, M., 1949, "On the distribution of certain Wiener functionals," Trans. Am. Math. Soc. **65**, 1–13.

Kac, M., 1951, in *Proceedings of the 2nd Berkeley Symposium on Mathematics and Statistical Probability*, edited by J. Neyman (University of California, Berkeley), pp. 189–215.

Kac, M., 1966, "Can one hear the shape of a drum?" Am. Math. Monthly **73**, 1–23.

Kadlecek, S. J., K. Emami, M. C. Fischer, M. Ishii, J. Yu, J. M. Woodburn, M. NikKhah, V. Vahdat, D. A. Lipson, J. E. Baumgardner, and R. R. Rizi, 2005, "Imaging physiological parameters with hyperpolarized gas MRI," Prog. Nucl. Magn. Reson. Spectrosc. **47**, 187–212.

Kaiser, R., E. Bartholdi, and R. R. Ernst, 1974, "Diffusion and field-gradient effects in NMR Fourier spectroscopy," J. Chem. Phys. **60**, 2966–2979.

Kaplan, J. I., 1959, "Application of the diffusion-modified Bloch equation to electron spin resonance in ordinary and ferromagnetic metals," Phys. Rev. **115**, 575–577.

Kärger, J., F. Grinberg, and P. Heitjans, 2005, Eds., *Diffusion Fundamentals* (Leipziger Universitätsverlag, Leipzig).

Kärger, J., and W. Heink, 1983, "The propagator representation of molecular transport in microporous crystallites," J. Magn. Reson. (1969-1992) **51**, 1–7.

Kärger, J., H. Pfeifer, and W. Heink, 1988, in *Advances in Magnetic Resonance*, edited by J. S. Waugh (Academic, San Diego), Vol. 12, pp. 1–89.

Kärger, J., H. Pfeifer, and G. Vojta, 1988, "Time correlation during anomalous diffusion in fractal systems and signal attenuation in NMR field-gradient spectroscopy," Phys. Rev. A **37**, 4514–4517.

Kärger, J., and D. M. Ruthven, 1992, *Diffusion in Zeolites and Other Microporous Solids* (Wiley, New York).

Kayser, R. F., and J. B. Hubbard, 1983, "Diffusion in a medium with a random distribution of static traps," Phys. Rev. Lett. **51**, 79–82.

Kayser, R. F., and J. B. Hubbard, 1984, "Reaction diffusion in a medium containing a random distribution of nonoverlapping traps," J. Chem. Phys. **80**, 1127–1130.

Kenyon, W. E., 1992, "Nuclear magnetic resonance as a petrophysical measurement," Nucl. Geophys. **6**, 153–171.

Kimmich, R., 1997, *NMR—Tomography, Diffusometry, Relaxometry* (Springer-Verlag, Berlin).

Kimmich, R., 2002, "Strange kinetics, porous media, and NMR," Chem. Phys. **284**, 253–285.

Kimmich, R., and E. Fischer, 1994, "One- and two-dimensional pulse sequences for diffusion experiments in the fringe field of superconducting magnets," J. Magn. Reson., Ser. A **106**, 229–235.

Kimmich, R., S. Stapf, P. T. Callaghan, and A. Coy, 1994, "Microstructure of porous media probed by NMR techniques in sub-micrometer length scales," Magn. Reson. Imaging **12**, 339–343.

King, M. D., J. Houseman, S. A. Roussel, N. van Bruggen, S. R. Williams, and D. G. Gadian, 1994, "q-space imaging of the brain," Magn. Reson. Med. **32**, 707–713.

Kingsley, P. B., 2006, "Introduction to diffusion tensor imaging mathematics," Concepts Magn. Reson. **28A**, 101–179.

Kirkpatrick, T. R., 1982, "Time dependent transport in a fluid with static traps," J. Chem. Phys. **76**, 4255–4259.

Kiselev, V. G., and D. S. Novikov, 2002, "Transverse NMR relaxation as a probe of mesoscopic structure," Phys. Rev. Lett. **89**, 278101 [see also Comment by Song, and Sen, 2003, Phys. Rev. Lett. **91**, 029801; and Reply by Kiselev, and Novikov, 2003, Phys. Rev. Lett. **91**, 029802].

Kiselev, V. G., and S. Posse, 1998, "Analytical theory of susceptibility induced NMR signal dephasing in a crebrovascular network," Phys. Rev. Lett. **81**, 5696–5699; **83**, 1487(E) (1999).

Klafter, J., and J. M. Drake, 1989, Eds., *Molecular Dynamics in Restricted Geometries* (Wiley, New York).

Kleinberg, R. L., 1994, "Pore size distribution, pore coupling, and transverse relaxation spectra of porous rocks," Magn. Reson. Imaging **12**, 271–274.

Kleinberg, R. L., 1996a, in *Encyclopedia of Nuclear Magnetic Resonance*, edited by D. M. Grant and Robin K. Harris (John Wiley, Chichester), Vol. 8, pp. 4960–4969.

Kleinberg, R. L., 1996b, "Utility of NMR T_2 distributions, connection with capillary pressure, clay effect, and determination of the surface relaxivity parameter ρ_2," Magn. Reson. Imaging **14**, 761−767.

Kleinberg, R. L., and M. A. Horsfield, 1990, "Transverse relaxation processes in porous sedimentary rock," J. Magn. Reson. (1969-1992) **88**, 9–19.

Kleinberg, R. L., W. E. Kenyon, and P. P. Mitra, 1994, "Mechanism of NMR relaxation of fluids in rock," J. Magn. Reson., Ser. A **108**, 206–214.

Kuchel, P. W., A. J. Lennon, and C. Durrant, 1996, "Analytical solutions and simulations for spin-echo measurements of diffusion of spins in a sphere with surface and bulk relaxation," J. Magn. Reson., Ser. B **112**, 1–17. The results of this reference should be taken with care since the condition of spin survival was not included in its Eq. (35). In particular, the existence of the second minimum on Fig. 2 of this reference is doubtful.

Lapidus, M. L., 1991, "Fractal drum, inverse spectral problems for elliptic operators and a partial resolution of the Weyl-Berry conjecture," Trans. Am. Math. Soc. **325**, 465–529.

Lapidus, M. L., and C. Pomerance, 1993, "The Riemann zeta-function and the one-dimensional Weyl-Berry conjecture for fractal drums," Proc. London Math. Soc. **66**, 41–69.

Lapidus, M. L., and M. van Frankenhuysen, 2000, *Fractal Geometry and Number Theory. Complex Dimensions of Fractal Strings and Zeros of Zeta Functions* (Birkhäuser, Boston).

Latour, L. L., R. L. Kleinberg, P. P. Mitra, and C. H. Sotak, 1995, "Pore-size distributions and tortuosity in heterogeneous porous media," J. Magn. Reson., Ser. A **112**, 83–91.

Latour, L. L., P. P. Mitra, R. L. Kleinberg, and C. H. Sotak, 1993, "Time-dependent diffusion coefficient of fluids in porous media as a probe of surface-to-volume ratio," J. Magn. Reson., Ser. A **101**, 342–346.

Latour, L. L., K. Svoboda, P. P. Mitra, and C. H. Sotak, 1994, "Time-dependent diffusion of water in a biological model system," Proc. Natl. Acad. Sci. U.S.A. **91**, 1229–1233.

Le Bihan, D., 2003, "Looking into the functional architecture of the brain with diffusion MRI," Nat. Rev. Neurosci. **4**, 469–480.

Le Bihan, D., 1995, Ed., *Diffusion and Perfusion Magnetic Resonance Imaging: Application to Functional MRI* (Raven, New York).

Le Doussal, P., and P. N. Sen, 1992, "Decay of nuclear magnetization by diffusion in a parabolic magnetic field: An exactly solvable model," Phys. Rev. B **46**, 3465–3485.

Leibig, M., 1993, "Random walks and NMR measurements in porous media," J. Phys. A **26**, 3349–3367.

Lennon, A. J., and P. W. Kuchel, 1994, "Enhancement of the 'diffraction-like' effect in NMR diffusion experiments," J. Magn. Reson., Ser. A **111**, 208–211.

Levitz, P. E., 2005, "Random flights in confining interfacial systems," J. Phys.: Condens. Matter **17**, S4059–S4074.

Levitz, P. E., D. S. Grebenkov, M. Zinsmeister, K. Kolwankar, and B. Sapoval, 2006, "Brownian flights over a fractal nest and first passage statistics on irregular surfaces," Phys. Rev. Lett. **96**, 180601.

Li, Y., G. Farrher, and R. Kimmich, 2006, "Sub- and superdiffusive molecular displacement laws in disordered porous media probed by nuclear magnetic resonance," Phys. Rev. E **74**, 066309.

Linse, P., and O. Söderman, 1995, "The validity of the short-gradient-pulse approximation in NMR studies of restricted diffusion. Simulations of molecules diffusing between planes, in cylinders and spheres," J. Magn. Reson., Ser. A **116**, 77–86.

Lisitza, N. V., and Y.-Q. Song, 2001, "The behavior of diffusion eigenmodes in the presence of internal magnetic field in porous media," J. Chem. Phys. **114**, 9120–9124.

Lisitza, N. V., and Y.-Q. Song, 2002, "Manipulation of the diffusion eigenmodes in porous media," Phys. Rev. B **65**, 172406.

Lori, N. F., T. E. Conturo, and D. Le Bihan, 2003, "Definition of displacement probability and diffusion time in q-space magnetic resonance measurements that use finite-duration diffusion-encoding gradients," J. Magn. Reson. **165**, 185–195.

Macfall, J. R., H. C. Charles, R. D. Black, H. Middleton, J. C. Swartz, B. Saam, B. Driehuys, C. Erickson, W. Happer, G. D. Cates, G. A. Johnson, and C. E. Ravin, 1996, "Human lung air spaces: Potential for MR imaging with hyperpolarized He-3," Radiology **200**, 553–558.

Mair, R. W., D. G. Cory, S. Peled, C.-H. Tseng, S. Patz, and R. L. Walsworth, 1998, "Pulsed-field-gradient measurements of time-dependent gas diffusion," J. Magn. Reson. **135**, 478–486.

Mair, R. W., M. D. Hürlimann, P. N. Sen, L. M. Schwartz, S. Patz, and R. L. Walsworth, 2001, "Tortuosity measurement and the effects of finite pulse widths on xenon gas diffusion NMR studies of porous media," Magn. Reson. Imaging **19**, 345–351.

Mair, R. W., M. S. Rosen, R. Wang, D. G. Cory, and R. L. Walsworth, 2002, "Diffusion NMR methods applied to xenon gas for materials study," Magn. Reson. Chem. **40**, S29–S39.

Mair, R. W., P. N. Sen, M. D. Hürlimann, S. Patz, D. G. Cory, and R. L. Walsworth, 2002, "The narrow pulse approximation and long length scale determination in xenon gas diffusion NMR studies of model porous media," J. Magn. Reson. **156**, 202–212.

Mair, R. W., G. P. Wong, D. Hoffmann, M. D. Hürlimann, S. Patz, L. M. Schwartz, and R. L. Walsworth, 1999, "Probing porous media with gas diffusion NMR," Phys. Rev. Lett. **83**, 3324–3327.

Majumdar, S., and J. C. Gore, 1988, "Studies of diffusion in random fields produced by variations in susceptibility," J. Magn. Reson. (1969-1992) **78**, 41–55.

Majumdar, S., 2005, "Brownian functionals in physics and computer science," Curr. Sci. **89**, 2076–2092.

Malmborg, C., D. Topgaard, and O. Söderman, 2004, "NMR

diffusometry and the short gradient pulse limit approximation," J. Magn. Reson. **169**, 85–91.
Marinelli, L., M. D. Hürlimann, and P. N. Sen, 2003, "Modal analysis of q-space-relaxation correlation experiments," J. Chem. Phys. **118**, 8927–8940.
Markushevich, A. I., 1965, *Theory of Functions of a Complex Variable* (Prentice-Hall, Englewood Cliffs, NJ), Vol. 2, pp. 299–304.
McAvity, D. M., 1992, "Heat kernel asymptotics for mixed boundary conditions," Class. Quantum Grav. **9**, 1983–1997.
McAvity, D. M., and H. Osborn, 1991, "A DeWitt expansion of the heat kernel for manifolds with a boundary," Class. Quantum Grav. **8**, 603–638; **9**, 317(E) (1991).
McCall, K. R., R. A. Guyer, and D. L. Johnson, 1993, "Magnetization evolution in connected pore systems. II. Pulsed-field-gradient NMR and pore-space geometry," Phys. Rev. B **48**, 5997–6006.
McCall, K. R., D. L. Johnson, and R. A. Guyer, 1991, "Magnetization evolution in connected pore systems," Phys. Rev. B **44**, 7344–7355.
McDonald, P. J., 1997, "Stray field magnetic resonance imaging," Prog. Nucl. Magn. Reson. Spectrosc. **30**, 69–99.
McDonald, P. J., J.-P. Korb, J. Mitchell, and L. Monteilhet, 2005, "Surface relaxation and chemical exchange in hydrating cement pastes: A two-dimensional NMR relaxation study," Phys. Rev. E **72**, 011409.
McGregor, D. D., 1990, "Transverse relaxation of spin-polarized ^{3}He gas due to a magnetic field gradient," Phys. Rev. A **41**, 2631–2635.
Meiboom, S., and D. Gill, 1958, "Modified spin-echo method for measuring nuclear relaxation times," Rev. Sci. Instrum. **29**, 688–691.
Mendelson, K. S., 1990, "Percolation model of nuclear magnetic relaxation in porous media," Phys. Rev. B **41**, 562–567.
Meriles, C. A., D. Sakellariou, H. Heise, A. J. Moulé, and A. Pines, 2001, "Approach to high-resolution ex situ NMR spectroscopy," Science **293**, 82–85.
Metzler, R., and J. Klafter, 2000, "The random walk's guide to anomalous diffusion: A fractional dynamics approach," Phys. Rep. **339**, 1–77.
Miller, J. B., 1998, "NMR imaging of materials," Prog. Nucl. Magn. Reson. Spectrosc. **33**, 273–308.
Mitra, P. P., and B. I. Halperin, 1995, "Effects of finite gradient pulse widths in pulsed field gradient diffusion measurements," J. Magn. Reson., Ser. A **113**, 94–101.
Mitra, P. P., L. L. Latour, R. L. Kleinberg, and C. H. Sotak, 1995, "Pulsed-field-gradient NMR measurements of restricted diffusion and the return-to-the-origin probability," J. Magn. Reson., Ser. A **114**, 47–58.
Mitra, P. P., and P. Le Doussal, 1991, "Long-time magnetization relaxation of spins diffusing in a random field," Phys. Rev. B **44**, 12035–12038.
Mitra, P. P., and P. N. Sen, 1992, "Effects of microgeometry and surface relaxation on NMR pulsed-field-gradient experiments: Simple pore geometries," Phys. Rev. B **45**, 143–156. Veeman (2003) pointed out an error in Eq. (6.11).
Mitra, P. P., P. N. Sen, and L. M. Schwartz, 1993, "Short-time behavior of the diffusion coefficient as a geometrical probe of porous media," Phys. Rev. B **47**, 8565–8574 [Sen (2003) pointed out typographical mistakes which can be fixed by multiplying the right side of Eq. (30) in Mitra's paper by $(\kappa D_0+\rho)/(\kappa D_0-\rho)$; a factor S/V_p is also missed in the last term of Eq. (29)].
Mitra, P. P., P. N. Sen, L. M. Schwartz, and P. Le Doussal, 1992, "Diffusion propagator as a probe of the structure of porous media," Phys. Rev. Lett. **68**, 3555–3558.
Mohr, P. J., and B. N. Taylor, 2005, "CODATA recommended values of the fundamental physical constants: 2002," Rev. Mod. Phys. **77**, 1–107.
Möller, H. E., X. J. Chen, B. Saam, K. D. Hagspiel, G. A. Johnson, T. A. Altes, E. E. de Lange, and H.-U. Kauczor, 2002, "MRI of the lungs using hyperpolarized noble gases," Magn. Reson. Med. **47**, 1029–1051.
Murday, J. S., and R. M. Cotts, 1968, "Self-diffusion coefficient of liquid lithium," J. Chem. Phys. **48**, 4938–4945.
Nestle, N., P. Galvosas, O. Geier, M. Dakkouri, C. Zimmermann, and J. Kärger, 2001, "NMR studies of water diffusion and relaxation in hydrating slag-based construction materials," Magn. Reson. Imaging **19**, 547–548.
Neuman, C. H., 1974, "Spin echo of spins diffusion in a bounded medium," J. Chem. Phys. **60**, 4508–4511 (note a typographical mistake: the coefficient ζ_{-1} for a cylinder is 7/96, not 7/296).
Nicholson, C., 1985, "Diffusion from an injected volume of a substance in brain-tissue with arbitrary volume fraction and tortuosity," Brain Res. **333**, 325–329.
Nicholson, C., 2001, "Diffusion and related transport mechanisms in brain tissue," Rep. Prog. Phys. **64**, 815–884.
Nyikos, L., and T. Pajkossy, 1985, "Fractal dimension and fractional power frequency-dependent impedance of blocking electrodes," Electrochim. Acta **30**, 1533–1540.
Nyikos, L., and T. Pajkossy, 1986, "Diffusion to fractal surfaces," Electrochim. Acta **31**, 1347–1350.
Packer, K. J., 1973, "The effects of diffusion through locally inhomogeneous magnetic fields on transverse nuclear spin relaxation in heterogeneous systems. Proton transverse relaxation in striated muscle tissue," J. Magn. Reson. (1969-1992) **9**, 438–443.
Packer, K. J., and C. Rees, 1972, "Pulsed NMR studies of restricted diffusion 1. Droplet size distributions in emulsions," J. Colloid Interface Sci. **40**, 206–218.
Perlo, J., V. Demas, F. Casanova, C. A. Meriles, J. Reimer, A. Pines, and B. Blümich, 2005, "High-resolution NMR spectroscopy with a portable single-sided sensor," Science **308**, 1279–1279.
Pfeuffer, J., U. Flögel, W. Dreher, and D. Leibfritz, 1998, "Restricted diffusion and exchange of intracellular water: Theoretical modelling and diffusion time dependence of 1H NMR measurements on perfused glial cells," NMR Biomed. **11**, 19–31.
Plassais, A., M.-P. Pomies, N. Lequeux, P. Boch, J.-P. Korb, D. Petit, and F. Barberon, 2003, "Micropore size analysis by NMR in hydrated cement," Magn. Reson. Imaging **21**, 369–371.
Plassais, A., M.-P. Pomies, N. Lequeux, J.-P. Korb, D. Petit, F. Barberon, and B. Bresson, 2005, "Microstructure evolution of hydrated cement pastes," Phys. Rev. E **72**, 041401.
Platte, R. B., and T. A. Driscoll, 2004, "Computing eigenmodes of elliptic operators using radial basis functions," Comput. Math. Appl. **48**, 561–576.
Port, S. C., and C. J. Stone, 1978, *Brownian Motion and Classical Potential Theory* (Academic, New York).
Price, W. S., 1997, "Pulsed-field gradient nuclear magnetic resonance as a tool for studying translational diffusion: Part 1. Basic theory," Concepts Magn. Reson. **9**, 299–336.
Price, W. S., 1998, "Pulsed-field gradient nuclear magnetic

resonance as a tool for studying translational diffusion: Part 2. Experimental aspects," Concepts Magn. Reson. **10**, 197–237.
Price, W. S., P. Stilbs, and O. Söderman, 2003, "Determination of pore space shape and size in porous systems using NMR diffusometry. Beyond the short gradient pulse approximation," J. Magn. Reson. **160**, 139–143.
Pütz, B., D. Barsky, and K. Schulten, 1992, "Edge enhancement by diffusion in microscopic MRI," J. Magn. Reson. (1969-1992) **97**, 27–53.
Revuz, D. R. J., and M. Yor, 1999, *Continuous Martingales and Brownian Motion* (Springer, Berlin).
Robertson, B., 1966, "Spin-echo decay of spins diffusion in a bounded region," Phys. Rev. **151**, 273–277.
Rodts, S., and P. E. Levitz, 2001, "Time domain analysis: An alternative way to interpret PGSE experiment," Magn. Reson. Imaging **19**, 465–467.
Ryu, S., 2001, "Probing pores using elementary quantum mechanics," Magn. Reson. Imaging **19**, 411–415.
Saad, Y., 1992, *Numerical Methods for Large Eigenvalue Problems* (Halstead, New York).
Saam, B., N. Drukker, and W. Happer, 1996, "Edge enhancement observed with hyperpolarized 3He," Chem. Phys. Lett. **263**, 481–487.
Saam, B., D. A. Yablonskiy, V. D. Kodibagkar, J. C. Leawoods, D. S. Gierada, J. D. Cooper, S. S. Lefrak, and M. S. Conradi, 2000, "MR imaging of diffusion of 3He gas in healthy and diseased lungs," Magn. Reson. Med. **44**, 174–179.
Sahimi, M., 1993, "Flow phenomena in rocks: From continuum models to fractals, percolation, cellular automata, and simulated annealing," Rev. Mod. Phys. **65**, 1393–1534.
Sahimi, M., 1995, *Flow and Transport in Porous Media an Fractured Rock* (VCH, Weinheim).
Sahimi, M., G. R. Gavalas, and T. T. Tsotsis, 1990, "Statistical and continuum models of fluid-solid reactions in porous media," Chem. Eng. Sci. **45**, 1443–1502.
Sapoval, B., 1994, "General formulation of Laplacian transfer across irregular surfaces," Phys. Rev. Lett. **73**, 3314–3316.
Sapoval, B., 1996, in *Fractals and Disordered Systems*, edited by A. Bunde and S. Havlin (Springer-Verlag, Berlin), pp. 233–261.
Sapoval, B., J.-N. Chazalviel, and J. Peyrière, 1988, "Electrical response of fractal and porous interfaces," Phys. Rev. A **38**, 5867–5887.
Sapoval, B., M. Filoche, and E. R. Weibel, 2002, "Smaller is better—but not too small: A physical scale for the design of the mammalian pulmonary acinus," Proc. Natl. Acad. Sci. U.S.A. **99**, 10411–10416.
Sapoval, B., S. Russ, D. Petit, and J.-P. Korb, 1996, "Fractal geometry impact on nuclear relaxation in irregular pores," Magn. Reson. Imaging **14**, 863–867.
Schearer, L. D., and G. K. Walters, 1965, "Nuclear spin-lattice relaxation in the presence of magnetic-field gradients," Phys. Rev. **139**, A1398–A1402.
Scheidegger, A. E., 1974, *The Physics of Flow through Porous Media*, 3rd ed. (University of Toronto, Toronto).
Schmidt, D. M., J. S. George, S. I. Penttila, A. Caprihan, and E. Fukushima, 1997, "Diffusion imaging with hyperpolarized 3He gas," J. Magn. Reson. **129**, 184–187.
Schwartz, L. M., M. D. Hürlimann, K.-J. Dunn, P. P. Mitra, and D. J. Bergman, 1997, "Restricted diffusion and the return to the origin probability at intermediate and long times," Phys. Rev. E **55**, 4225–4234.
Seland, J. G., G. H. Sørland, K. Zick, and B. Hafskjold, 2000, "Diffusion measurements at long observation times in the presence of spatially variable internal magnetic field gradients," J. Magn. Reson. **146**, 14–19.
Seland, J. G., K. E. Washburn, H. W. Anthonson, and J. Krane, 2004, "Correlations between diffusion, internal magnetic field gradients, and transverse relaxation in porous systems containing oil and water," Phys. Rev. E **70**, 051305.
Sen, P. N., 2003, "Time-dependent diffusion coefficient as a probe of permeability of the pore-wall," J. Chem. Phys. **119**, 9871–9876; **120**, 11965–11966(E) (2004).
Sen, P. N., 2004, "Time-dependent diffusion coefficient as a probe of geometry," Concepts Magn. Reson. **23A**, 1–21.
Sen, P. N., A. André, and S. Axelrod, 1999, "Spin echoes of nuclear magnetization diffusing in a constant magnetic field gradient and in a restricted geometry," J. Chem. Phys. **111**, 6548–6555 [note a few errors in this paper pointed out by Axelrod and Sen (2001), see their comment 24].
Sen, P. N., and S. Axelrod, 1999, "Inhomogeneity in local magnetic field due to susceptibility contrast," J. Appl. Phys. **86**, 4548–4554.
Sen, P. N., M. D. Hürlimann, and T. M. de Swiet, 1995, "Debye-Porod law of diffraction for diffusion in porous media," Phys. Rev. B **51**, 601–604.
Sen, P. N., L. M. Schwartz, P. P. Mitra, and B. I. Halperin, 1994, "Surface relaxation and the long-time diffusion coefficient in porous media: Periodic geometries," Phys. Rev. B **49**, 215–225.
Shanbhag, D. D., T. A. Altes, G. W. Miller, J. F. Mata, and J. Knight-Scott, 2006, "q-space analysis of lung morphometry in vivo with hyperpolarized 3He spectroscopy," J. Magn. Reson Imaging **24**, 84–94.
Shlesinger, M. F., J. Klafter, and G. Zumofen, 1999, "Above, below and beyond Brownian motion," Am. J. Phys. **67**, 1253–1259.
Smith, I. C. P., and L. C. Stewart, 2002, "Magnetic resonance spectroscopy in medicine: Clinical impact," Prog. Nucl. Magn. Reson. Spectrosc. **40**, 1–34.
Söderman, O., and B. Jönsson, 1995, "Restricted diffusion in cylindrical geometry," J. Magn. Reson., Ser. A **117**, 94–97.
Song, Y.-Q., 2000a, "Detection of the high eigenmodes of spin diffusion in porous media," Phys. Rev. Lett. **85**, 3878–3881.
Song, Y.-Q., 2000b, "Determining pore sizes using an internal magnetic field," J. Magn. Reson. **143**, 397–401.
Song, Y.-Q., 2002, "Categories of coherence pathways for the CPMG sequence," J. Magn. Reson. **157**, 82–91.
Song, Y.-Q., 2003, "Using internal magnetic fields to obtain pore size distributions of porous media," Concepts Magn. Reson. **18A**, 97–110.
Song, Y.-Q., H. C. Gaede, T. Pietrass, G. A. Barrall, G. C. Chingas, M. R. Ayers, and A. Pines, 1995, "Spin-polarized 129Xe gas imaging of materials," J. Magn. Reson., Ser. A **115**, 127–130.
Song, Y.-Q., B. M. Goodson, B. Sheridan, T. M. de Swiet, and A. Pines, 1998, "Effects of diffusion on magnetic resonance imaging of laser-polarized xenon gas," J. Chem. Phys. **108**, 6233–6239.
Song, Y.-Q., M. D. Hürlimann, and C. Flaum, 2003, "A method for rapid characterization of diffusion," J. Magn. Reson. **161**, 222–233.
Song, Y.-Q., S. Ryu, and P. N. Sen, 2000, "Determining multiple length scales in rocks," Nature (London) **406**, 178–181.
Song, Y.-Q., L. Venkataramanan, M. D. Hürlimann, M. Flaum,

P. Frulla, and C. Straley, 2002, "T1-T2 correlation spectra obtained using a fast two-dimensional Laplace inversion," J. Magn. Reson. **154**, 261–268.
Sridhar, S., and A. Kudrolli, 1994, "Experiments on not 'hearing the shape' of drums," Phys. Rev. Lett. **72**, 2175–2178.
Stallmach, F., C. Vogt, J. Kärger, K. Helbig, and F. Jacobs, 2002, "Fractal geometry of surface areas of sand grains probed by pulsed field gradient NMR," Phys. Rev. Lett. **88**, 105505 (see also Comment by D. Candela and P. Z. Wong, 2003, Phys. Rev. Lett. **90**, 039601; and Reply by F. Stallmach and J. Kärger, 2003, Phys. Rev. Lett. **90**, 039602).
Stapf, S., R. Kimmich, and R.-O. Seitter, 1995, "Proton and deuteron field-cycling NMR relaxometry of liquids in porous glasses: Evidence for Levy-Walk statistics," Phys. Rev. Lett. **75**, 2855–2858.
Stejskal, E. O., 1965, "Use of spin echoes in a pulsed magnetic-field gradient to study anisotropic, restricted diffusion and flow," J. Chem. Phys. **43**, 3597–3603.
Stejskal, E. O., and J. E. Tanner, 1965, "Spin diffusion measurements: Spin echoes in the presence of a time-dependent field gradient," J. Chem. Phys. **42**, 288–292.
Stepišnik, J., 1981, "Analysis of NMR self-diffusion measurements by density matrix calculation," Physica B & C **104**, 350–364.
Stepišnik, J., 1985, "Measuring and imaging of flow by NMR," Prog. Nucl. Magn. Reson. Spectrosc. **17**, 187–209.
Stepišnik, J., 1993, "Time-dependent self-diffusion by NMR spin-echo," Physica B **183**, 343–350.
Stepišnik, J., 1998, "Spin echo attenuation of restricted diffusion as a discord of spin phase structure," J. Magn. Reson. **131**, 339–346.
Stepišnik, J., 1999, "Validity limits of Gaussian approximation in cumulant expansion for diffusion attenuation of spin echo," Physica B **270**, 110–117. The upper estimates deduced in this paper should be taken with caution, as discussed in Sec. II.H.
Stepišnik, J., and P. T. Callaghan, 2000, "The long time tail of molecular velocity correlation in a confined fluid: Observation by modulated gradient spin-echo NMR," Physica B **292**, 296–301.
Stepišnik, J., A. Mohorič, and A. Duh, 2001, "Diffusion and flow in a porous structure by the gradient spin echo spectral analysis," Physica B **307**, 158–168.
Stilbs, P., 1987, "Fourier transform pulsed-gradient spin-echo studies of molecular diffusion," Prog. Nucl. Magn. Reson. Spectrosc. **19**, 1–45.
Stoller, S. D., W. Happer, and F. J. Dyson, 1991, "Transverse spin relaxation in inhomogeneous magnetic fields," Phys. Rev. A **44**, 7459–7477.
Sukstanskii, A. L., and D. A. Yablonskiy, 2002, "Effects of restricted diffusion on MR signal formation," J. Magn. Reson. **157**, 92–105.
Sukstanskii, A. L., and D. A. Yablonskiy, 2003, "Gaussian approximation in the theory of MR signal formation in the presence of structure-specific magnetic field inhomogeneities," J. Magn. Reson. **163**, 236–247.
Sukstanskii, A. L., and D. A. Yablonskiy, 2004, "Gaussian approximation in the theory of MR signal formation in the presence of structure-specific magnetic field inhomogeneities. Effects of impermeable susceptibility inclusions," J. Magn. Reson. **167**, 56–67.
Sukstanskii, A. L., D. A. Yablonskiy, and J. J. H. Ackerman, 2004, "Effects of permeable boundaries on the diffusion-attenuated MR signal: Insights from a one-dimensional model," J. Magn. Reson. **170**, 56–66.
Sun, B., and K.-J. Dunn, 2002, "Probing the internal field gradients of porous media," Phys. Rev. E **65**, 051309.
Swift, A. J., J. M. Wild, S. Fichele, N. Woodhouse, S. Fleming, J. Waterhouse, R. A. Lawson, M. N. J. Paley, and E. J. R. van Beek, 2005, "Emphysematous changes and normal variation in smokers and COPD patients using diffusion 3He MRI," Eur. J. Radiol. **54**, 352–358.
Taflove, A., and S. C. Hagness, 2005, *Computational Electrodynamics: The Finite-Difference Time-Domain Method*, 3rd ed. (Artech House, Boston).
Tanner, J. E., 1978, "Transient diffusion in a system partitioned by permeable barriers. Application to NMR measurements with a pulsed field gradient," J. Chem. Phys. **69**, 1748–1754.
Tanner, J. E., and E. O. Stejskal, 1968, "Restricted self-diffusion of protons in colloidal systems by the pulsed-gradient, spin-echo method," J. Chem. Phys. **49**, 1768–1777.
Tarczon, J. C., and W. P. Halperin, 1985, "Interpretation of NMR diffusion measurements in uniform- and nonuniform-field profiles," Phys. Rev. B **32**, 2798–2807.
Torquato, S., and M. Avellaneda, 1991, "Diffusion and reaction in heterogeneous media—Pore-size distribution, relaxation times, and mean survival time," J. Chem. Phys. **95**, 6477–6489.
Torrey, H. C., 1956, "Bloch equations with diffusion terms," Phys. Rev. **104**, 563–565.
Trottenberg, U., C. W. Oosterlee, and A. Schuller, 2001, *Multigrid* (Academic, New York).
Valckenborg, R. M. E., H. P. Huinink, J. J. v. d. Sande, and K. Kopinga, 2002, "Random-walk simulations of NMR dephasing effects due to uniform magnetic-field gradients in a pore," Phys. Rev. E **65**, 021306.
van Beek, E. J. R., J. M. Wild, H.-U. Kauczor, W. Schreiber, J. P. Mugler III, and E. E. de Lange, 2004, "Functional MRI of the lung using hyperpolarized 3-helium gas," J. Magn. Reson Imaging **20**, 540–554.
van den Berg, M., and P. B. Gilkey, 1994, "Heat content asymptotics of a Riemannian manifold with boundary," J. Funct. Anal. **120**, 48–71.
Veeman, W. S., 2003, "Diffusion in a closed sphere," Annu. Rep. NMR Spectrosc. **50**, 201–216.
Venkataramanan, L., Y.-Q. Song, and M. D. Hürlimann, 2002, "Solving Fredholm integrals of the first kind with tensor product structure in 2 and 2.5 dimensions," IEEE Trans. Signal Process. **50**, 1017–1026.
Wang, L. Z., A. Caprihan, and E. Fukushima, 1995, "The narrow-pulse criterion for pulsed-gradient spin-echo diffusion measurements," J. Magn. Reson., Ser. A **117**, 209–219.
Watson, A. T., J. T. Hollenshead, J. Uh, and C. T. P. Chang, 2002, "NMR determination of porous media property distributions," Annu. Rep. NMR Spectrosc. **48**, 113–144.
Watson, G. N., 1962, *A Treatise on the Theory of Bessel Functions* (Cambridge University, Cambridge, England).
Watson, A. T., and C. T. P. Chang, 1997, "Characterizing porous media with NMR methods," Prog. Nucl. Magn. Reson. Spectrosc. **31**, 343–386.
Wayne, R. C., and R. M. Cotts, 1966, "Nuclear-magnetic-resonance study of self-diffusion in a bounded medium," Phys. Rev. **151**, 264–272.
Wehrli, F. W., 1995, "From NMR diffraction and zeugmatography to modern imaging and beyond," Prog. Nucl. Magn. Reson. Spectrosc. **28**, 87–135.

Weibel, E. R., 1984, *The Pathway for Oxygen. Structure and Function in the Mammalian Respiratory System* (Harvard University, Cambridge, MA and London).

Weisskoff, R., C. S. Zuo, J. L. Boxerman, and B. R. Rosen, 1994, "Microscopic susceptibility variation and transverse relaxation: Theory and experiment," Magn. Reson. Med. **31**, 601–610.

Wesseling, P., 1991, *An Introduction to Multigrid Methods* (Wiley, New York).

Wilkinson, D. J., D. L. Johnson, and L. M. Schwartz, 1991, "Nuclear magnetic relaxation in porous media: The role of the mean lifetime $\tau(\rho,D)$," Phys. Rev. B **44**, 4960–4973.

Wilson, R. C., and M. D. Hürlimann, 2006, "Relationship between susceptibility induced field inhomogeneities, restricted diffusion, and relaxation in sedimentary rocks," J. Magn. Reson. **183**, 1–12.

Woessner, D. E., 1960, "Self-diffusion measurements in liquids by the spin-echo technique," Rev. Sci. Instrum. **31**, 1146–1146.

Woessner, D. E., 1961, "Effects of diffusion in nuclear magnetic resonance spin-echo experiments," J. Chem. Phys. **34**, 2057–2061.

Woessner, D. E., 1963, "NMR spin-echo self-diffusion measurements on fluids undergoing restricted diffusion," J. Phys. Chem. **67**, 1365–1367.

Wong, P. Z., 1999, *Methods in the Physics of Porous Media* (Academic, London).

Yablonskiy, D. A., A. L. Sukstanskii, J. C. Leawoods, D. S. Gierada, G. L. Bretthorst, S. S. Lefrak, J. D. Cooper, and M. S. Conradi, 2002, "Quantitative in vivo assessment of lung microstructure at the alveolar level with hyperpolarized 3He diffusion MRI," Proc. Natl. Acad. Sci. U.S.A. **99**, 3111–3116.

Yor, M., 2001, *Exponential Functionals of Brownian Motion and Related Processes* (Springer, Berlin).

Zaslavsky, G. M., 2002, "Chaos, fractional kinetics, and anomalous transport," Phys. Rep. **371**, 461–580.

Zavada, T., N. Südland, R. Kimmich, and T. F. Nonnenmacher, 1999, "Propagator representation of anomalous diffusion: The orientational structure factor formalism in NMR," Phys. Rev. E **60**, 1292–1298.

Zhang, G. Q., and G. J. Hirasaki, 2003, "CPMG relaxation by diffusion with constant magnetic field gradient in a restricted geometry: Numerical simulation and application," J. Magn. Reson. **163**, 81–91.

Zhong, J., R. P. Kennan, and J. C. Gore, 1991, "Effects of susceptibility variations on NMR measurements of diffusion," J. Magn. Reson. (1969-1992) **95**, 267–280.

Zielinski, L. J., 2004, "Effect of internal gradients in the nuclear magnetic resonance measurement of the surface-to-volume ratio," J. Chem. Phys. **121**, 352–361.

Zielinski, L. J., and M. D. Hürlimann, 2004, "Short-time restricted diffusion in a static gradient and the attenuation of individual coherence pathways," J. Magn. Reson. **171**, 107–117.

Zielinski, L. J., and M. D. Hürlimann, 2005, "Probing short length scales with restricted diffusion in a static gradient using the CPMG sequence," J. Magn. Reson. **172**, 161–167.

Zielinski, L. J., and P. N. Sen, 2000, "Relaxation of nuclear magnetization in a nonuniform magnetic field gradient and in a restricted geometry," J. Magn. Reson. **147**, 95–103.

Zielinski, L. J., and P. N. Sen, 2003a, "Combined effects of diffusion, nonuniform-gradient magnetic fields, and restriction on an arbitrary coherence pathway," J. Chem. Phys. **119**, 1093–1104.

Zielinski, L. J., and P. N. Sen, 2003b, "Restricted diffusion in grossly inhomogeneous fields," J. Magn. Reson. **164**, 145–153.

Zielinski, L. J., and P. N. Sen, 2003c, "Effects of finite-width pulses in the pulsed-field gradient measurement of the diffusion coefficient in connected porous media," J. Magn. Reson. **165**, 153–161.

Zielinski, L. J., Y.-Q. Song, S. Ryu, and P. N. Sen, 2002, "Characterization of coupled pore systems from the diffusion eigenspectrum," J. Chem. Phys. **117**, 5361–5365.